INVESTIGATION OF REACTIVELY SPUTTERED BORON CARBON NITRIDE THIN FILMS

by

VINIT O. TODI

B.E. University of Mumbai, 2006
M.S.E.E University of Central Florida, 2008

A dissertation submitted in partial fulfillment of the requirements
for the degree of Doctor of Philosophy
in the Department of Electrical Engineering and Computer Science
in the College of Engineering and Computer Science
at the University of Central Florida
Orlando, Florida

Summer Term
2011

Major Professor: Kalpathy B. Sundaram

ABSTRACT

Research efforts have been focused in the development of hard and wear resistant coatings over the last few decades. These protective coatings find applications in the industry such as cutting tools, automobile and machine part etc. Various ceramic thin films like TiN, TiAlN, TiC, SiC and diamond-like carbon (DLC) are examples of the films used in above applications. However, increasing technological and industrial demands request thin films with more complicated and advanced properties. For this purpose, B-C-N ternary system which is based on carbon, boron and nitrogen which exhibit exceptional properties and attract much attention from mechanical, optical and electronic perspectives. Also, boron carbonitride (BCN) thin films contains interesting phases such as diamond, cubic BN (c-BN), hexagonal boron nitride (h-BN), B_4C, β-C_3N_4. Attempts have been made to form a material with semiconducting properties between the semi metallic graphite and the insulating h-BN, or to combine the cubic phases of diamond and c-BN (BC_2N heterodiamond) in order to merge the higher hardness of the diamond with the advantages of c-BN, in particular with its better chemical resistance to iron and oxygen at elevated temperatures.

New microprocessor CMOS technologies require interlayer dielectric materials with lower dielectric constant than those used in current technologies to meet RC delay goals and to minimize cross-talk. Silicon oxide or fluorinated silicon oxide (SiOF) materials having dielectric constant in the range of 3.6 to 4 have been used for many technology nodes. In order to meet the aggressive RC delay goals, new technologies require dielectric materials with $K<3$. BCN shows promise as a low dielectric constant material with good mechanical strength suitable to be used

in newer CMOS technologies. For optical applications, the deposition of BCN coatings on polymers is a promising method for protecting the polymer surface against wear and scratching. BCN films have high optical transparency and thus can be used as mask substrates for X-ray lithography.

Most of the efforts from different researchers were focused to deposit cubic boron nitride and boron carbide films. Several methods of preparing boron carbon nitride films have been reported, such as chemical vapor deposition (CVD), plasma assisted CVD, pulsed laser ablation and ion beam deposition. Very limited studies could be found focusing on the effect of nitrogen incorporation into boron carbide structure by sputtering.

In this work, the deposition and characterization of amorphous thin films of boron carbon nitride (BCN) is reported. The BCN thin films were deposited by radio frequency (rf) magnetron sputtering system. The BCN films were deposited by sputtering from a high purity B_4C target with the incorporation of nitrogen gas in the sputtering ambient. Films of different compositions were deposited by varying the ratios of argon and nitrogen gas in the sputtering ambient. Investigation of the oxidation kinetics of these materials was performed to study high temperature compatibility of the material. Surface characterization of the deposited films was performed using X-ray photoelectron spectroscopy and optical profilometry. Studies reveal that the chemical state of the films is highly sensitive to nitrogen flow ratios during sputtering. Surface analysis shows that smooth and uniform BCN films can be produced using this technique. Carbon and nitrogen content in the films seem to be sensitive to annealing temperatures. However depth profile studies reveal certain stoichiometric compositions to be stable after high temperature anneal up to 700ºC. Electrical and optical characteristics are also

investigated with interesting results. The optical band gap of the films ranged from 2.0 eV - 3.1 eV and increased with N_2/Ar gas flow ratio except at the highest ratio. The optical band gap showed an increasing trend when annealed at higher temperatures.

The effect of deposition temperature on the optical and chemical compositions of the BCN films was also studied. The band gap increased with the deposition temperature and the films deposited at 500^{o}C had the highest band gap. Dielectric constant was calculated from the Capacitance-Voltage curves obtained for the MOS structures with BCN as the insulating material. Aluminum was used as the top electrode and the substrate was p-type Si. Effect of N_2/Ar gas flow ratio and annealing on the values of dielectric constant was studied and the dielectric constant of 2.5 was obtained for the annealed BCN films. This by far is the lowest value of dielectric constant reported for BCN film deposited by sputtering. Lastly, the future research work on the BCN films that will be carried out as a part of the dissertation is proposed.

dedicated to my grandparents, parents and brother

Shri Late Gaurishankar Todi & Smt. Savitri Devi Todi

Shri Omprakash Todi and Smt. Usha Todi

Shri Late Rahul Todi

who have always been inspirational sources in helping me realize and achieve my goals

ACKNOWLEDGMENTS

PhD dissertation is a journey and would not have been possible without the help of the following people. I would like to express my sincere gratitude to all who have helped me achieve this success in life. Firstly, I am heartily thankful to my advisors, Dr. K. B. Sundaram and Dr. Kevin R. Coffey whose encouragement, supervision and support from the preliminary to the concluding level of my PhD enabled me to develop an understanding of the subject. Thanks to Prof. J.S. Yuan, Prof. Vikram Kapoor and Prof. Praveen Wahid for serving on my dissertation committee and for their valuable comments which helped me in improving the quality of my dissertation. Special acknowledgement to my promoter at K. U. Leuven Dr. Cor Claeys and my manager Steffen Kaldor for facilitating my summer internships at IMEC and IBM respectively.

I am grateful to Edward Dein for giving me my first lessons in the clean room and for helpful suggestions at all times. I also wish to acknowledge advanced micro fabrication facility (AMF) and the materials characterization facility (MCF) at the advanced materials processing and analysis center (AMPAC) for laboratory support at the University of Central Florida (UCF). I gratefully acknowledge the faculty and staff at AMPAC, the School of Electrical Engineering and Computer Science and the College of Engineering and Computer Science at UCF for academic support for nearly five years.

I would especially like to thank Dr. Ravi Todi who has been a tremendous motivator and for his help with all aspects of my doctoral research including his proofing and commenting on my journal articles. His timely phone calls and suggestions have put me in the right perspective during tough times. I couldn't imagine completing this dissertation in time without his moral support and guidance.

I would like to thank my current and former colleagues at UCF: Mr. Bojanna Shantheyanda, Mr. Prabhu Doss Mani and Mr. Andrew Warren, who have helped me tremendously throughout all the experiments. I would like to express my sincere thanks to Dr. Arun Vijayakumar for his valuable comments and innovative suggestions during the course of my research work.

At this time I would also like to acknowledge all my peers for their valuable suggestions at all times. I would like to acknowledge the student government association and the division of graduate studies at UCF for numerous travel awards that helped me present research at various international conferences. I would also acknowledge professional organizations like IEEE, AVS and ECS for providing me with the opportunity for professional development.

Last but not the least I would like to thank the love of my life Miss Rupam Sharma for her love, support and patience which helped me get through difficult stages of my PhD dissertation. I would also like to thank all my family members and friends for always being there for me and making each day worth living. Finally, with deep gratitude, I would like to thank my brother; my ANGEL, Late Rahul Todi whose presence I have always felt around me which helped me in getting across any hurdle through earning this PhD and in life.

TABLE OF CONTENTS

LIST OF FIGURES

LIST OF TABLES

CHAPTER 1: INTRODUCTION

Today, surface coatings finds a wide range of applications in the industry including microelectronics, display devices, corrosion and wear-resistance including cutting tools and polymers, high temperature oxidation, solar cells, aerospace, decorative coatings etc. Efforts are directed to find ways to improve the performance, extending the life and enhancing the appearance of the materials.

1.1 Overview

With increasing advancements in technology there has been an increasing growth of performance enhancing electronics on a wide variety of industrial applications. Hard and wear resistant coatings are extensively studied by thin film researchers and constitute an important part of surface engineering. Ceramic thin films of TiN, TiAlN, TiC, SiC and diamond like carbon (DLC) have been studied previously for use in industrial applications such as cutting tools, automobiles and machining parts. However due to ever increasing industrial demands there is a need to research for thin films with more complicated properties. The thin films also finds applications as inter level dielectrics (ILD) in Si- based microelectronics.

Binary, ternary and quaternary compounds formed through combinations of silicon, boron, carbon and nitrogen are gaining importance due to possible applications in harsh environments. Vijayakumar, et. al., have presented results on one such quaternary compound of silicon boron carbon nitride that demonstrated good thermal stability and improved performance at high temperature, thus, allowing the compound to be used in low cost and easy-to-fabricate high temperature photodetector applications [1, 2]. Similarly, a ternary compound of boron carbonitride (BCN) has gained increased attention due to its potential applications in electronic,

optoelectronic and luminescent devices. [3] [4]. The boron-carbon-nitrogen phase diagram contains interesting phases, such as diamond, graphite, fullerene, cubic-BN, B_4C and there is also a hypothetical C_3N_4 as shown in Fig.1.

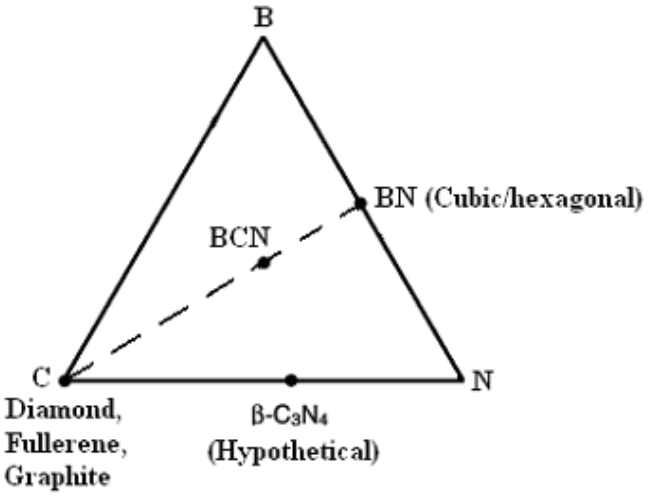

Figure 1.1: Ternary Triangle

Carbon nitride (C-N) thin films are predicted to have hardness comparable to diamond due to the small bond length and low ionicity of this material [5]. Boron nitride (BN) films have high hardness and wide band gap but typically have poor adhesion due to high internal stress [6]. In addition to their super-hardness, these materials have in general high melting point, semiconducting, excellent resistance to wear and chemicals.

1.2 Motivation

There exist atomic bonding similarities amongst boron, carbon, and nitrogen that allow the formation of compounds with a wide compositional range. BCN compounds have been expected to combine the excellent properties of B_4C, BN and C_3N_4, with their properties adjustable, depending on composition and structure [7-9]. For example, C.Morant, et. al., have reported BCN films with hardness > 20GPa [10]. The BCN alloy has been regarded as a

promising candidate for novel super hard materials to be used as protective coatings. The most interesting aspect of BCN films results from its electrical properties. As graphite is semi metallic and h-BN is insulating (band gap >3.8eV), it is expected that such a hybrid between semi metallic graphite and insulating h-BN may show adjusted semiconductor properties [11].

Moreover, recent efforts have been devoted to develop a low dielectric constant BCN film in order to reduce the stray capacitance induced signal delay of interconnections in Si ultra large scale integrated circuits (ULSI). Dense (pore-free) BCN films with a low dielectric constant in the range of 1.9 to 2.1 have been successfully demonstrated [12] [13]. The use of BCN films in the CMOS back end technology is really very interesting and promising. A material with a low dielectric constant and with high mechanical hardness is a perfect match for inter layer dielectrics. Also, it has been reported that the band gap energy of BCN films decreases with increasing carbon ratio [14]. The control of band gap energy and refractive index may make it possible to develop optical components such as filters and mirrors for use in the UV wavelength region. Montasser et al. have initially prepared transparent BCN films to light of wavelength of 200-1000 nm using plasma-assisted CVD [15]. Weber et al. have reported the BCN films could be used as mask substrates for X-ray lithography [16].

Many attempts have been made for the preparation of thin films of BCN materials with various amounts of carbon, boron and nitrogen including binary and ternary compounds as well as diamond and other carbon materials. The composition and structures of the prepared materials strongly depend on the preparation method and the corresponding precursors used for the preparation process. Several methods of preparing boron carbon nitride films have been reported, such as chemical vapor deposition (CVD) [17, 18], plasma assisted CVD [19, 20], pulsed laser ablation [21-23], ion beam deposition [24], and sputtering [25, 26]. Also, shock wave

compression [27] or high pressure/high temperature techniques (HP/HT) have been used [28]. However, it is still not easy to synthesize boron carbon nitride compounds with controllable composition by changing deposition parameters. In Itoh [29], theoretical and experimental data are compared concerning the stability of bonds between the elements boron, nitrogen and carbon. The energetically most preferred bonds are B-N and C-C, while N-C, B-C, B-B and N-N have a much lower binding energy. This suggests that it can be difficult to form real ternary composites where all three elements are bound. Provided that there is enough mobility, the most stable bonds will form and hence, a phase separation should be expected. In most research publications, the investigated composition range within the ternary triangle is closely limited. Sometimes, only a few compositions are investigated. In other works the limitations in composition are due to experimental restrictions like target composition or precursor mixing, so that one element is always incorporated in approximately the same while other two can be varied over a greater range. For example, in Teodorescu et al, N is always below 15%, but B and C are varied from 43 to 91% and 7 to 46%, respectively [30]. Another kind of restriction is that the given compositions lie on a line within the triangle where the ratio between two elements is more or less constant [31, 32]

The sputtering technique provides unique advantages over other techniques such as freedom to choose the substrate material and a uniform deposition over relatively large area. Furthermore, it is possible to control the deposition parameters to prepare BCN films of various compositions. Some work has been reported on BCN films produced by sputtering. Sputtered BCN films with excellent mechanical properties, such as adhesion, high hardness and good wear resistance, have been reported [33-34]. According to the chemical properties of the B, C and N during the depositing process of the BCN films, B and C can exist both as elements and as

compounds reacting with N or each other, while N could be existed in the films only as compounds by reacting with B or C. Therefore, the process of N deposited into the films and the reciprocity among B, C, and N during the deposition of films becomes the main factors, which affect the composition and properties of films.

1.3 Objective and Outline

The focus of this work was to synthesize the ternary boron carbon nitrogen (BCN) alloy through reactive sputtering and investigating various physical, chemical and electrical properties and access its optical applications and the feasibility to use as a low-κ material in the CMOS back end technology.

Chapter 2 is intended to provide the background on the work done on ternary alloy of boron carbon nitrogen. A historical outlook on different methods of synthesis as well as the significant properties of the materials that makes them so useful is presented.

Chapter 3 includes experimental details, the system used for the deposition of thin films including deposition parameters followed by the presentation of various characterization techniques used to evaluate different properties of the thin films materials deposited for this study.

Chapter 4 forms the core of this dissertation and includes results and discussion. Initially we focus on the BCN film deposition and characterizing different process parameters. Later we discuss the important properties of the different films obtained to identify the optimum deposition conditions. Chemical structure, optical and electrical properties are also discussed in detail with correlation between important parameters affecting each observation. Finally the feasibility of BCN material as a low dielectric constant material is demonstrated.

Chapter 5 gives a summary of the work with concluding remarks based on the observations discussed in chapter 4. Finally, we discuss other deposition configurations using reactive sputtering to deposit BCN films and suggest future experimental work to explore this material further.

CHAPTER 2: LITERATURE REVIEW

2.1 Boron Carbide Thin Films

Boron carbide (B_4C), one of the important alloys in the family of non-metallic hard materials is the third largest hardest material at room temperature. At temperatures over 1100^oC, the hardness of B_4C is more than diamond and cubic boron nitride. Other attractive properties include good wear resistance, low specific weight, high modulus and high thermal stability [35-40]. The bulk form of boron carbide finds applications in sharpening cutting tools, abrasives in polishing, lapping and grinding media and in sand blasting nozzles [41]. Electrically, boron carbide is p-type semiconductor material at even high temperatures which suggests is thermally very stable. In thin film form too, this material finds applications as hard and protective coatings, hard disk drives and other corrosion-resistance applications [42]. Harris et al. reported that boron carbide can be used in tribological systems under high load also at elevated temperatures [43-44]. Due to its high thermal stability it is a promising material for electronic devices operating at high temperatures and an excellent thermoelectric material [45]. It can also be used for semiconductor devices in harsh environments as heterojunction diodes with silicon [46]. Aoqui et al. has reported its usage in high intensity electron emitting devices [47].

Several techniques have been used for depositing boron carbide thin films, including chemical vapor deposition (CVD) [48-49], plasma-enhanced CVD [50-51], laser CVD [52], ion-beam evaporation [53], pulsed laser deposition [54-55], vacuum plasma spraying [56], ion beam sputtering [57], RF magnetron sputtering [37] and DC magnetron sputtering [58-60]. Sputtering techniques have been commercialized more successfully in big manufacturing fabs because of their high film deposition rate and low temperature features [61]. General properties of boron carbide are shown in the following table.

Table 2. 1: General properties of boron carbide [35, 40, 62].

Properties of boron carbide	
Molecular weight (g/mol)	55.26
Density (g/cm^3)	2.52 for B_4C
Melting Point (^oC)	~ 2400
Specific Heat (Cal/mol K at 300 K)	12.7
Thermal conductivity (W/cm K)	0.35-0.16 (25-800^oC)
Thermal expansion (1/K)	4-8 E^{-6} (25-800^oC)
Electrical Resistivity (Ω-cm)	5 (at 298K)
Electrical conductivity (1/ Ω-cm)	~10^3
Band Gap (eV)	0.77-1.80
Dielectric Constant	5
Seeback coefficient (μV/K)	200-300
Vickers Hardness (GPa)	27.4-40
Young's Modulus (GPa)	290-460
Shear Modulus (GPa)	158-200
Bulk Modulus (GPa)	190-250
Tensile Strength (N/mm^2)	155 (980^oC) 162 (1425^oC)
Poisson's Ratio	0.14-0.18
Flexural Strength (MPa)	323-430
Lattice constant (nm)	c=1.207 a=0.561
Oxidation resistance	in air up to 600^oC
Chemical resistance	Excellent. Reacts with halogens at high temperature.

Fig. 2.1 and 2.2 show rhombohedral unit cell and crystal structure of boron carbide respectively. The crystal structure of boron carbide is represented by a rhombohedral unit cell with icosahedral arrangement of 12 atoms [62]. A unit cell containing of 15 atoms is formed by 12 atoms of the icosahedra and 3 atoms of the intericosihedral chain. As seen, four sites are

available for 15 B and C atoms in the crystal arrangement thereby allowing B and C atoms to substitute for each other within both icosahedra and the intericosehedral chains. This is the reason behind the existence of large homogeneity range of boron carbide [35, 40].

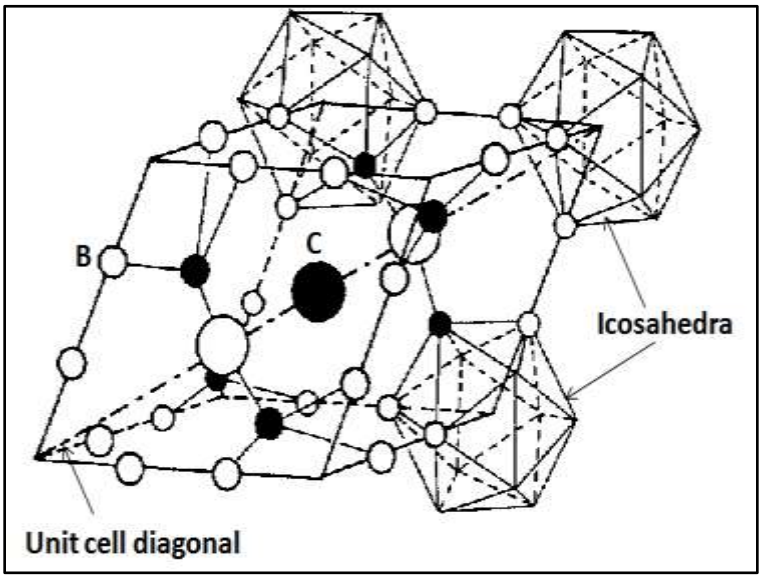

Figure 2. 1: Rhombohedral unit cell of boron carbide

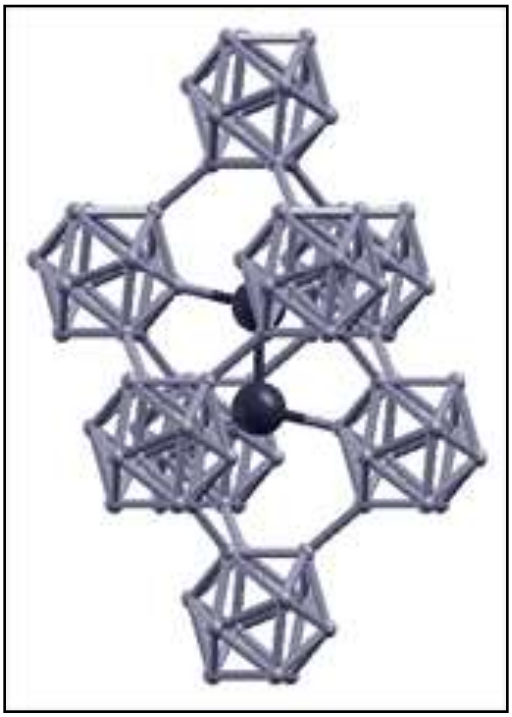

Figure 2. 2: Rhombohedral crystal struture

All sputter deposited thin films of boron carbide reported in the literature are amorphous. Even for the amorphous thin films the structure is still based on a random icosahedral network at carbon content less than 50 at.% [57]. Crystalline boron carbide films prepared by RF sputtering above 950^{o}C have been reported by Chian et al. [63]. Similarly, Han et al. observed a tendency of crystallization for boron carbide films if sputtered at a temperature above 450^{o}C [64]. Boron carbide films prepared by using ion beam sputtering showed crystal phases when deposited at about 350^{o}C [65]. Kulikovsky et al. demonstrated the possibility to deposit crystalline B_4C films by DC magnetron sputtering at temperature above 900^{o}C [66].

Polycrystalline boron carbide films were reported by few techniques other than sputtering. Using pulsed ion-beam evaporation technique, Suematsu et al. were able to deposit crystalline boron carbide thin films at room temperature without external heating [45]. For CVD techniques, polycrystalline boron carbide films can be grown but at the temperature range of 1000-1600^{o}C [52]. Partially crystallized boron carbide films were obtained by cathode arcing [67]. The shortcoming of this technique is that it utilizes a high conductivity target and hence is not effectively suitable for mostly semiconducting boron carbide targets. This can be overcome again by raising the temperature of the cathode while increasing the amount of droplets incorporated into the resultant boron carbide coatings.

Thus, it is clear from the literature that the sputtering is the most preferred method for boron carbide deposition for its use of operation and relatively high deposition rates. Mostly amorphous films are obtained from sputtering and the sputter deposited films tend to crystallize at high temperatures. Though the boron carbide films obtained from sputtering are amorphous, they have mechanical hardness comparable and at times superior to that of crystalline bulk boron carbide.

2.1.1 Mechanical Properties

The reported values of the hardness and Young's modulus for boron carbide thin films are very much scattered. S. Ulrich et al. reported the sputtered deposited boron carbide film with the hardness value of 72 GPa [68]. This is by far the highest value reported in the literature and the films were prepared by sputtering from B_4C target by applying bias voltages. Other values reported in the literature include films prepared without external heating by H. Y. Chen et al. and they reported hardness values of 13 GPa [65]. A list of the literature survey on the mechanical properties of the boron carbide films is as shown in Table 2.2.

Table 2. 2: Mechanical properties of boron carbide [35, 40, 62].

Hardness (GPa)	Young's Modulus (GPa)	Technique	Reference
20-40	180-280	Nanoindentation	T. Eckardt et al. [44]
8-18	90-140	Nanoindentation	H.S. Ahn et al. [61]
15.4	138.5	Nanoindentation	P.D.Cuong et al. [69]
42.5-50.4	300-420	Nanoindentation	Z.Han et al. [64]
30	250	Nanoindentation	Y. Chen et al. [39]
10-35	145-275	Nanoindentation	T. Hu et al. [70]
14-32	175-313	Nanoindentation	F. Kokai et al. [54]
17-27	210-245	Nanoindentation	L.G. Jacobsohn [59]
19-25	250-300	Nanoindentation	E.Pascual et al. [71]
25-30	290-350	Nanoindentation	A. Lousa et al. [38]
16	200	Nanoindentation	K.E.Lee et al. [72]
23-29	252-348	Nanoindentation	J. Sun et al. [55]
15.6-26	16-210	Nanoindentation	O.R.Monterio et [67]
20.8-60	255-518	Nanoindentation	V.Kulikovsky et [66]

Most of the work reported in Table 2.2 focuses on studying the effect of deposition temperature and bias voltages on the values of the hardness. Ulrich et al. have studied the effect of bias voltages in the range of 0 to 175 V, on the hardness of the boron carbide films and found an increase in hardness from 30GPa to about 72 GPa and compressive stress from 4 GPa to 7 GPa with the increase in bias voltages from floating to 75V [68]. Similar trend was observed by Lousa et al. whereby the hardness increased from 24 to 30 GPa with increasing negative bias voltage and the values of the stress increased linearly from about 4 to 5.5 GPa with increasing bias voltages [38]. Knotek et al. found an increase in hardness from about 20 to 35 GPa for the films deposited at 100^{o}C and 20 to 30 GPa at 300^{o}C. They varied the bias voltages between 0 and 100V. According to them both heating and bias voltages increases the hardness [73].

Thus from Table 2.2 it can be said that the reported hardness and modulus values for boron carbide thin films are comparable and even superior to that of bulk boron carbide reported previously in Table 2.1. Also it is noteworthy to mention that for all the studies reporting the mechanical properties with respect to increase in deposition temperature, the authors observed an increase in hardness with the increase in the deposition temperature. This is regardless of whether the films are amorphous or crystalline. On the other hand, some researchers reported a continuous increase of the hardness with increase of the applied negative bias voltage [73], while others observed a rise and fall trend with the increasing bias voltages and few others have reported a continuous decrease in the hardness while increasing the bias voltages [38, 68]. In brief, it is difficult to make any concluding remarks describing a general dependence of the applied bias voltages on the mechanical properties of the boron carbide thin films.

2.1.2 Wear properties

Similar to the hardness data the data reported for the friction and wear properties of the boron carbide films are scattered too. Knotek et al. reported the friction coefficient values of about -.7-0.8 for DC sputtered and 0.2 for rf sputtered films. They used a pin-on-disc tribometer against a 100Cr6 counterface [73]. Friction coefficient values of about 0.9 were reported by Eckardt et al. and they also used 100Cr6 ball with 4.67 mm diameter and a load of 1N [44]. Erdemir et al. studied the tribological properties of post annealed boron carbide thin films and found a decrease in friction coefficient by the formation of boron oxide on the film as a result of annealing. The friction coefficient values reported by them were as low as 0.03 [74]. Frictional properties of B_4C at various temperatures were studied by Rabinowicz and Imai and they found that B_2O_3 layers become lubricious above 650^oC thereby providing a friction coefficient as low as 0.1 [75]. Larsson et al. confirmed the formation of a solid lubricant boric acid layer on sintered bulk boron carbide [75]. A different arrangement was used by Guruz et al. to find the friction and wear properties of the boron carbide films. They used a block-on-ring apparatus for the tests and M2 steel as counterface. They found friction coefficient values of about 0.06 for the M2 steel-boron carbide pair and 7.3 x 10^{-9} mm^3/Nm wear rates [76]. Yet another method was used by Martinez et al. to study the nano wear properties. The friction coefficient was measured by a micro scratch test with a diamond tip and was found about 0.12 [34]. Reigada et al. also investigated the nanowear properties of boron carbide coatings prepared by DC sputtering. The effect of applied bias voltages on the wear properties was studied and they observed a decrease in both friction and wear with the increase in negative bias voltages [77]. The wear rates of metal doped (Mo, W, Ni-Cr) boron carbide coatings prepared by rf sputtering was researched by

Kustas et al. They observed the improvement in wear properties of the coatings with bias voltages by a process of densification of the coatings [78].

2.1.3 Electrical Properties

Boron Carbide is a p-type semiconductor with a band gap of 1.2-1.8 eV [79]. Also, B_4C phase is stable at high temperatures because of its high melting point [35]. These combined properties of B_4C phase makes this material a good candidate to be used for electronic devices that can be operated at high temperatures thus can be used in harsh environment applications. Carbon content was showed to play an important role in the electrical properties of the boron carbide films studied by Suematsu et al. and synthesized using ion beam evaporation. The increase in carbon content from 14 % to 20% led to the decrease in the conductivity from about $10^5\ \Omega^{-1}cm^{-1}$ to $10^4\ \Omega^{-1}cm^{-1.}$ Also the Seeback coefficient also decreased from about 300 μVK^{-1} to 150 μVK^{-1} with an increase in the carbon content [53].

Sylvester et al. reported amorphous hydrogenated boron carbide thin films with boron concentrations ranging from 0 to 18 atomic percent by plasma decomposition of a feedstock of diborane and methane. They observed that boron acts like a dopant with increasing boron concentrations leading to increasing acceptor densities [80]. Similar work on amorphous hydrogenated carbon doped with boron was first done by Jones and Stewart and they reported a increase by a factor of ten in conductivity [81]. Some work on the use of boron carbide material in semiconducting devices in harsh environments was done by Ahmad et al. whereby they describe the fabrication of boron carbide/silicon hetero junction diodes [82]. To be a good candidate to be used in junction with silicon the boron carbide films is expected to have resistivity but the films they obtained by sputtering had low resistivity value of 10 Ω-cm and thus did not form rectifying contact with silicon. Another very interesting work on boron carbide is

done by Kormann et al. where they study the electrical properties of powder pressed boron carbide. They measure Seeback-coefficient, dc conductivity, ac conductivity and dielectric constant between room temperature and 4.2K. They observed a decreasing trend is Seeback-coefficient with respect to temperature and values down to 10-30 μV/K around 5 to 20K has been reported. The dc conductivity was measured to be in the range of 10^{-9} to 10^{-11} $(\Omega\text{-cm})^{-1}$ [83].

2.2 Boron Nitride

Boron nitride is very similar to diamond and can be used to make crystals that are as hard as diamond. Boron nitride is an excellent conductor of heat in spite being an insulator electrically. Boron nitride is mostly found in cubic (c-BN or β-BN) and heaxagonal (h-BN) phases. BN is general is not found naturally. Cubic BN has properties close to diamond and is known to the second hardest material after diamond. Also, c-BN can be made either n or p type conductivity for electronic applications. On the other hand h-BN is a soft material with insulating properties and has a band gap of 5 eV [84-85].

2.2.1 Cubic boron nitride

Cubic boron nitride is an allotrope of boron nitride and is made of tetrahedrally bonded light elements. It is also known as c-BN, β-BN or z-BN (after zinc blende crystalline structure). The cubic form of boron nitride was first discovered in 1957 [86] and during past years research focus has been on the deposition of thin films of small area crystals under high temperature and high pressure conditions. The powdered form of c-BN finds extensive use as industrial abrasive and boron nitride deposits are used to minimize friction and wear. Its usefulness is derived from the fact that boron nitride is insoluble in iron, nickel and related alloys at high temperatures.

High pressure-high temperature (HPHT) method is used to prepare cubic BN in powder form from a submicron size up to small crystals with a size 0.8 mm [87-88]. Such c-BN materials in granular form are used in the tooling industry with the help of sintering. Other techniques used to synthesize cubic boron nitride includes physical vapor deposition (PVD) and plasma enhanced chemical vapor deposition (PECVD), pulsed laser deposition, DC and RF magnetron sputtering from conductive or non-conductive targets (h-BN, boron, B_4C composite) [89-90]. However the c-BN films still suffer from following shortcomings;

a) Low quality of crystallinity
b) Presence on interfacial softer layers
c) Low phase purity
d) High internal stress
e) Poor adhesion to the substrate

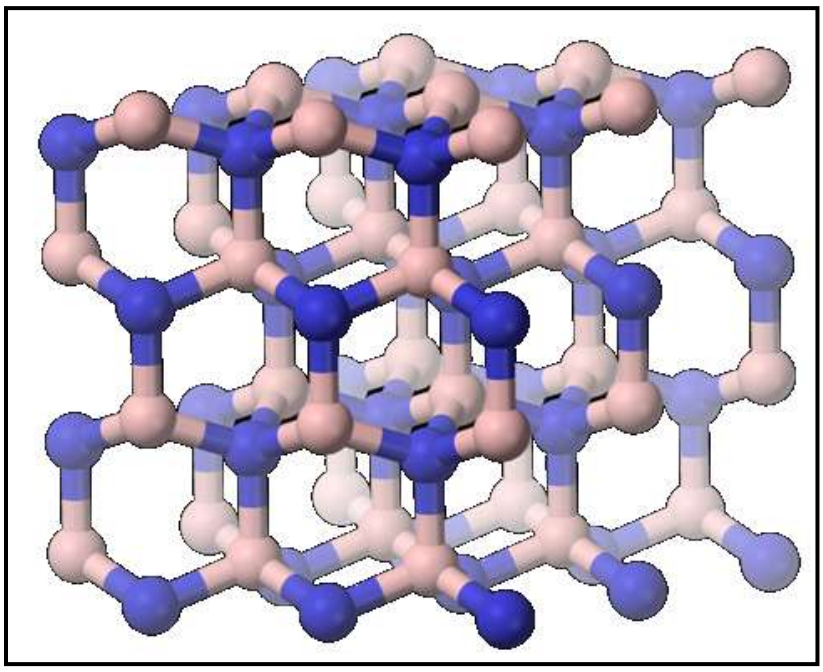

Figure 2. 3: BN, wurtzite structure

Because of adhesion issues there is a limitation to the thickness of the c-BN film prepared which limits its use in the industry. The thickest films have been produced using dc plasma jet and electron cyclotron resonance ECR deposition using complex gas mixtures [91].

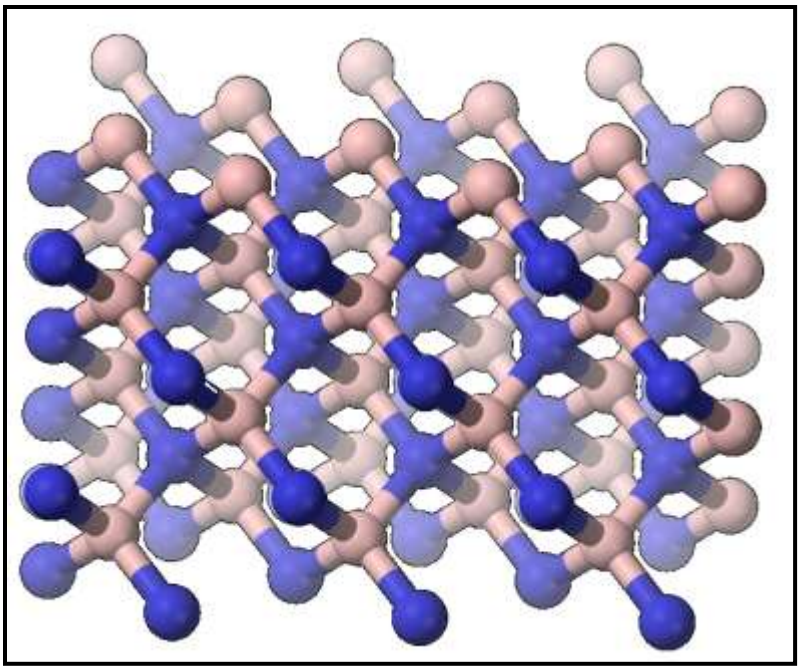

Figure 2. 4: β-BN sphalerite structure

These techniques involve use of complex precursor mixture which can be expensive and thus inadaptable into a production flow. Further, c-BN is almost as hard as diamond, 5 x 10^3 kp/mm^2 for c-BN as compared to 8 x 10^3 kp/mm^2 for diamond [92] and has a very large indirect energy band gap E_g varying between 5.4 and 7.0 eV at room temperature. A p-n junction when fabricated from c-BN material can operate at temperatures above 500^{o}C [93]. Also, c-BN can easily be doped n-type using Si and p-type using Be and Mg. This is something that cannot be achieved with diamond. Lastly, c-BN does not react with foreign materials at high altitudes and in harsh environments [94-95].

2.2.2 Hexagonal boron nitride

Hexagonal boron nitride (h-BN) or α-BN or g-BN (graphite BN) is used at both very low temperature and at high temperature as a lubricant and in situations where the electrical conductivity or chemical reactivity would be problematic [96]. Boron nitride lubricants can be

used even in vacuum for space applications as the lubricity mechanism does not contain water molecules which will be trapped between the layers. h-BN can be included in ceramics, alloys, resins, plastics, rubbers and other materials, giving them self-lubricating properties. Such materials are used in construction of bearings. Plastics filled with BN have decreased thermal expansion, increased thermal conductivity, increases electrical insulation and case reduced wear to adjacent parts.

Hexagonal boron nitride is stable at temperatures up to 1000^{o}C in air, 1400^{o}C in vacuum and 2800^{o}C in inert gas thus is a material which has one of the best thermal conductivities of all electric insulators. Another important characteristic of h-BN is that it is fairly chemically inert and is not wetted by many melted materials (e.g. aluminum, copper, zinc and steels, germanium, silicon, glass and halide salts) [97]. The h-BN has hardness comparable to graphite and thus can be made by hot pressing with subsequent machining and also keeps the machining cost low. The parts are made from boron nitride powders, using boron oxide as a sintering agent.

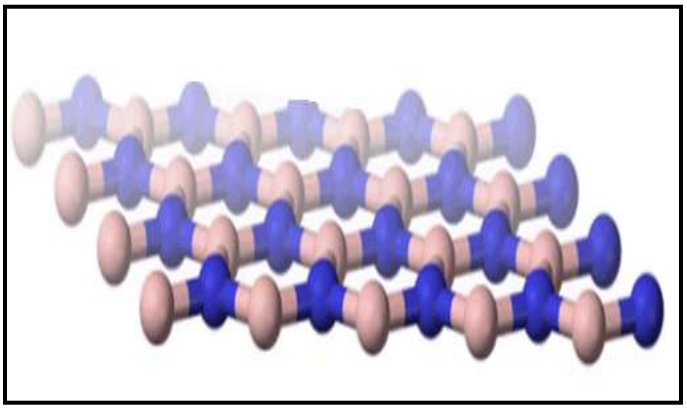

Figure 2. 5: h-BN hexagonal (graphite like)

Other applications of boron nitride include substrates for semiconductors, microwave transparent windows, structural material for seals, electrodes and catalyst carriers in fuel cells and batteries. Fine grained h-BN is used in some cosmetics, paints, dental cements, pencil leads etc. There has been another interest in electronic application of BN films as a low dielectric

constant insulating film. The switching performance of ultra large scale integrated (ULSI) semiconductor devices is degraded by the time delay due to interconnection of electron devices. In order to reduce the time delay, it is necessary to introduce a wiring metal with a low electrical resistivity and a high quality insulating film with a low wiring capacitance. The dielectric constants of h-BN and c-BN were reported to be 3.8 and 7.1 respectively [98].

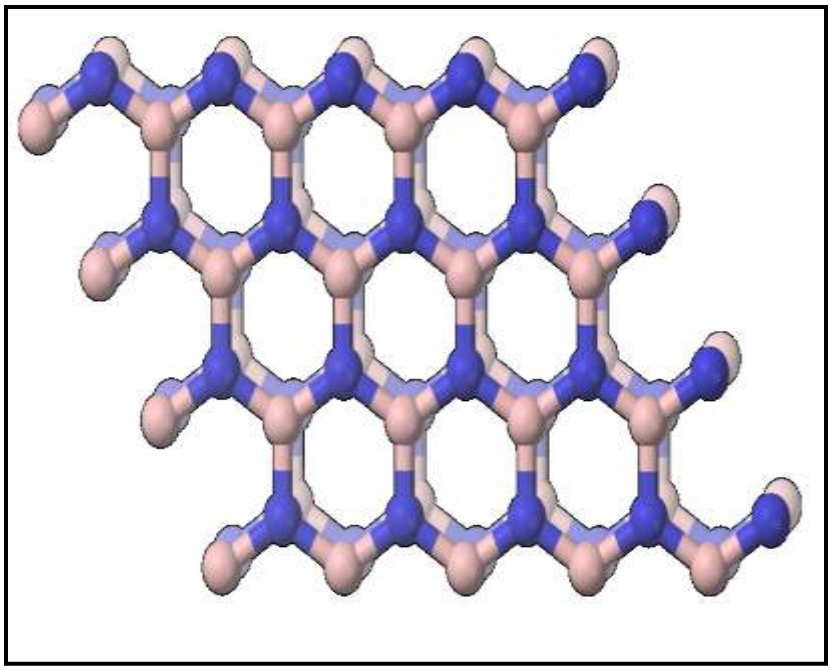

Figure 2. 6: h-BN hexagonal (diamond like)

Thin films of boron nitride can be obtained by chemical vapor deposition from boron tricholoride and nitrogen precursors. Takashi et al. reported BN films prepared by plasma assisted CVD and observed dielectric constant as low as 2.3 [99]. Combustion of boron powder in nitrogen plasma at 500^{o}C is used for production of ultra-fine boron nitride for lubricants and toners.

Table 2.3 compares the physical properties of BN with the properties of other well-known semiconductors [100].

Table 2. 3: : Comparison of various properties of BN with those of other semiconductors [100].

Parameter	c-BN	h-BN	Diamond	3C-SiC	GaAs	Si
Lattice Constant (A)	3.615	a=2.504	3.567	4.358	5.65	5.43
Thermal expansion Coefficient	3.5	2.7, 3.7	1.1	4.7	5.9	2.6
Density (gm/cm^3)	3.487	2.28	3.515	3.216	-	2.328
Melting Point (oC)	>2973	-	3800	2540	1238	1420
Energy bandgap (eV)	6.4	5.2	5.45	3.0	1.43	1.12
Electron mobility (cm^2/Vs)	-	-	2200	400	8500	1500
Hole mobility (cm^2/Vs)	-	-	1600	50	400	600
Dielectric constant	7.1	5.06	5.5	9.7	12.5	11.8
Breakdown(x10^5 Vcm^{-1})	~80	~80	100	40	60	3
Resistivity (Ω-cm)	10^{16}	10^{10}	10^{13}	150	10^8	10^3
Thermal conductivity	13	-	20	5	0.46	1.5
Absorption edge (μm)	0.205	0.212	0.20	0.40	-	1.40
Refractive index	2.117	1.700	2.42	2.65	3.4	3.5
Hardness (kg/mm)	9000	-	10,000	3500	600	1000

2.3 Carbon Nitride

Theoretical prediction was made by Liu and Cohen stating that β-C_3N_4 which is isomorphic with β-Si_3N_4 can possess a bulk modulus which can surpass that of diamond [5]. Figure 2.7 shows the structure of the carbon nitride. This has motivated a lot of research work in the development of C_3N_4 over the past two decades. Along with high hardness C-N material is expected to possess wide band gap, high thermal conductivity, high strength, high decomposition temperature and excellent resistance to corrosion and wear. The relatively shorter bond length (1.47 Å) and low bond iconicity (about 7%) of the C-N bond compared to β-Si_3N_4 with a Si-N bond length of 1.74Å and bond iconicity of 30% suggest the superiority of the former material over the latter in terms of hardness and high temperature applications [100, 101]. Carbon Nitride also finds applications in devices such as insulator in III-V metal-insulator-semiconductor

structures. C-N is a preferred material over Si_3N_4 for such applications because it doesn't introduce any shallow impurities.

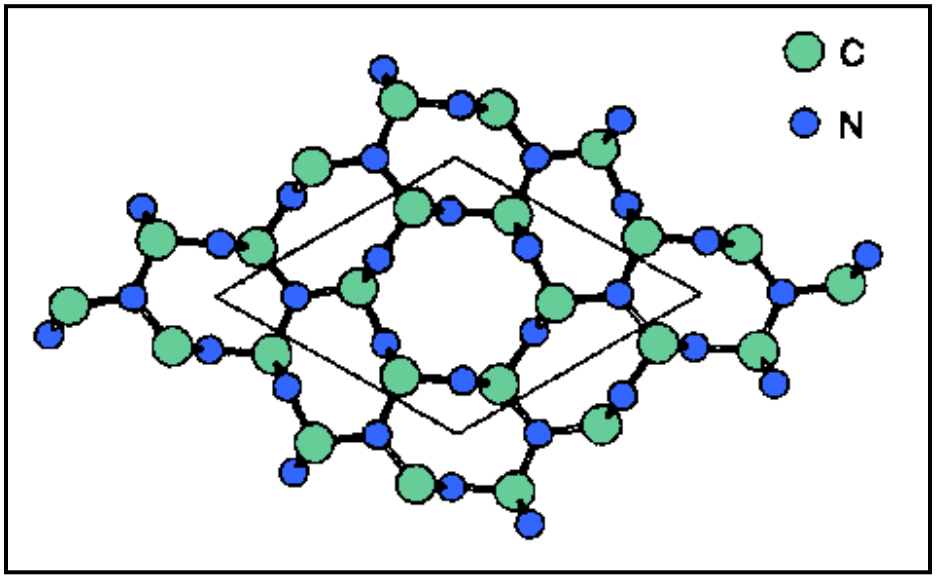

Figure 2. 7: Crystal structure of carbon nitride

Works have been reported on the deposition of C-N films by various deposition techniques such as reactive sputtering [102-105], plasma chemical vapor deposition (CVD) [106-107], laser ablation [108,109], ion-assisted deposition [110-112] and metal-organic chemical vapor deposition (MOCVD) [113]. The nitrogen incorporation in the C-N films in all the work reported above was about 40 at. % which is on a lower side than that expected for stoichemetric β-C_3N_4(57 at %). Higher amounts of nitrogen (50-57 at. %) has been reported in the hydrogenated C-N films prepared by plasma CVD [107] and the CN films obtained by dual ion beam sputtering [112], laser ablation [109] of graphite using a low-wavelength excimer laser and by using the MOCVD technique [113]. Thus sputtering being the most widely used deposition method in the industry results in relatively low nitrogen content in the carbon nitride films [114]. Mubumbila et al. used reactive sputtering and studied the effect of nitrogen incorporation on the growth kinetics, composition, structure and type on bonding. They observed that the introduction

of N_2 in the plasma leads to an increase in the growth rate and that the growth kinetics and N content in the films is dependent on physical and chemical sputtering. The changes in growth kinetics influenced the chemical, structural and optical properties [115]. Sunil Kumar et al. also deposited C-N films by reactive sputtering and observed that by lowering the power to the target and at high nitrogen pressure results in higher N_2 contents in the film. They achieved equal amounts of carbon and boron for a wide range of sputtering pressures at low temperature and the structure of the film was graphite-like [116].

2.4 Boron carbon Nitride (BCN) Thin Films

In past few years, thin films within the ternary system B-C-N have gained much interest. The ternary alloy of BCN is expected to combine the properties of diamond, cubic boron nitride, tetragonal amorphous carbon and boron carbide [8,117]. The phase diagram of the B-C-N is showed in Figure 1.1. One of the characteristic features of the materials in the BCN ternary phase system is that they have short bond lengths and thus expected to combine the specific properties of diamond, cubic boron nitride (c-BN), hexagonal boron nitride (h-BN) and boron carbide (B_4C). The properties of these materials include high hardness, low friction coefficients, lubricity and good wear resistance and thus are good candidate for hard and protective coatings for cutting tools and other wear-resistance applications [8, 34, 118].

Besides the excellent mechanical properties B-C-N ternary system also includes materials with good optical and electrical properties. Materials such as diamond and cubic boron nitride are known to have high refractive index and large band gap [119,120]. Also, the ability to control the band gap (E_g) by changing the atomic composition and structure makes them suitable for the application in electronic and photonic devices [121-123]. There are possibilities to form ternary materials in the BCN system which can take the advantages of less complex materials and form

different relaxed ternary phases and still preserve the structure and properties of the localized materials like diamond, c-BN and boron carbide. Several studies have been made to combine materials with extremely different properties, for example combining super hard diamond and soft h-BN, hard and wear resistant B_4C and soft and lubricating h-BN, semi metallic graphite and insulating h-BN etc [120].

Various deposition techniques have been reported in the literature for depositing BCN thin films, including chemical vapor deposition (CVD) [121,124], ion beam assisted deposition [125,126], cathodic arc plasma deposition [127], pulsed laser deposition [128] and DC and RF magnetron sputtering [129,130]. The experimental investigations reported above focuses mainly on the synthesis, characterization and mechanical properties. Yang et al. studied the effect of nitrogen pressure on structure and optical properties of BCN thin films deposited by pulsed laser ablation of a boron carbide (B_4C target). The nitrogen content in the films increased and then saturated up to ~26 at. %. The optical band gap (Eg) increased from 3.78 to 3.92 eV as the nitrogen pressure was increased from 2 to 15 Pa. The change in optical band gap was well in accordance with the change in film composition measured by XPS [131]. Yuki et al. synthesized BCN films by plasma-assisted chemical vapor deposition and studied the optical and electrical properties. They observed that the carbon composition had a strong dependence on the optical and electrical properties of the BCN films. The band gap of the film decreased from 5.3 to 3.4 eV with increasing C composition ratio from 9 to 30%. The electrical resistivity of the BCN film decreases from $1x10^{12}$ to 3.4×10^{9} Ω-cm as the carbon content in the films increased from 9 to 30%. The activation energy varied from 0.52 to 0.36 eV with increased carbon content in the films [14]. Watanabe et al. researched the electrical properties of BC_2N thin films with respect to temperature and reported the dependence of resistivity and Hall Effect measurements. The

resistivity and Hall Effect measurements results indicated that BC_2N thin films are p-type semiconductors and the acceptor levels were between 7.5 and 23 meV. They also studied the dependency of type of substrate and found that the quality of thin film is better on Ni substrates than on quartz [121].

Yap et al. studied BCN films deposited by RF plasma-assisted pulsed laser deposition (PLD) system. They were able to change the composition of the BCN films by controlling the quantities of the carbon and BN plumes together with the help of in situ nitrogen ion bombardment. They obtained a film composition of BC_2N at a temperature of around 800^oC [132]. Dinescu et al. reported the growth of c-BCN thin films by reactive pulsed laser ablation (RPLA). They used a rotating target formed of two semi disks one of h-BN and other one of graphite and the deposition was done at room temperature. They observed crystalline BCN films with the formation of c-BCN, h-BCN and h-BN. The films were hard, adherent and transparent [133]. In yet another report, BCN films were deposited by radio frequency plasma enhanced chemical vapor deposition by Mannan et al. Tris- dimethylamino borane (TDMAB) was used as a precursor in this study and the deposition was done at different RF powers of 400-800W. They observed that the predominant hybrid configuration of sp^2-BCN films oriented in the direction perpendicular to the Si substrate [19]. In another work by same group of researchers, they used radio frequency and microwave plasma enhanced chemical vapor deposition to deposit BCN thin films. The micro-hardness values reported were approximately 2~7 GPa [134].

Pan et al. prepared BCN films by pulsed laser deposition from a sintered B_4C target. The films prepared were found to be smooth and adhered well to the substrate. They also observed that with the help of reactive nitrogen plasma they can incorporate more amounts of nitrogen in the films [135]. Other works reported on BCN films includes work done by Perrone et al.

whereby they deposit BCN thin films using sequential pulsed laser ablation of graphite and hexagonal boron nitride (h-BN) target. They films deposited were crystalline and the grain size was in the range of 30-80 nm and the micro hardness value reported was around 2.9 GPa [21]. Tsai deposited BCN thin films using cathodic arc plasma deposition (CAPD). He varied the amount of N_2 gas in the chamber and the bias levels on the substrate. The hardness of the films reported ranged within 1-3 GPa and the surface roughness of the films were high: RMS values being 25-60 nm [127].

Electron affinity and field emission characteristics of BCN films were reported by Kimura et al. The films were synthesized by plasma-assisted chemical vapor deposition. Carbon was observed to play an important role in the emission characteristics. The positive electron affinity was as low as 0.7eV for the BCN film with carbon composition of 29 %. The negative electron affinity was observed for h-BN which contains no carbon. It was also reported that the turn on electric field increases with carbon composition ratio [136].

We now report on some of the work reported on BCN films prepared by sputtering. One of the works includes work reported by Yue et al. where they prepared BCN films by RF reactive sputtering from a hexagonal h-BN target in an Ar-CH_4 discharge. They obtained different films with different carbon contents by varying the CH_4 partial pressure. Under optimum processing conditions they observed polycrystalline BC_2N and the calculated activation energy was approximately 0.8 eV [25]. Another work reported in the literature is work done by Liu et al. in which they prepared BCN films by RF magnetron sputtering using a composite target consisting of h-BN and graphite in an Ar-N_2 atmosphere. They studied the effect of sputtering power on the composition of BCN films and found that the films deposited at 80W and 130W are close to the BC_3N stoichiometry and the sample deposited at 110 W is close to the stoichiometry of BCN.

Lastly the samples deposited at 100W and 120W have the chemical composition of BC_2N. Thus they were able to achieve the BCN films with different compositions by varying the power to the composite target [137]. Similar work using composite target for sputtering was reported by Yokomichi et al. whereby they deposited BCN films by magnetron sputtering using a composite target consisting of boron-nitride pellets and a graphite target in N_2 and Ar gas atmosphere. They observed that the addition of boron atoms improved the aging effect such as peeling off the substrate and that the deposition rate is lesser when sputtered in pure Ar environment than compared when sputtered in pure N_2 gas ambient [138].

Martinez et al. researched the influence of the composition of BCN films on the properties of BCN films. The films used in this study were deposited by reactive magnetron sputtering using h-BN and graphite targets operated in RF and DC mode respectively. The nitrogen content in their films was constant at about 40 at. %. The emphasis was to study the composition of the film of the first tens of mono layers. They observed that first three to four mono layers were hexagonal-like structure and underneath this layer a disordered sp^3 bonded bulk was found [139]. Dual cathode magnetron sputtering was used to deposit BCN films by Kusano et al. and they sputtered from graphite and boron targets. They varied the power to the sputtering targets and concentration of nitrogen gas in the sputtering chamber. They observed the variation of deposition rate with reactive gas and the BCN films deposited at pure nitrogen exhibited a higher content of sp and sp^2 carbon and had lower durability in friction tests as compared to other BCN films [140].

Lousa et al. reported BCN thin films near B_4C composition deposited by radio frequency magnetron sputtering from a sintered B_4C target. The observed the increase in nitrogen incorporation in the films from 0 to 40 at. % while the relative atomic composition of B/C was

relatively constant at 4 thus the films structure changed from B_4C to a mixture of h-BN and amorphous carbon. Also, there was a variation in the values of stress and hardness with nitrogen variation and the optimum value was found to be N_2/Ar gas composition of 2% [33]. Same group of researchers characterized BCN films by their micromechanical and micro tribological behavior. They evaluated the adhesion and friction coefficient against diamond by micro scratch and also characterized their wear behavior at the nano metric scale. They found that the hardness is higher in the films with lower nitrogen concentration and the least hard films had nitrogen content of around 20 at. % [34].

Xu et al. investigated BCN films deposited at various N_2/Ar flow ratios by DC reactive magnetron sputtering of conductive B_4C target. They observed the increasing trend of nitrogen content in the films with respect to increasing N_2/Ar flow ratio and the nitrogen content saturated at higher N_2/Ar gas ratios. The maximum nitrogen content in their films was 33.1 at. % and was obtained at N_2/Ar of 30/100. The carbon content in the films decreased with increasing N_2/Ar ratio whereas boron content decreased initially at low N_2/Ar flow ratio and then increased with increasing N_2/Ar flow ratio [141].

Few other works reported in the literature are based on deposition of multilayer films. One such work was reported by Bejarano et al. and they made multi-layer films of B_4C/BCN/c-BN structures. The films were deposited by r. f. magnetron sputtering from h-BN and B_4C targets in an Ar/N_2 gas mixture. The main objective of this work was to improve the adhesion of the c-BN films via a multi-step process on silicon substrates coated with a B_4C layer and a subsequent B-C-N gradient layer as well as multi layers of these two components. They observed that the structural and mechanical properties of both coatings types was crucial to increase the hardness and adhesion of the cubic boron nitride film and that they were able to deposit thick and

stable c-BN films up to approximately 4642 nm on silicon substrates [26]. M. P. Johansson et al. reported growth of CN_x/BN: C multilayer films prepared by magnetron sputtering from C (graphite) and B_4C targets in an Ar/N_2 discharge. The substrate was held at 225^oC and at a negative floating potential of ~30V. The film thickness was 0.5 μm. The films obtained had the composition of $CN_{0.33}$ and BN: C with boron 35 at.%, nitrogen 50 at.% and carbon 15 at.% respectively. The CN_x/BN: C interfaces obtained were relatively smooth. Furthermore, the multiyear films were very elastic in nature with elastic recovery of 90% at 3 to 10 mN maximum load. Thus the authors concluded that the multilayer films showed improved system response and therefore were more suitable for mechanical design [142].

Another interesting work was reported by Morant et al. where they deposited coatings of BCN/CN/BN multilayer films on Si substrates using a double ion beam sputtering. They obtained the multilayers by sequentially sputtering from BN, C and B_4C targets and at the same time bombarding the films with low energy nitrogen ions. The hardness of the coatings, measured in the BCN/CN/BN multilayer was 23, 18 and 5 GPa, respectively. Also, the multilayers possessed higher wear resistance than measures separately [10].

2.5 Low Dielectric Constant (low- κ) Materials

2.5.1 Need for low-κ materials

The manufacturing technology and reliability for advanced interconnects is impacted by the choice of metallization and interlayer dielectric (ILD) materials. At the 130-nm technology node aluminum was replaced by copper as the interconnect metal and this required notable changes in the areas of integration, metallization and patterning technologies. The reliability performance of the interconnect system was directly impacted by these changes. Various

research efforts have been focused on the improvement in interconnect performance by utilizing lower dielectric constant (low- κ) ILD materials from one technology node to another.

Fig. 2.8 shows the various elements of a simple two-layer interconnect system in which the electrical signal is transmitted through the metal lines from one end of the chip to another and from metallization level to another through conductive vias. Interconnects are charge carriers made out of metal lines and are separated by an insulating layer dielectric (ILD). The capacitive coupling of the metal lines to the ILD produces the so called RC delay where R and C represents the effective resistance and capacitance of the interconnects, respectively.

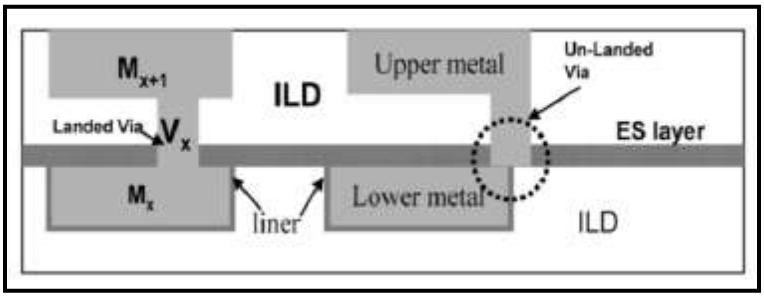

Figure 2. 8: Simple two-layer interconnect system (not to scale)

With the continuous scaling of the CMOS devices and for the dimensions below 0.5 μm, RC delay becomes dominant over the intrinsic gate delay in determining the overall circuit performance [143]. One way to improve the interconnect performance is to use repeaters which maintains the signal integrity and thus helps in circumventing the problem of overall chip delay.

The concept of RC delay can be explained by considering the case of a simple parallel plate capacitor. The RC delay is given by,

$$\mathrm{RC} = \varepsilon \left(\frac{\rho}{M}\right) \left(\frac{L^2}{S}\right)$$

where,

ρ = resistivity of the interconnect,
M = thickness of the interconnect,
L = length of the interconnect,
ε = permittivity of the ILD
S = thickness of the ILD

Thus, as seen from the above equation the RC delay can be reduced by reducing resistivity or length of the metal interconnects, increasing metal thickness, increasing ILD thickness or utilizing a lower permittivity ILD material. To meet the interconnect density targets, the number of metal layers increases and at the same time the dimension of the metal interconnects decreases and because of this we cannot achieve the improved performance by increasing the width and thickness of a metal line. Another way to reduce the RC delay is by using a more conductive metal and/or utilizing a low dielectric constant (low-κ) ILD material. Aluminum was replaced by copper in the 130-nm technology node which yielded an approximate 30% reduction in resistivity.

Table 2.4 shows comparison of properties for possible metal options for interconnects system. The possible options for metal include silver, copper and gold as low resistivity options. As seen from the table the other properties which influences the choice of metal includes corrosion resistance, thermal conductivity, adhesion characteristics to ILD, diffusion performance and manufacturability of both deposition and patterning processes. Silver possess the lowest resistivity but still cannot be utilized as a metal connect because it has extremely poor corrosion and adhesion performance. On the other hand, copper offers 2X reduction in resistivity than aluminum and is also integrateable in the semiconductor manufacturing environment.

Table 2. 4: Comparison of properties for possible metal options for an interconnect system.

	Aluminum	Copper	Silver	Gold
Resistivity (Ω-cm)	2.66	1.67	1.59	2.35
Thermal Conductivity (W/cm)	2.38	3.98	4.25	3.15
Corrosion Resistance in air	Good	Poor	Poor	Excellent
Adhesion to SiO_2	Good	Poor	Poor	Poor
Suitability for Semiconductor Processing				
Sputter deposition	OK	OK	OK	OK
Electroplating	OK	OK	OK	OK
Dry Etching	OK	NO	NO	NO
Wet Etching	OK	OK	OK	OK

There are several points to be noted as far as copper is considered which dictated the process technology strategy and integration scheme for interconnects utilizing copper metallization. Firstly, copper diffuses easily is silicon and silicon dioxide which may cause leakage problems. This required the need of a diffusion barrier that will encapsulate copper lines from all directions. Secondly, copper does not adhere well to the underlying ILD material and thus the surface of the copper needs to be pretreated to promote adhesion to both ILD and dielectric diffusion barrier. Thirdly, the difficulty associated with the dry etching of copper prohibited the continuation of subtractive etching used for patterning aluminum interconnects. This led to the introduction of the concept of dual damascene (DD) by which copper was poured into patterned trenches and vias within the ILD itself [144]. Moreover, in addition to DD patterning, copper electroplating and polishing technologies had to be introduced into the

manufacturing process. These techniques were used for filling the DD structures with copper and later removing the excess of copper by using a chemical-mechanical polishing (CMP) process. An example of the use of copper in high volume manufacturing of high performance microprocessors can be seen from the following Figure 2.9 which shows Intel's 130-nm and 90-nm technology.

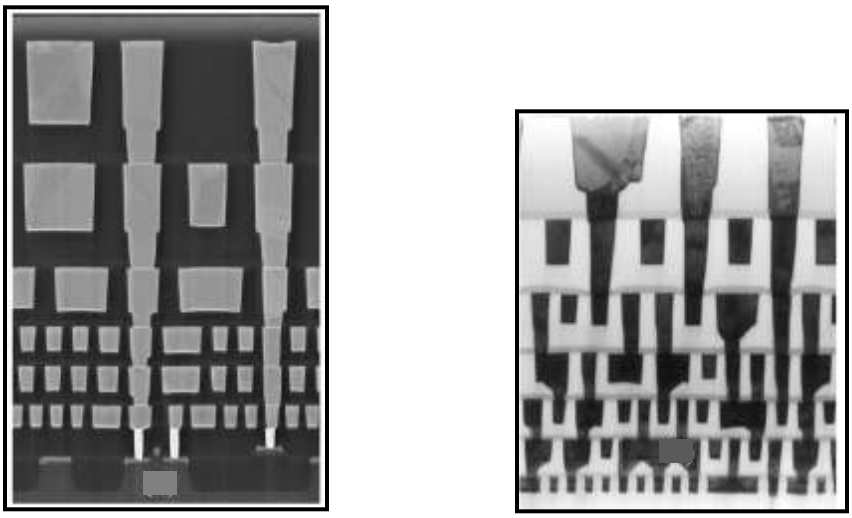

Figure 2. 9: Scanning electron microscope (SEM) images showing the cross section of Intel's 130 nm and 90 nm logic technology.

Another way to improve the interconnect performance is to use a low-κ ILD. Using low-k ILD has its own impact on the process technology for copper low- κ interconnects. Figure 2.10 shows the industry's inability to predict a practical target for the ILD dielectric constant for the future technology nodes [145]. It can be seen that in year 2000 the prediction was made to use ILD with κ as low as 1.5 for the 45-nm technology node and lower but the industry never followed the predicted curve and moved to the adoption of a higher κ material over the next years until the present time. Since the introduction of copper in late 1990s, the semiconductor industry is obsessed with finding low- κ ILD materials.

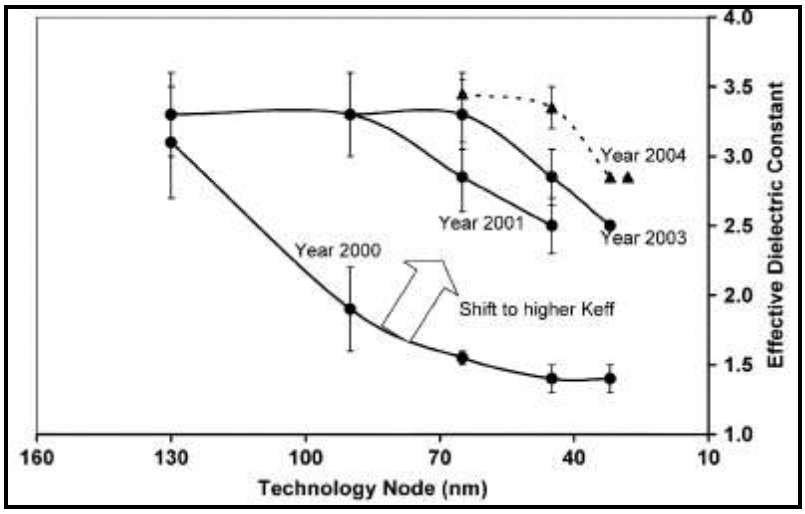

Figure 2. 10: ITRS trend of minimum K_{eff} with technology node.

However, the main technology limiter was not the ability to develop low- κ ILD materials but rather two fundamentally difficult problems associated with this category of materials. Firstly, is the inherent weak mechanical strength of low- κ ILD which seriously limits the ability to package chips made with such ILDs. Moreover, the lower the dielectric constant, the weaker the ILD gets as shown in Fig 2.11. The second problem is the degradation of the dielectric constant of the low-κ materials during processing. Typical processing steps used in the CMOS technology includes photo resist removal, dry and wet etch and metal cleans. All these steps extract carbon from the materials and render them to a higher dielectric constant.

An added benefit of switching to new low dielectric constant dielectrics is that low- κ dielectrics reduces the power required to operate transistors in an ultra-large scale integration (ULSI) integration scheme. The required drive power scales as CV^2, where C is the capacitance of the circuit and V is the drive voltage. A notable point here is that this benefit is not obtained by merely replacing aluminum with copper.

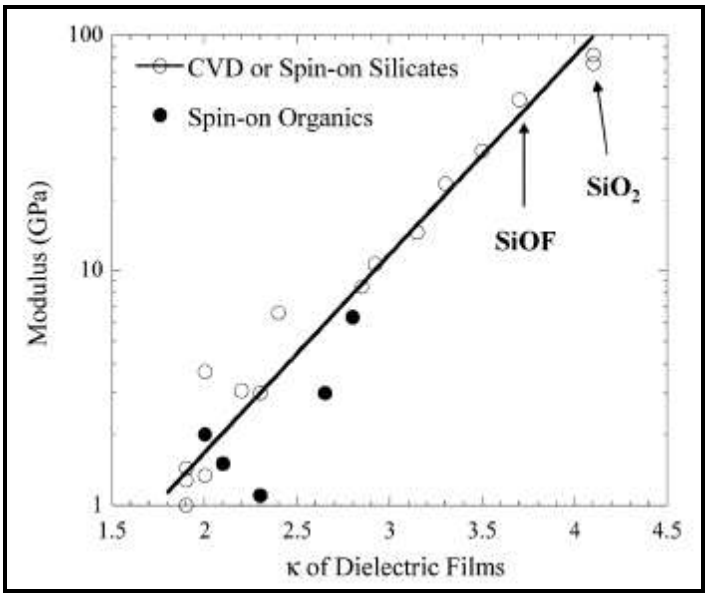

Figure 2. 11: Relationship between the dielectric constant and mechanical strength, as represented by modulus of a representative ILD material.

Figure 2.12 shows the drive power per gate and time delay for three interconnect technologies. For comparison purposes, if a 1 Volt design rule is assumed, it is very clear that we can achieve more benefits by replacing the ILD as compared to benefits achieved by replacing the interconnect metal. Replacing the ILD leads to larger reductions both in time delay and drive power. One more advantage of using low- κ ILD is that as the density of the interconnect lines increases; there is greater cross-talk between one line to another which can be reduced by switching to a low- κ ILD.

While the existence of a low dielectric constant is a critical requirement for any new low κ dielectric material, it is far being the only requirement. It is equally important that the new material be chemically stable and compatible with Si microelectronics processing. In a typical device fabrication facility, the list of approved elements only includes H, B, C, N, O, F, Al, Si, P, Ti, As, W and possibly, Co, Cu and Ta. The development of a new low- κ material containing

any other elements than those described above might face a serious challenge for meeting approval.

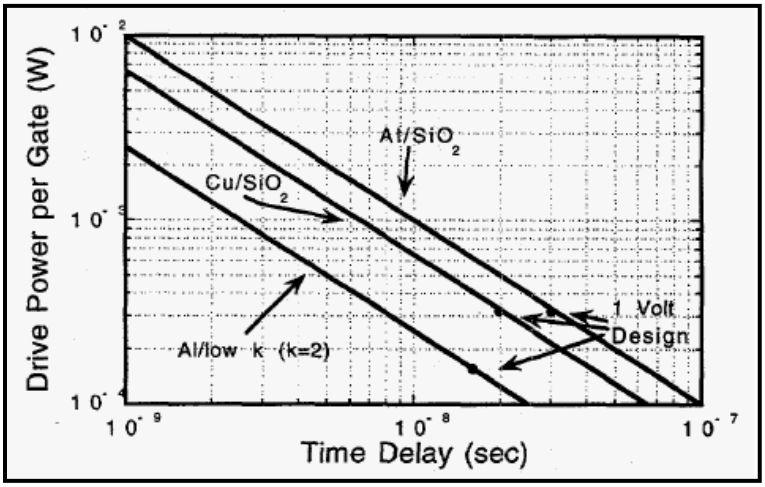

Figure 2. 12: Comparison of drive power per gate and time delay for three interconnects technologies.

The list of the requirements of the low- κ material is as given below;

1) Dielectric constant < 3.0
2) Chemical compatibility with Si
3) Highly insulating
4) Good thermal stability (up to 400^{o}C)
5) High resistance to environmental degradation
6) Low hydrogen/moisture content
7) Compatibility with planarization, lithographic and etching processes
8) Low diffusivity for metallic impurities
9) High breakdown voltage
10) Low dissipation factor
11) Compositional uniformity
12) Low void/crack/defect density
13) Low compressive stress
14) Conformal deposition

15) Good adhesion
16) Low deposition temperature
17) Thickness uniformity over large areas
18) Low particle density
19) High elastic modulus
20) Low shrinkage
21) Low thermal expansion

2.5.2 Amorphous carbon and Boron Nitride

Insulators formed from first row elements are good candidates for low permittivity dielectrics, with their bulk dielectric constants in the range of 5 to 8. Few examples of such insulators include BeO, cubic BN (c-BN) and diamond. Out of these insulating films of carbon and BN are more promising as they are very compatible with the Si processing. Most of the literatures reported have concentrated on chemical vapor or plasma-enhanced chemical vapor deposition (CVD or PECVD) which leads to insulating diamond-like carbon, DLC and films of predominantly hexagonal BN (h-BN). The reported values of dielectric constant for these materials range less than or approaching that of SiO_2 [146-155].

Despite of the fact that these films show low dielectric constant, they cannot be used as inter level dielectrics due to thermal or environmental degradation. It is reported in the literature that at temperatures above 300^{o}C, hydrogen comes out of the DLC resulting in the transformation of C-C:H sp^3 bonds to C-C sp^2 bonds [156]. This degrades the property of the insulating films and renders them unsuitable as an inter-level dielectric. On the other hand, h-BN films are hygroscopic which means these films deteriorate under conditions of high humidity. To overcome these deficiencies, one can deposit insulating carbon films free of hydrogen, called amorphous tetrahedrally-coordinated carbon (a-tC) and by depositing cubic BN (c-BN) films. a-

tC films are stable at temperatures up to 800^{o}C in inert ambient while c-BN is known to be environmentally stable bulk ceramic [157]

Table 2. 5: Reported dielectric constants for DLC and BN films.

Film	Dielectric Constant	Deposition	Ref.
DLC	3.9	PECVD	146
DLC	4.2	PECVD	147
DLC	4.5	PECVD	148
DLC	< 4	PECVD	149
h-BN	4.0 - 4.7	PECVD	150
h-BN	2.2 - 4.41	PECVD	151
h-BN	2.9	PECVD	152
h-BN	2.9 - 4.3	PECVD	153
h-BN	3.3 - 3.5	CVD	154
h-BN	3.7	CVD	155

We now provide an overview of one of the work reported by J. P. Sullivan from Sandia National Laboratories [158]. They characterized the a-tC and BN films with respect to dielectric constant.

Evaluation of a-tC

The amorphous-tetra carbon (a-tC) films were deposited using PLD in high vacuum (10^{-8} – 10^{-7} Torr) with a KrF laser and a rotating graphite target. The energy density of the laser light was focused onto the rotating graphite target and was adjusted between 5 to 48 J/cm^{2}. The deposition was performed at the room temperature with no subsequent annealing.

For dielectric characterization, the a-tC films were deposited on heavily doped (~0.01Ω-cm) n and p-type Si substrates. Square and circular Ti-Au or Al contacts were made to the dielectric films either by photolithography and lift-off or by metal evaporation through a shadow mask. Diode sizes defined lithographically ranged from 50 μm to 400 μm while those defined by shadow mask ranged from ~127 μm to 1270 μm. Back side contacts were made to the p-type wafers by an In-Ga eutectic alloy and to the n-type wafers by heat diffused Sb, followed by the In-Ga eutectic. Typical thickness for the a-tC was 1000A^{o}. They measured the film thicknesses by profilometer and confirmed the same by ellipsometer and transmission electron microscopy. Current-voltage (IV) and Capacitance-voltage (CV) characterization were performed on the metal-insulator-metal (MIM) and metal-insulator-semiconductor (MIS) diodes.

The dielectric characteristics of a-tC films depend greatly on the deposition conditions, particularly the laser energy density impinging on the graphite target. The measured resistivities from MIM diodes for a-tC films are shown in the figure . At the smallest diode sizes there is a monotonic decrease in resistivity with decreasing laser energy density. Films deposited at 45 J/cm^2 in 10 mTorr ambient of H_2 and N_2 showed resistivities > 10^6 Ω-cm and less than 100 Ω-cm respectively.

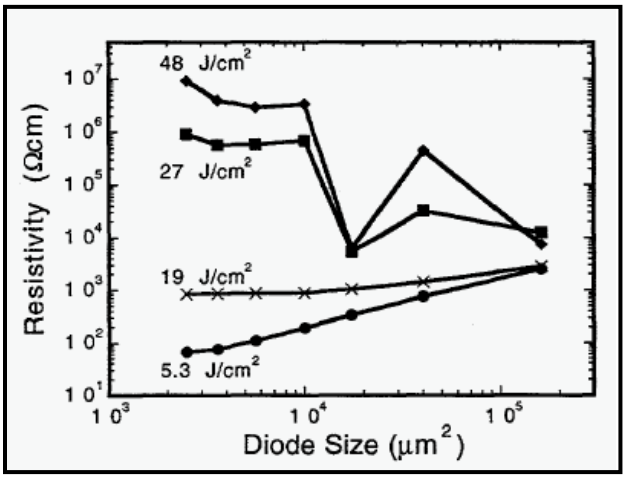

Figure 2. 13: Median resistivities of a-tC films measured from MIM structures [158]

Sheet resistance measurements performed for the 48 J/cm^2 and 19 J/cm^2 a-tC films on insulating substrates uniformly show high resistivities, > 10^6 Ω-cm, suggesting that the resistivity drop at larger diode sizes and the low resistivities in the samples deposited at low energy density are due to low resistivity shorts between the top and bottom electrodes in the film.

They measured dielectric constant of a-tC films, from MIM structures as a function of laser energy density and the results obtained are shown in figure . The result from the samples grown in 10 mTorr H_2 is also shown. As seen from the results, the samples deposited in vacuum the dielectric constant were independent of laser energy density and was within the range of 5 to 8. Also, the sample deposited at 10 mTorr H_2 exhibited a dielectric constant exceeding 8.

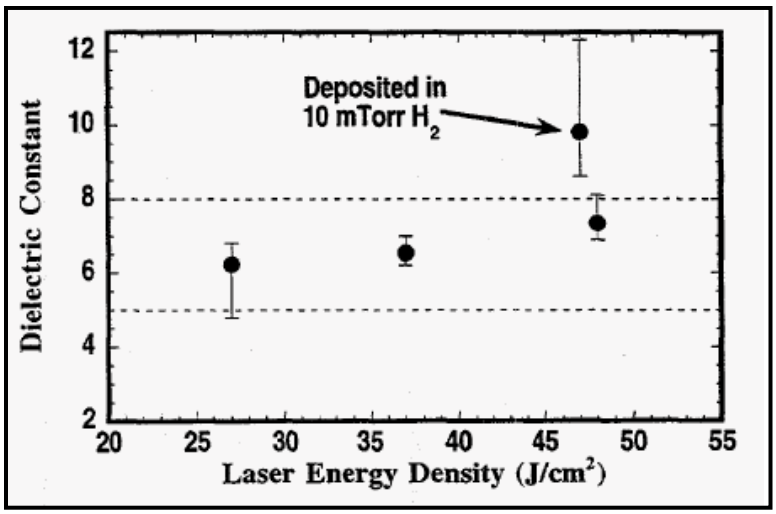

Figure 2. 14: Measured dielectric constants for a-tC films deposited in vacuum and hydrogen as a function of laser energy density [158].

Evaluation of BN

The c-BN and h-BN films deposited by PLD were found to be highly resistive, with resistivities approaching 10^{14} Ω-cm. Figure shows a histogram of the dielectric constant measured from MIS diodes with PLD c-BN and h-BN films and ECR deposited h-BN films. They observed that the c-BN possessed highest dielectric constant of around 7.5 and the PLD

deposited h-BN samples had dielectric constant values clustered at 5.5. The ECR deposited h-BN had dielectric constant values less than 4.0. They observed difference values of dielectric constant on different regions of a sample deposited by ECR. This variation was not well understood by them and they speculated the reason could be differences in film density or non-stoichiometry in the films near the edge of the wafer.

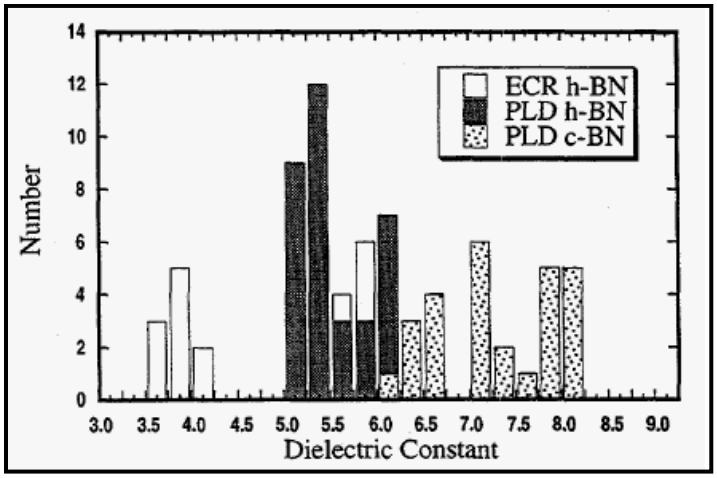

Figure 2. 15: Histogram of measured dielectric constants of BN films [158].

Table 2.6 summarizes the average dielectric constant measured for the PLD a-tC and BN films and ECR BN films along with the dielectric constant of bulk diamond and BN. The dielectric constants for the PLD films are both higher than the PECVD films and are almost comparable to the bulk values. This difference was attributed to the density difference of the films obtained by these two methods where low film densities results in low values of dielectric constant. When the films are deposited by non CVD like techniques the results films are dense, bulk-like densities and the observed dielectric constant obtained are bulk-like. The enhanced film density improved the film resistance to thermal and environmental degradation.

Table 2. 6: Measured dielectric constants of a-tC and BN films [158].

Material	Dielectric Constant
a-tC	~6.5
Bulk Diamond	5.7
PLD c-BN	6.5-8.0
Bulk c-BN	7.1
PLD h-BN	5.0-6.0
ECR h-BN #1	~3.75
ECR h-BN #2	~5.75
Bulk h-BN	~5.7

CHAPTER 3: METHODOLOGY

In this chapter, the experimental procedures and techniques used to fabricate and characterize the BCN based thin films and devices are reported. This chapter also outlines various materials and electrical characterization techniques used to study the thin film samples. The chapter is broadly divided into four main sub-sections; one explaining the actual film processing method and then moving on to the various characterization methods and the specific analytical techniques that were applied in each case.

3.1 Thin film deposition

Sputter deposition technique was used to obtain thin film samples. Sputter deposition is a physical vapor deposition PVD method of depositing thin films by eroding, material from a source, which then deposits onto a substrate. One advantage of sputtering as a deposition technique is that the deposited films have the same composition as the source material. The similarity of the film and target stoichiometry is due to the fact that the sputter yield depends on the atomic weight of the atoms in the target. Magnetron sputtering was used to utilize strong electric and magnetic fields to trap electrons close to the surface of the target. Insulating targets can cause charge build up hence varied biasing of the anode and cathode was obtained with a radio frequency (rf) power source. Sputter deposition sources (also called sputter “guns”) creates low pressure plasma by the excitation of an inert gas (typically argon) contained at 1 to 30 millitorr in a vacuum chamber. This process extracts energetic ions which accelerate toward the cathode target, striking it with kinetic energy up to several hundred electron volts. Energy transfer then ejects material from the target with approximately 90% leaving as neutral atoms and 10% as ions. Gas phase collisions between target atoms and argon atoms scatter the ejected

material into a distributed cloud. As the cloud migrates towards the substrate, the random approach angles result in deposition of a uniform film, even on surfaces that have micron-sized vertical structures.

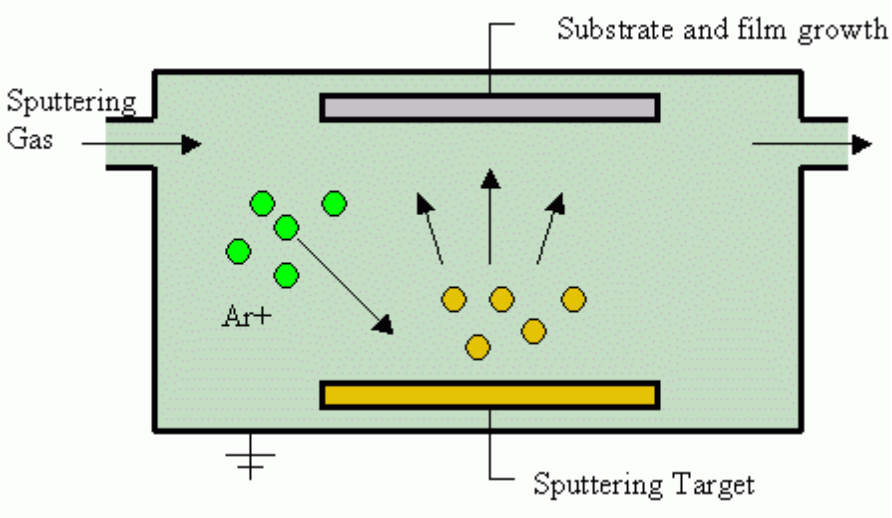

Figure 3. 1: Sputtering Process Cartoon

Thin films of BCN were deposited by reactive RF magnetron sputtering in a UHV system. Three inch, powder pressed, B_4C target with a purity of 99.5% was used. The system base pressure was approximately 1×10^{-8} Torr and the purity of the process gas was maintained by a hot reactive metal getter. Process gas contamination in the deposition chamber at the typical deposition pressure of 4 mTorr was confirmed to be less than 10 ppm (the instrumental sensitivity limit) by closed ion source quadrapole mass spectrometry. Reactive sputtering was used where the deposited film is formed by chemical reaction between the target material and a gas which is introduced into the vacuum chamber. Oxide and nitride films are fabricated using this technique. The composition of the film is controlled by changing relative flow of inert and reactive gases. In this case nitrogen was used as the reactive gas and, the N_2 to Ar ratio was

varied from 0 to 1, in steps of 0.25 by changing the individual gas flow rate, while total gas flow was kept constant at 20 sccm and a constant deposition pressure of 4 mTorr.

3.2. Material Characterization

Material characterization is an essential part of thin film analysis. Several characterization techniques are involved that can give us information ranging from surface morphology and roughness of the sample to chemical nature and bonding structure of the material. Appropriate tools used in correlation with observed properties can help correlate properties in turn explaining some uniquely observed phenomena in the material. High temperature oxidation kinetics of the BCN films was investigated. The films were oxidized in a programmable box furnace from room temperature to 700 ºC. Oxygen as well as air was used to study effect of oxidation ambient on film characteristics. Analysis of the films before and after anneal can reveal more information about the high temperature behavior of the BCN material.

3.2.1. Surface Morphology

Surface roughness of the thin films is an important factor in determining their reliability. Degradation in film properties occurs when the thickness is reduced to the point that the surface roughness of the film becomes comparable the film thickness. When the root mean square (RMS) roughness of the film exceeds 20% relative to the film thickness then thin spots in the film can start to dominate the thin film properties. The surface profile of the deposited films was measured using a VEECO NT3300 Optical profilometer. The NT3300 is a non-contact surface profiler which was used to measure the thickness and surface roughness of the sputtered dielectric and metal films. This profilometer uses two different technologies to measure a wide variety of surface heights. Phase shifting interferometry (PSI) is reliable for smooth surfaces and small steps in which the height change between two adjacent points is not more than 160 nm.

The vertical resolution for PSI mode is 3Å for a single measurement and 1Å for multiple averaged measurements. Vertical scanning interferometry (VSI) allows measurement of rough surface profiles and steps up to few millimeters high. The vertical resolution is 3nm for a single measurement and <1nm for averaged multiple measurements. The average roughness and peak to valley roughness was measured for oxygen annealed BCN thin films. Average roughness (RBaB) represents the two dimensional roughness averages, the arithmetic mean of the absolute values of the surface departures from the mean plane.

$$R_a = \frac{1}{MN} \sum_{j=1}^{M} \sum_{i=1}^{N} \left| Z_{ji} \right|$$

where, M and N are the number of data points in the X and Y direction, respectively of the array, and Z is the surface height relative to the surface reference mean plane.

3.2.2. X-ray Photoelectron Spectroscopy

In X-ray photoelectron spectroscopy (XPS), also called electron spectroscopy for chemical analysis (ESCA), X-rays excite photoelectrons, and the emitted electron signal is plotted as a spectrum of binding energies. Differing chemical states resulting from compound formation are reflected in the photoelectron peak positions and shapes. Spectral information is collected from a depth of 2-20 atomic layers, depending on the material studied (Schroeder, 1998) [35]. The energy of the photoelectrons leaving the sample is determined using a chemical analyzer (Concentric hemispherical analyzer-CHA) and this gives a spectrum with a series of photoelectron peaks. The binding energy of the peaks is characteristic of each element. The peak areas can be used (with appropriate sensitivity factors) to determine the composition of the materials surface. The shape of each peak and the binding energy can be slightly altered by the

chemical state of the emitting atom. Hence XPS can provide chemical bonding information as well.

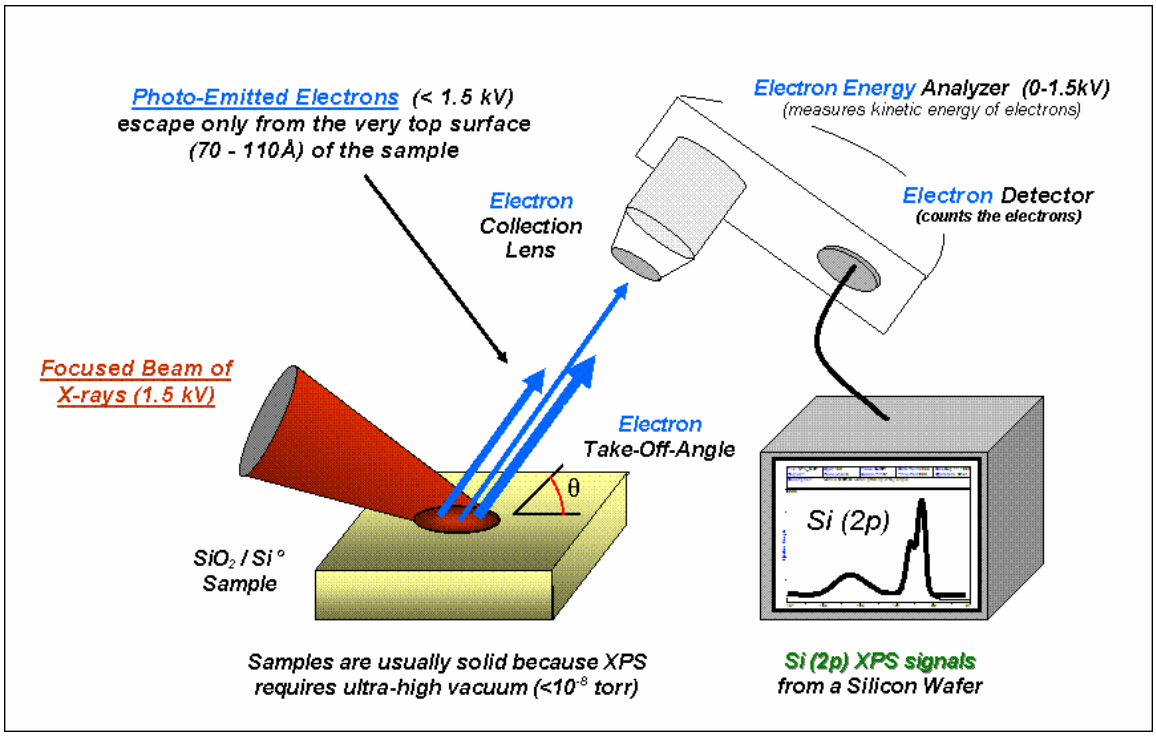

Figure 3. 2: Schematic Representation of a XPS System

XPS was performed using a PHI 5400 ESCA system. The base pressure during analysis was 10^{-9} Torr and Mg K-α X-ray source (hν= 1253.6 eV) at a power of 350 watts was used for the analysis, samples were transferred in a sealed petri-dish to the XPS analysis chamber. Although care was taken to minimize the exposure time in air, the atmospheric exposure could not be completely avoided.

Both the survey and the high-resolution narrow spectra were recorded with electron pass energy of 44.75 eV and 35.75 eV, respectively, to achieve the maximum spectral resolution. Any charging shift produced by the samples was carefully removed by using a B.E. scale referred toC (1s) B.E. of the hydrocarbon part of the adventitious carbon line at 284.6 eV [159]. Non-linear

least square curve fitting was performed using a Gaussian/Lorentzian peak shape after the background removal.

3.2.3. Secondary Ion Mass Spectroscopy

Secondary ion mass spectroscopy (SIMS) is a technique for the characterization of solid surfaces and thin films. It uses the process of ion formation by bombarding the surface to be tested with a highly collimated beam of primary ions. The surface then emits material through a sputtering process - only a fraction of these emitted particles is ionized. These secondary ions are measured with a mass spectrometer to determine the quantitative elemental, isotopic or molecular composition of the surface.

The SIMS technique requires high vacuum to ensure undisturbed movement of secondary ions to the detector. The primary ion beam used (often Cs^{+}, O^{2-}, Ga^{+} or Bi clusters like Bi_3^{2-}) determines the detection limits of the instrument. Two surface analysis modes are static and dynamic. Static SIMS is the process involved in surface atomic monolayer analysis, usually with a pulsed ion beam and a time of flight mass spectrometer, while Dynamic SIMS is the process involved in bulk analysis, closely related to the sputtering process, using a DC primary ion beam and a magnetic sector or quadrupole mass spectrometer.

SIMS analysis was performed using a PHI Adept 1010 Dynamic quadrupole SIMS system capable of depth resolution up to 1nm. A cesium (Cs^{+}) ion source operated at 3 kV and 25nA was used so that oxygen detection can be possible. For depth profile the depth scale was quantified by measuring the analysis craters with a stylus profilometer.

3.3 Optical Characterization

Optical properties of thin films can be very informative about the application prospects as electronic devices. Wavelengths from ultra violet (UV) through the visible and infrared to the

millimeter range have enormous power to examine all aspects of solids, especially semiconductors such as; crystal lattice, the electronic band structure and bang gap. Characteristics such as optical transmission, absorption, reflectance and band gap studies are considered. Samples for optical transmission were deposited on quartz substrates.

3.3.1. UV-Visible Spectroscopy

The instrument used in ultraviolet-visible spectroscopy is called a UV/Vis spectrophotometer. It measures the intensity of light passing through a sample (I), and compares it to the intensity of light before it passes through the sample (Io). The ratio I / Io is called the transmittance, (see Figure 3.3) and is usually expressed as a percentage (%T). The absorbance, A, is based on the transmittance:

$$A = -\log (\%T) \qquad [1]$$

The basic parts of a spectrophotometer are a light source (often an incandescent bulb for the visible wavelengths, or a deuterium arc lamp in the ultraviolet), a holder for the sample, a diffraction grating or mono chromator to separate the different wavelengths of light, and a detector. The detector is typically a photodiode or a CCD. Photodiodes are used with monochromators, which filter the light so that only light of a single wavelength reaches the detector. Diffraction gratings are used with CCDs, which collects light of different wavelengths on different pixels.

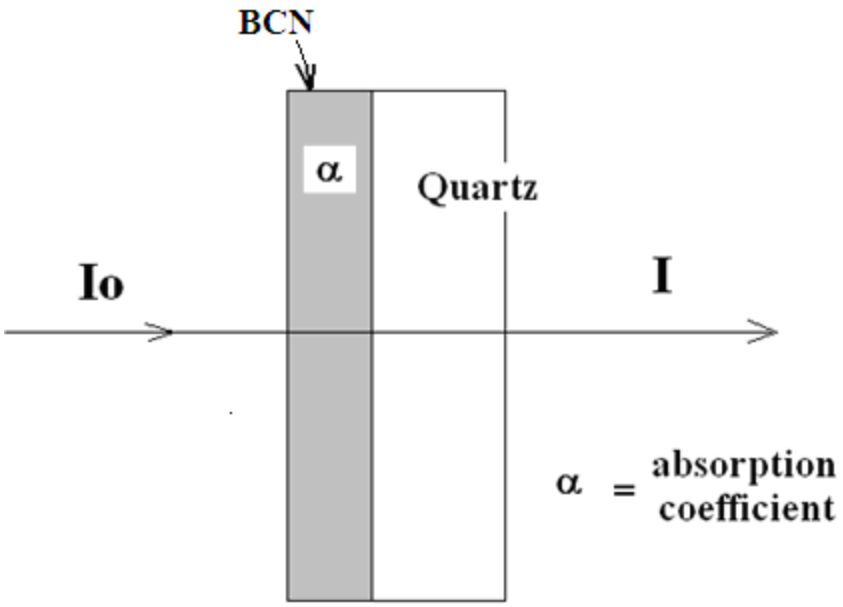

Figure 3. 3: Schematic of Transmission Measurement using UV-VIS Spectroscopy

A Cary 5E high resolution spectrophotometer was used to study the optical characteristics of the thin film samples. This is a double beam instrument controlled by a microprocessor and has a measurement range of 3150 -185 nm. The ratio of transmitted light to that of incident light (*%T*) and absorption data were collected and base line correction (obtained using blank substrate) was applied prior to collection of spectral data.

3.4: Electrical Characterization

Capacitance-Voltage (C-V) testing was performed on MIS devices fabricated with BCN as an insulator. The accumulation region capacitance was measured from the C-V plots and from the accumulation region capacitance the dielectric constant (κ-value) of the BCN films were calculated. The resistivity was measured from Metal-Insulator-Metal (MIM) structures with Ta as the top and bottom electrodes and BCN as the insulating layer.

3.4.1 Fabrication of MIS devices

MIS stands for Metal-Insulator-Semiconductor devices. The p-type silicon wafer with <100> orientation and resistivity of 50 Ω-cm^2 was used as the substrate and which acts as a semiconductor for the MIS devices. The substrate was subjected to standard cleaning procedure which includes rinsing with acetone, methanol and DI water. The wafer was then dipped in HF acid to remove any native oxide on the surface of the wafer. The substrate was then rinsed thoroughly with DI water and loaded immediately in to the sputtering chamber for subsequent BCN deposition. It is important to make sure there is no surface oxide before depositing the insulating film. The surface oxide if present will add an additional capacitance which will jeopardize the accuracy of the C-V measurements.

BCN film was then sputter deposited on top of the silicon substrate. The reactive sputtering from a 3 inch B_4C target was used to deposit BCN films. The base pressure of the chamber was in the range of 7 x 10^{-8} Torr. The ratio of N_2/Ar gas flow was varied in the steps of 0.25 whereas the total flow in the sputtering chamber was kept constant at 20 sccm. The R.F power to the B_4C target was kept constant at 200 Watts. All the depositions were done at 5m Torr. The deposition time was 2 hours and the thickness of the BCN film was measured by step profilometer. The BCN thicknesses ranged from 250-300 nm. The samples were deposited at room temperature and also at 300^{o}C and 500^{o}C. The temperature of the substrate was measured by a thermocouple attached to the substrate. The temperature was measured in steady state condition.

Lastly, aluminum dots were deposited on the BCN layer to form the top layer of the MIS structures. Aluminum was evaporated using an evaporation chamber which was evacuated to a base pressure of 2 x 10^{-5} Torr. Shadow masks with circular dots of 3mm in diameter were used

for aluminum deposition. The thickness of aluminum was about 130nm. Figure 3.4 shows a picture of the fabricated MIS structures.

Figure 3. 4: Actual Fabricated MIS structures.

Annealing of the MOS structures was carried out in a programmable box furnace. The samples were kept on the quartz plate which was loaded into the furnace. The box furnace was then flushed with high purity argon gas for about 2 hours. This is to eliminate any effect of oxidation while annealing. At the end of 2 hours argon flushing the furnace was then programmed. The temperature was set at 400^{o}C with the ramping rate of 10^{o}C/minute. The flow of argon was 100 sccm which was measured on the flow meter. The samples were annealed at 400^{o}C for 20 minutes and at the end of 20 minutes the samples were allowed to cool down to room temperature. The samples were then taken out from the box furnace.

3.4.2 Fabrication of MIM Structures

Metal-Insulator-Metal (MIM) structures were fabricated for the I-V measurements. Resistivity data was then calculated from the slope of the I-V curve. Aluminum was chosen as the top and bottom metal electrodes because it is very easy to evaporate aluminum. Firstly, we started with depositing strips of aluminum on the glass substrates using a mechanical mask. This

will serve as bottom electrode. Aluminum was evaporated in the evaporation chamber evacuated in the range of 10^{-5} Torr. Current was passed through the filament to melt the aluminum and at certain amperage aluminum evaporated to deposit on the glass substrates. Next we deposit BCN films to serve as an insulator layer. BCN film was sputter deposited using reactive sputtering from a B_4C target in the gas mixture of argon and nitrogen. The thickness of the BCN film ranged from 160 nm-180 nm and was measured using a alpha step profilometer. Lastly, aluminum was evaporated to form the top electrodes in the same manner as bottom electrodes using the mechanical mask. This time the strips of aluminum were deposited perpendicular to the strips of aluminum deposited as bottom electrodes. Figure 3.4 shows a snap shot of such a fabricated Metal-Insulator-Metal (MIM) structure using aluminum as metal electrodes and BCN as insulating layer.

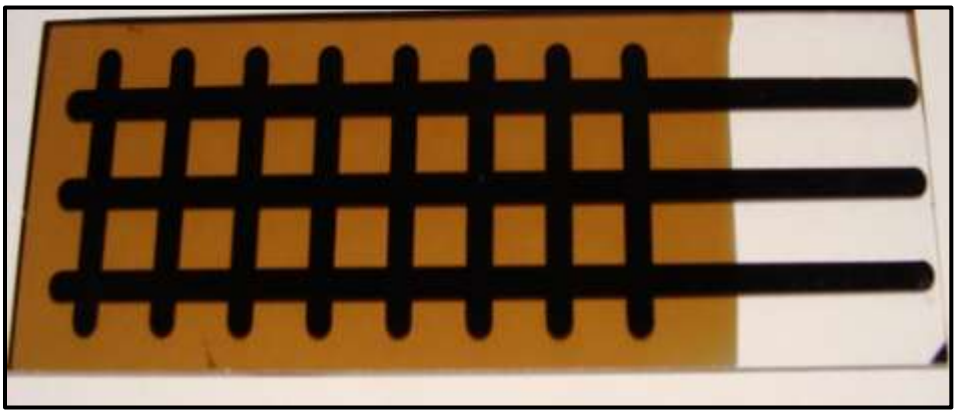

Figure 3. 5: Fabricated MIM (Al-BCN-Al) structure for electrical testing.

3.4.3 Capacitance-Voltage (CV) Testing

Capacitance-voltage (C-V) testing is widely used to determine semiconductor parameters, particularly in MOSCAP and MOSFET structures. However, other types of semiconductor devices and technologies can also be characterized with C-V measurements, including bipolar

junction transistors (BJTs), JFETs, III-V compound devices, photovoltaic cells, MEMs devices, organic TFT displays, photodiodes, carbon nanotubes (CNTs), and many others.

The fundamental nature of these measurements makes them useful in a wide range of applications and disciplines. They are used in the research labs of universities and semiconductor manufacturers to evaluate new materials, processes, devices, and circuits. C-V measurements are extremely important to product and yield enhancement engineers, who are responsible for improving processes and device performance. Reliability engineers use these measurements to qualify material suppliers, monitor process parameters, and analyze failure mechanisms. With appropriate methodologies, instrumentation, and software, a multitude of semiconductor device and material parameters can be derived. This information is used all along the production chain beginning with evaluation of epitaxially grown crystals, including parameters such as average doping concentration, doping profiles, and carrier lifetimes. In wafer processes, C-V measurements can reveal oxide thickness, oxide charges, mobile ions (contamination), and interface trap density. These measurements continue to be used after other process steps, such as lithography, etching, cleaning, dielectric and polysilicon depositions, and metallization. After devices are fully fabricated on the wafer, C-V is used to characterize threshold voltages and other parameters during reliability and basic device testing and to model the performance of these devices.

A MOSCAP structure is a fundamental device formed during semiconductor fabrication (see Figure 3.6). Although these devices may be used in actual circuits, they are typically integrated into fabrication processes as a test structure. Since they are simple structures and their fabrication is easy to control, they are a convenient way to evaluate the underlying processes.

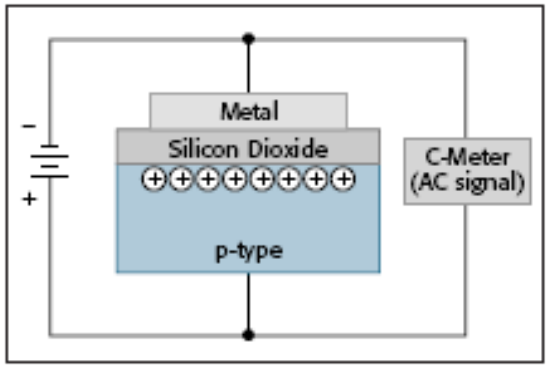

Figure 3. 6: C-V Measurement circuit for a MOSCAP structure on a p-type substrate.

The metal/polysilicon layer shown in Fig. 3.6 is one plate of the capacitor, and silicon dioxide is the insulator. Since the substrate below the insulating layer is a semiconducting material, it is not by itself the other plate of the capacitor. In effect, the majority charge carriers become the other plate. Physically, capacitance, *C*, is determined from the variables in the following equation:

$$C = A\,(\kappa/d),$$

Where,

A is the area of the capacitor,
κ is the dielectric constant of the insulator, and
d is the separation of the two plates.

Therefore, the larger *A* and κ are, and the thinner the insulator is, the higher the capacitance will be. Typically, semiconductor capacitance values range from nanofarads to picofarads, or smaller.

The procedure for taking C-V measurements involves the application of DC bias voltages across the capacitor while making the measurements with an AC signal. Commonly, AC frequencies from about 10kHz to 10MHz are used for these measurements. The bias is applied as

a DC voltage sweep that drives the MOSCAP structure from its accumulation region into the depletion region, and then into inversion.

CHAPTER 4: RESULTS AND DISCUSSION

4.1 Characteristics of sputtered BCN thin films

4.1.1 Deposition Rate

Figure 4.1 shows the deposition rate of BCN films as a function of N_2/Ar gas flow ratio during sputtering. It is observed that the deposition rate initially increases to 7.5 Å/min when the N_2/Ar ratio increases up from zero to 0.5. Further increase in N_2/Ar ratio causes the deposition rate to reduce to ~6.5Å/min. This trend can be attributed to the nitridation of the target during sputtering processes. Initially, with low nitrogen flow the boron and carbon sputtered from the target forms a layer of BCN on the substrate and the thickness of this layer increases with the increased nitrogen incorporation for the gas phase.

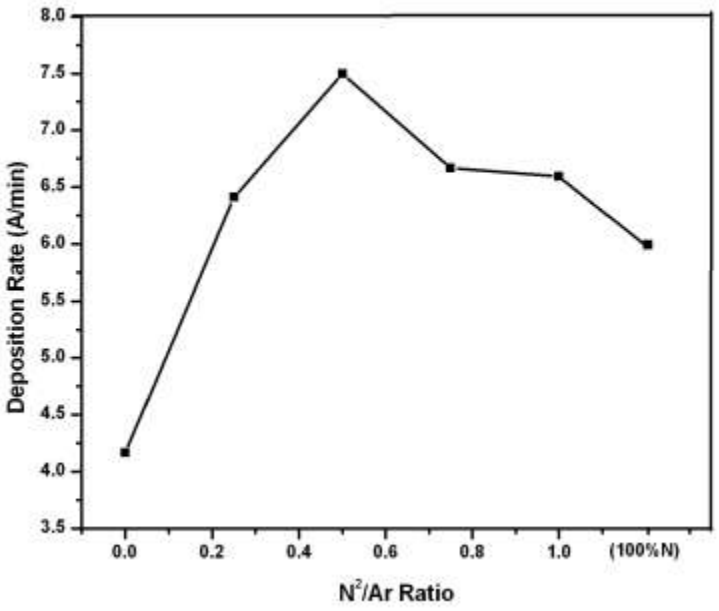

Figure 4. 1: Deposition rate v/s N_2/Ar gas flow ratio.

During this period the rate of formation of a BCN layer of the target surface is less than the removal rate by argon ions thereby maintaining a constant sputtering rate of boron and carbon. As the nitrogen ratio is increased above 0.5, the removal rate drops below the rate of formation, resulting in the formation of a stable BCN layer in the target surface and a reduced overall deposition rate on the substrate. Moreover, when the sputtering was performed in pure nitrogen ambient, a further decrease in deposition rate to 5.8 Å/min was observed.

4.1.2 Chemical composition

The elemental compositions of the films were obtained from XPS surface scans. The relative atomic concentrations of boron, carbon, and nitrogen are shown in Table 4.1

Table 4. 1: Relative surface atomic concentrations of boron carbon and nitrogen as a function of N_2/Ar flow ratios from XPS data.

N_2/Ar Ratio	**Boron atomic concentration (%)**	**Carbon atomic concentration (%)**	**Nitrogen atomic concentration (%)**
0	62	38	0
0.25	29	38.35	32.65
0.50	30.3	33.7	36
0.75	29.5	31.5	39
	29	30	41
100% N_2	30.5	29.5	40

Once nitrogen is introduced at the 0.25 N_2/Ar flow ratio, the carbon content in the films steadily decreases as the N_2/Ar ratio further increases. This carbon loss is understood as the replacement of C with N in the amorphous carbonitride network. The relative amount of boron in

the films drops dramatically with the introduction of nitrogen, then remains fairly constant for the BCN films at all N_2/Ar ratios. As expected, the nitrogen content initially increases for the BCN films with the N_2/Ar flow ratio reaching ~40% for nitrogen flow ratios of 0.75 and higher. The XPS measurements were done ex-situ, wherein the surface was exposed to reaction with atmospheric oxygen and thus the surface of the films was sputtered clean before each XPS survey scan to make sure that the surface is free from any oxygen contamination.

High resolution XPS scans were obtained to analyze the chemical nature of the films. Fig. 4.2 shows the raw data and deconvolved peaks from the high-resolution scans of the C 1s peak. The broad and asymmetric raw data peak indicates that more than one type of bonding is present for C 1s state. The deconvolved peak at 284.6 eV is attributed to adventitious carbon. [159].The peaks located at 286-286.9 eV are attributed to the presence of C-N bonds [24, 31]. The peaks located at 288-288.5 eV are primarily due to the presence of C-O contamination bonds [160].

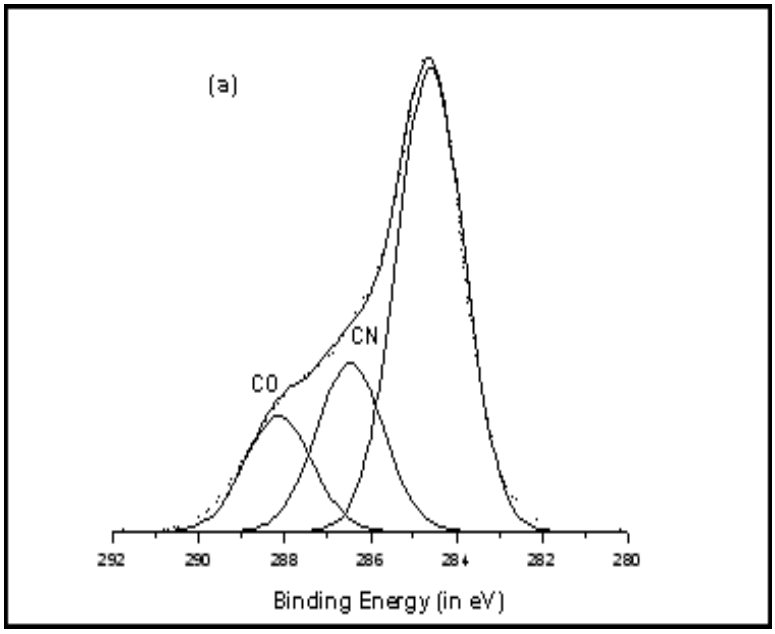

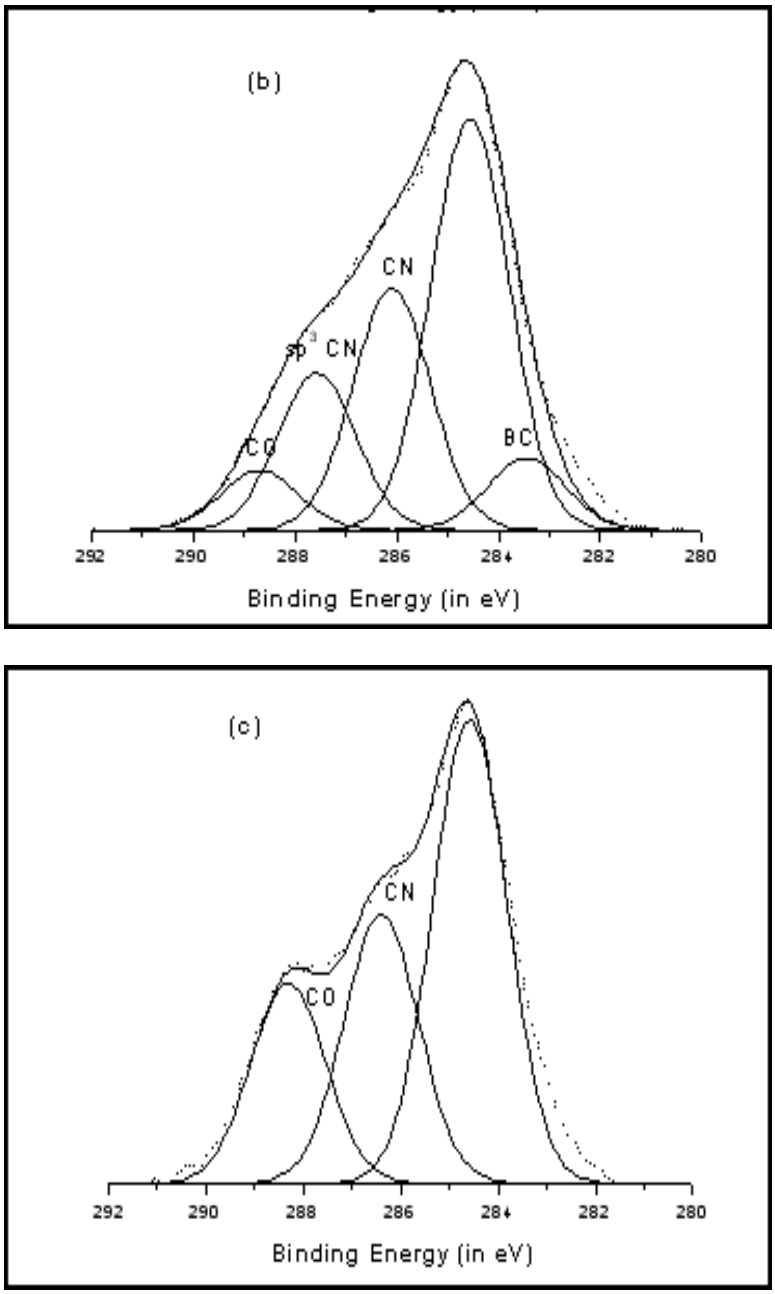

Figure 4. 2: XPS C 1s spectra for sputter deposited BCN films as a function of N2/Ar ratio (a) 0.25 (b) 1 and (c) pure N_2 ambient

Figure 4.3 shows the deconvoluted N 1s spectra for the films deposited with N_2/Ar ratios of 0.25, 1 and 100% N_2 respectively. This peak indicates the presence of N in several bonding states. The deconvolved peak found between 397-397.5 eV can be attributed to hexagonal B-N

bonding [161, 162], and is evident in all BCN samples, suggesting that nitrogen binds well with boron. This peak varies little with the N_2/Ar gas flow ratio. A second peak between 399-399.5 eV is due to sp^2 N-C bonding (N bonded to sp^2-hybridized C) [163, 164]. The small peak at 400-400.5 eV can be assigned to N-C bonding [165, 166]. Thus we see N-C bonds appear in several states. Moreover, the intensity of CN bond peak decreases with the increase in N_2/Ar ratio.

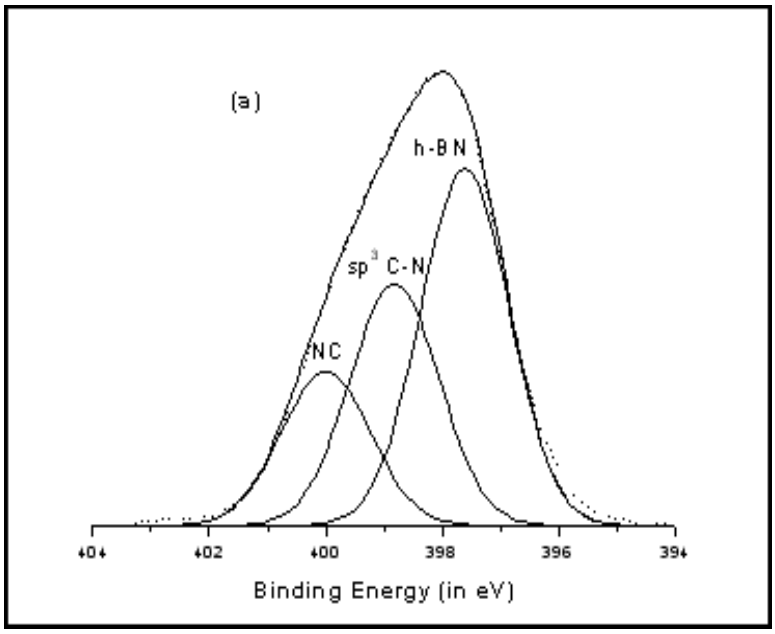

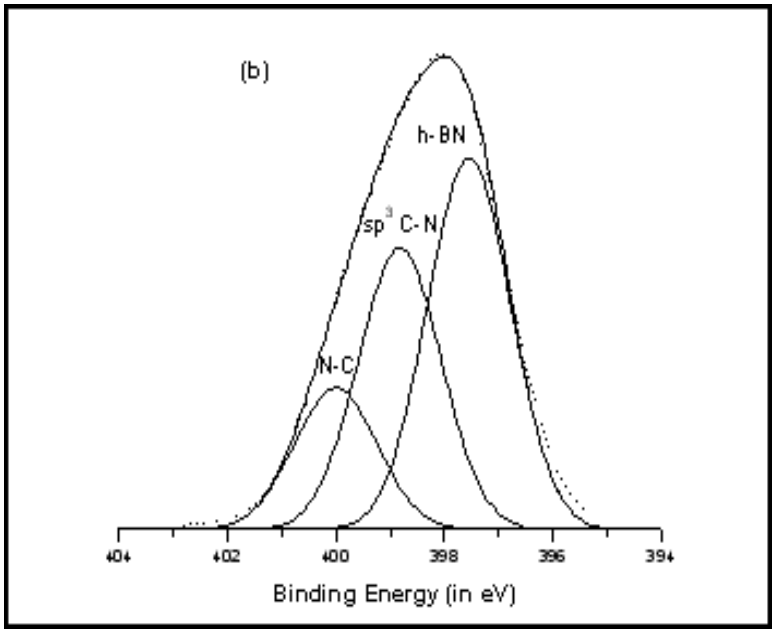

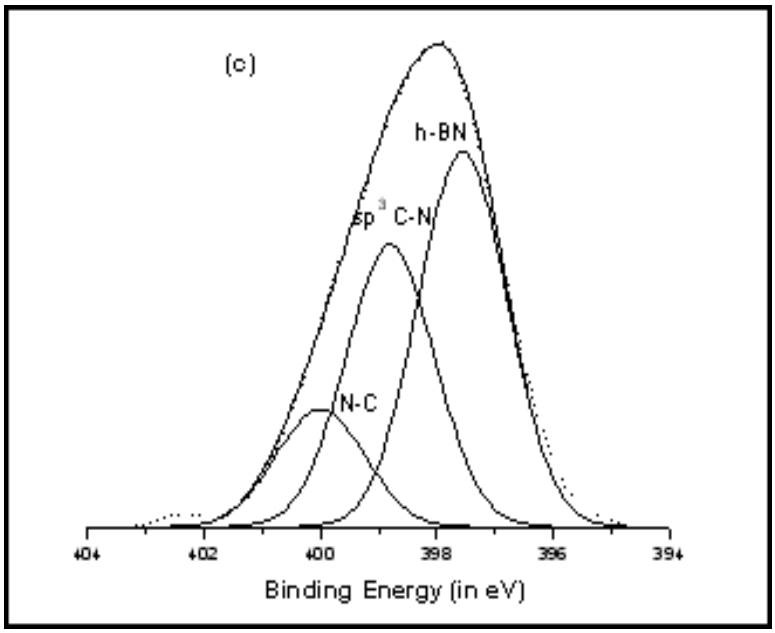

Figure 4. 3: XPS N 1s spectra for sputter deposited BCN films as a function of N_2/Ar ratio.

The deconvolved peak for boron (Fig. 4.4) also shows multiple peaks combining to form the observed intensity. It was reported that the B1s binding energy for the B-N bond in hexagonal BN is the range of 190-191 eV [167, 168]. Thus, the major portion of the deconvoluted area which is at a peak centered at 190.5 eV can be ascribed to hexagonal B-N bonding. This suggests that the B atoms in the BCN films are bonded to N in the chemical environment similar to the sp^2 B-N bonds in hexagonal BN. The peak at 189.4-189.8 eV is attributed to B-C bonds. Kunzli et al. suggested that the B-C binding energy in a boron carbide compound with lower carbon concentration ($BC_{3.4}$) experiences a shift towards a higher value of 189.6, compared to that of 188.4 eV in those with higher carbon concentration (BC_4) [169]. The peak at 192 eV is considered to correspond to B-O bonds due to the high reactivity between B and O [170] which results from the surface contamination.

Thus, from the XPS measurements it can be concluded that the bonding in the BCN films is complex and includes a variety of sp^2-BCN atomic hybrid configurations. The prominent and

distinctive hexagonal B-N peak indicates that boron binds more preferably to nitrogen than to carbon. This is consistent with the increase in nitrogen content observed.

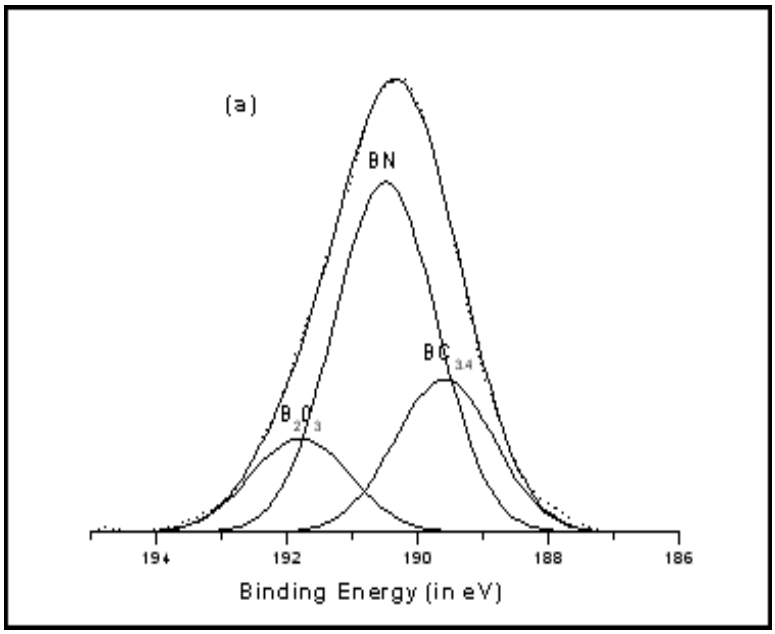

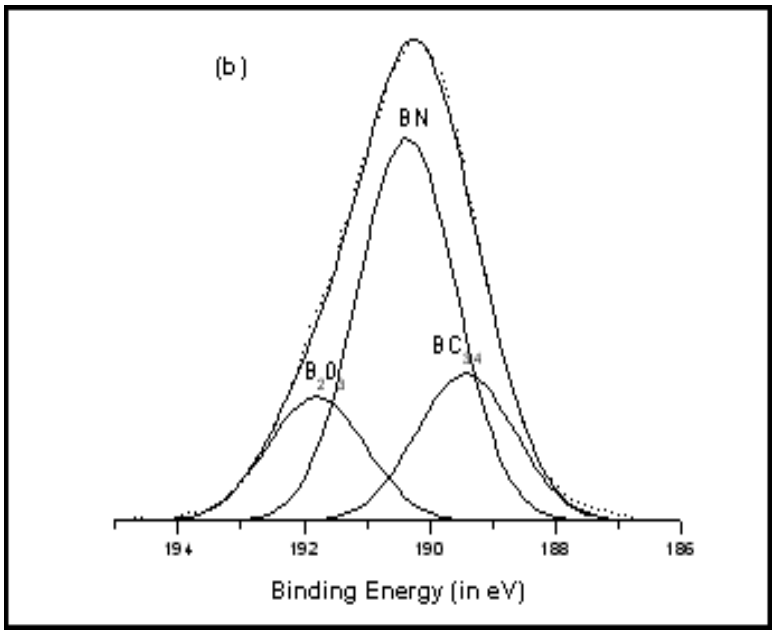

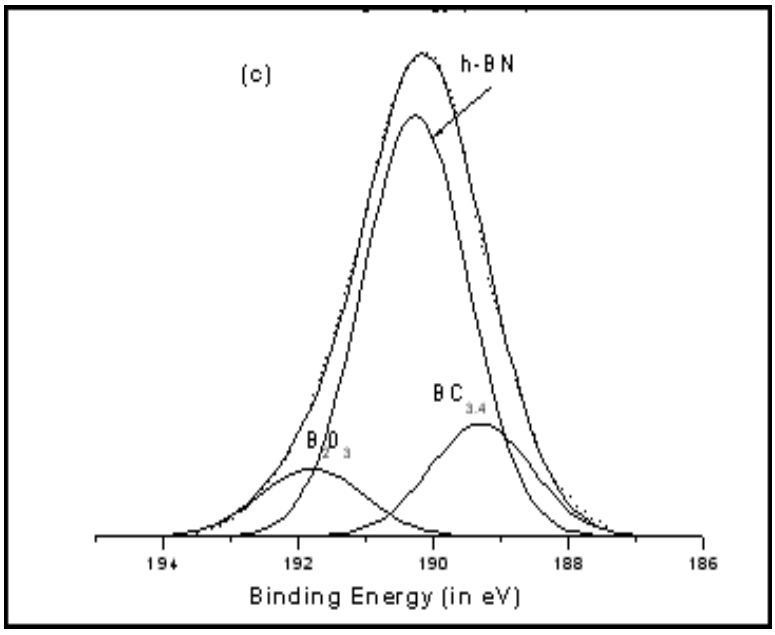

Figure 4. 4: XPS B 1s spectra for sputter deposited BCN films as a function of N_2/Ar ratio

Figure 4.5 shows a plot of the average roughness of the sputtered samples at different N_2/Ar gas ratios. The roughness of the films increases with N_2 flow ratio during sputtering clearly indicating that the N_2 concentration in the ambient also affects the surface morphology of the deposited film. Surface morphology of the films also shows that the films deposited at lower N_2 rates have fewer voids than the ones deposited at higher N_2 rates. Since the films are formed by a reactive sputter process higher concentration of N_2 in the sputtering ambient could cause additional ion bombardment of the films surface during deposition and lead to increased surface roughness.

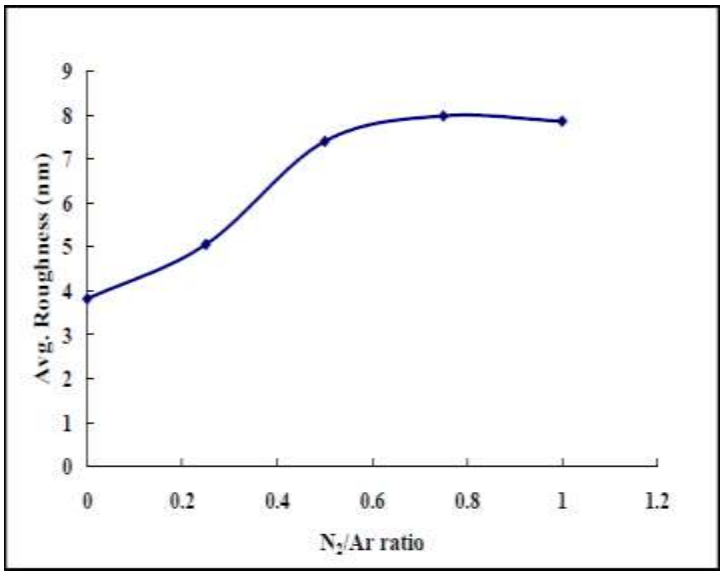

Figure 4. 5: Variation of average surface roughness as a function of N_2/Ar flow ratios for sputter deposited BCN films.

4.1.3 SIMS depth profiling

Figure 4.6 how the SIMS scans for the BCN thin films deposited at N_2 gas flow ration of 0.25. It can be observed that there exists a very uniform distribution of the three elements B, C and N in the film, suggesting that the film is quite homogeneous. Also, the SIMS analysis clearly distinguishes two regions of BCN samples. The first region is the actual BCN films on the surface and the second region is the thermally grown SiO_2 oxide layer. It can also be observed that the film is very low on oxygen content.

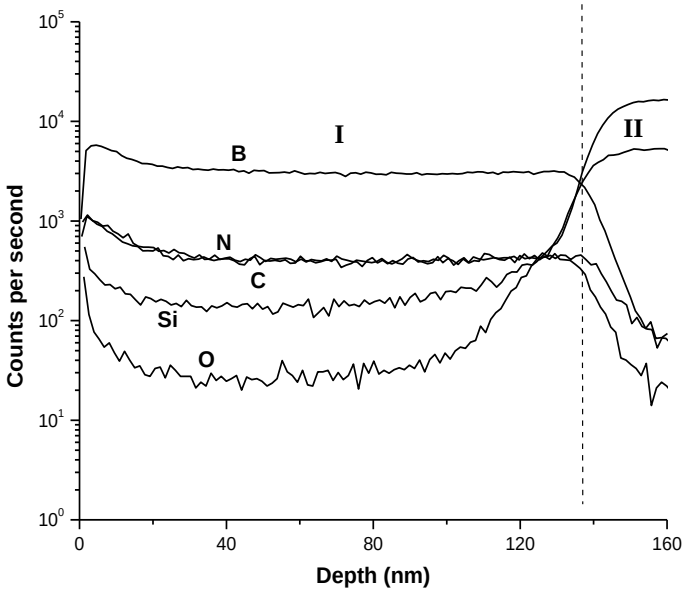

Figure 4. 6: SIMS profile for the sample deposited at N_2/Ar ratio of 0.25. Region I shows the BCN films on the surface and region II shows the SiO_2 layer

4.2 High temperature oxidation studies

Initial analysis of the sputtered films has revealed that nitrogen flow rate change in the sputtering chamber also affects the film surface characteristics. Roughness of the films increases with higher N_2 flow rates and could be due to increased ion activity in the chamber at these flow rates. Characterization of the sputtered films under high temperature conditions is also essential to understand potential for applications under such conditions. We now consider annealing the thin film samples at various incremental temperatures under oxygen ambient to accelerate the degradation (oxidation) of the film. Table 4.2 shows the samples studied and temperatures as well as labeling convention used.

Table 4. 2: Sample labeling and Temperature Annealing Matrix

N_2/Ar Gas Flow Ratio	Annealing Temperature (^oC)			
	room	300	500	700
0	x	x	x	x
0.25	x	x	x	x
0.5	x	x	x	x
0.75	x	x	x	x
1	x	x	x	x

4.2.1. Chemical analysis through XPS

Surface atomic composition was obtained from XPS scans and the normalized atomic concentrations of carbon and nitrogen detected are shown in Figure 4.7. It can be observed that the carbon concentration decreases steadily with increasing temperatures with almost a linear trend. The nitrogen concentration also follows a similar trend but at a more rapid rate and almost no nitrogen was detected in the films beyond 700°C anneal. The boron concentration decreased as the annealing temperature was increased but the decrease in boron was not that extreme. As seen there were still around 6 at. % of boron content lefts in the films annealed at 700^{o}C. The oxygen content showed an increasing trend with respect to annealing temperatures which is very obvious as it means rapid oxidation of the films with higher annealing temperatures.

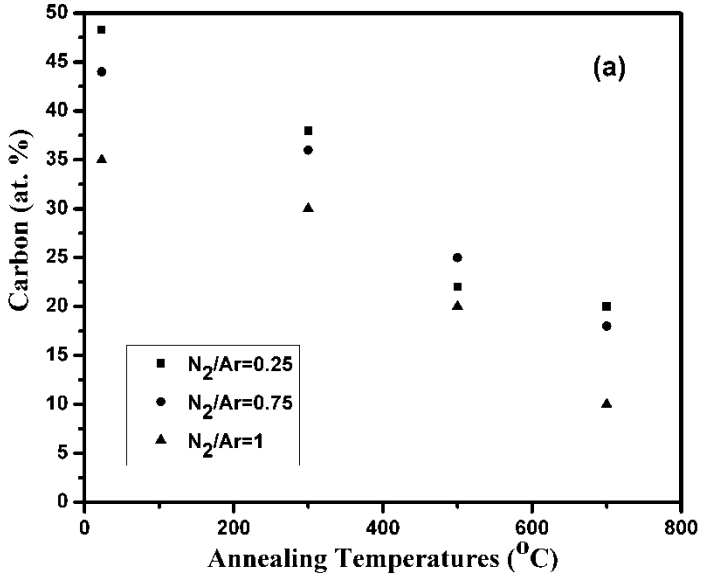
(a)
Carbon (at. %)
Annealing Temperatures (°C)
N2/Ar=0.25
N2/Ar=0.75
N2/Ar=1
0
5
10
15
20
25
30
35
40
45
50
0
200
400
600
800

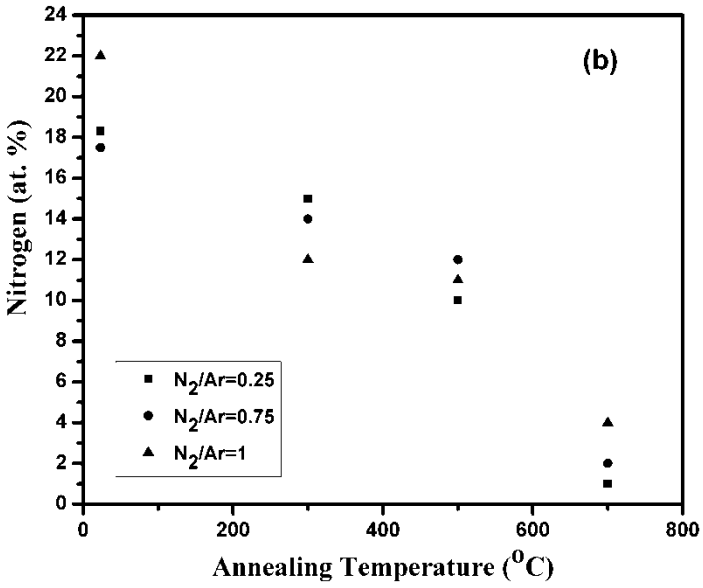
(b)
Nitrogen (at. %)
Annealing Temperature (°C)
N2/Ar=0.25
N2/Ar=0.75
N2/Ar=1
0
2
4
6
8
10
12
14
16
18
20
22
24
0
200
400
600
800

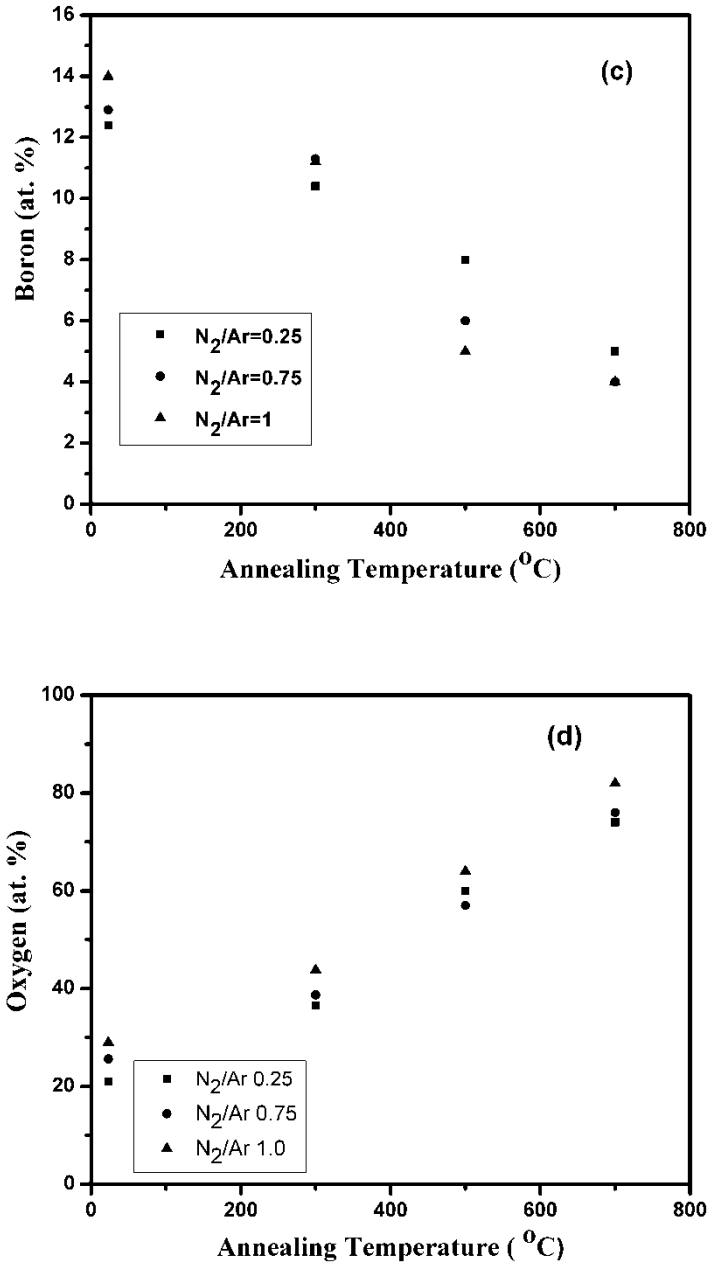

Figure 4. 7: Surface atomic concentration calculated from XPS peaks of (a) C, (b) N, (c) B and (d) O for different N2/Ar deposition ratios and annealing temperatures.

High resolution XPS scans were obtained to analyze the chemical nature of the BCN films. Fig. 4.8 shows the deconvolved high resolution carbon (C 1s) spectral data for as deposited and films annealed after 500°C and 700°C respectively. The broad envelope of the

peaks clearly indicates the presence of different C 1s states. The deconvolved peak at 284.6 eV is attributed to adventitious carbon. [159].The peaks located at 286-286.9 eV are attributed to the presence of C-N bonds [24, 31]. The peaks located at 288-288.5 eV are primarily due to the presence of C-O contamination bonds [160]. It can be observed that the C-N peak intensity decreases after the annealing process and there is no C-N peak in the sample annealed at 700^{o}C. This implies that there is a loss of carbon and nitrogen in the films. The C-N bonds break due to annealing, leaving nitrogen free to escape as gas and the carbon would combine with oxygen to form CO or CO_2 and escape as gas during annealing.

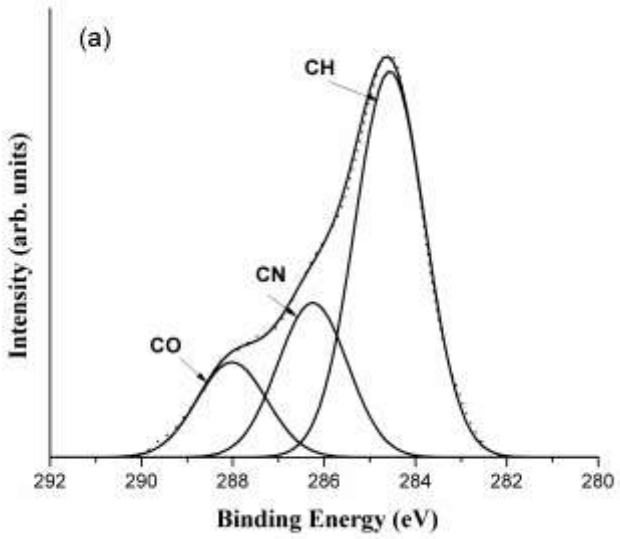

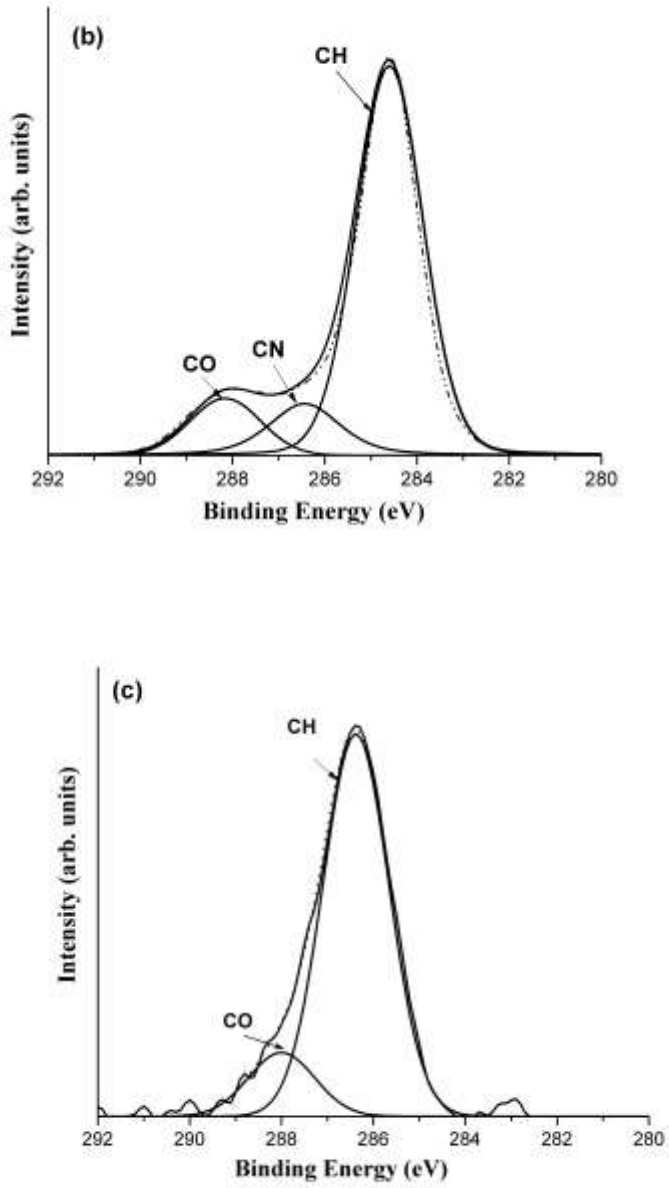

Figure 4. 8: XPS C 1s spectra for BCN films deposited at 1 N_2/Ar at different anneal temperatures (a) un-annealed, (b) 500^{o}C and (c) 700^{o}C

Fig. 4.9 shows the deconvolved high resolution Nitrogen (N 1s) spectral data for as deposited as well as films annealed at 500^{o}C and 700^{o}C. This peak indicates the presence of N in several bonding states. The deconvolved peak found between 397-397.5 eV can be attributed to hexagonal B-N bonding [161, 162] and is evident in all BCN samples, suggesting that nitrogen

binds well with boron. A second peak between 399-399.5 eV is due to sp^2 N-C bonding (N bonded to sp^2-hybridized C) [163, 164]. The peak between 400.5-401 eV can be attributed to the presence of some surface contamination in the form of N-O bonds. It can be seen that the sp^2 N-C peak decreases with annealing at higher temperatures. This also confirms the loss of carbon and nitrogen in the films at higher annealing temperatures.

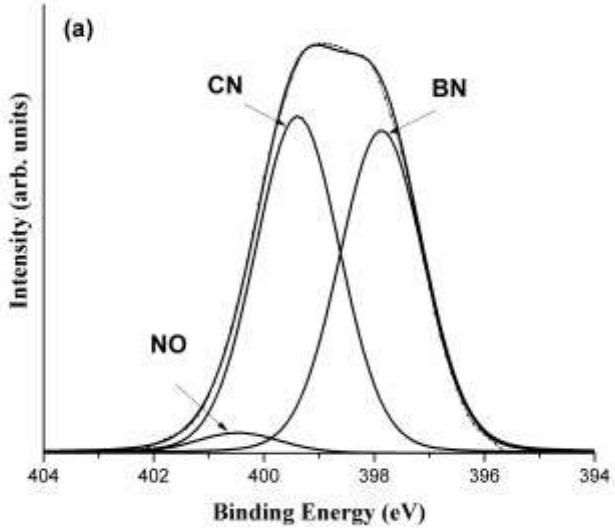

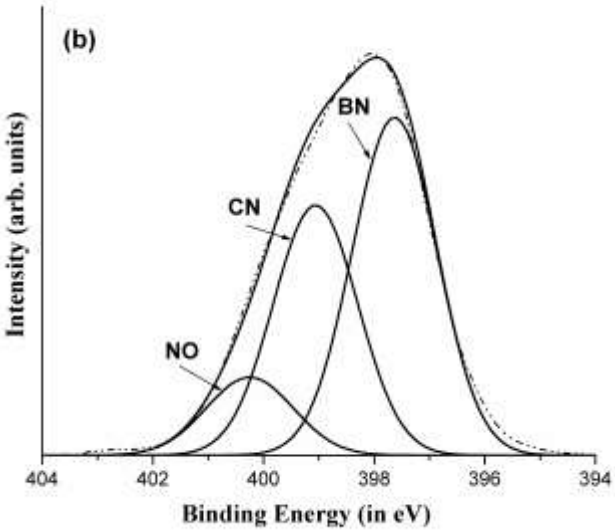

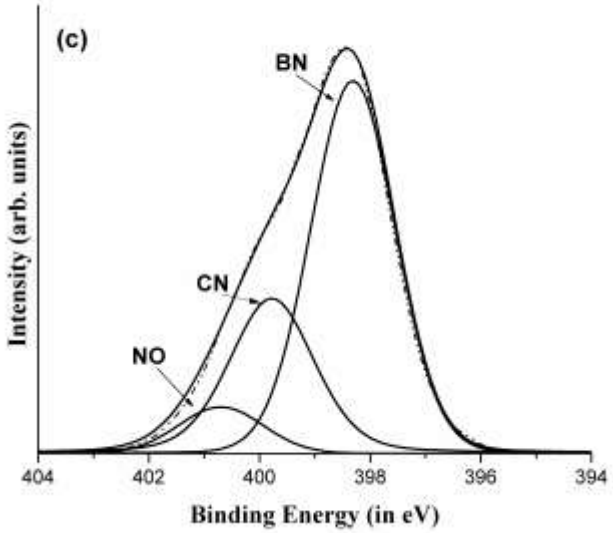

Figure 4. 9: XPS N 1s spectra for BCN films deposited at 1 N_2/Ar at different anneal temperatures (a) un-annealed, (b) 500^{o}C and (c) 700^{o}C

Fig. 4.10 shows deconvolved high resolution Boron (B 1s) spectral data for as deposited and films annealed at 500^{o}C and 700^{o}C. For un-annealed sample, the peak at 190.5eV is a clear indication of a BN peak [167, 168]. The peak at 189.5 eV can be attributed to the BC bonding [169]. Finally, the peak at 192 eV is due to B_2O_3 bonding [170]. It can be seen that the intensity of BN and BC peaks decreased with annealing temperatures. At the same time the intensity of B_2O_3 peak increased significantly with annealing temperature indicating the presence of boron oxide phases in the films. At 700^{o}C, boron reaction with oxygen is maximum and the film predominantly consists of B_2O_3 phases. It is also observed that the BC peak completely vanished after annealing at 700^{o}C indicating the complete oxidation of BC phases in the film. Dang Li et. al. reported B_2O_3 as an insulator with band gaps in the range of 6.20 eV- 8.85 eV [171].

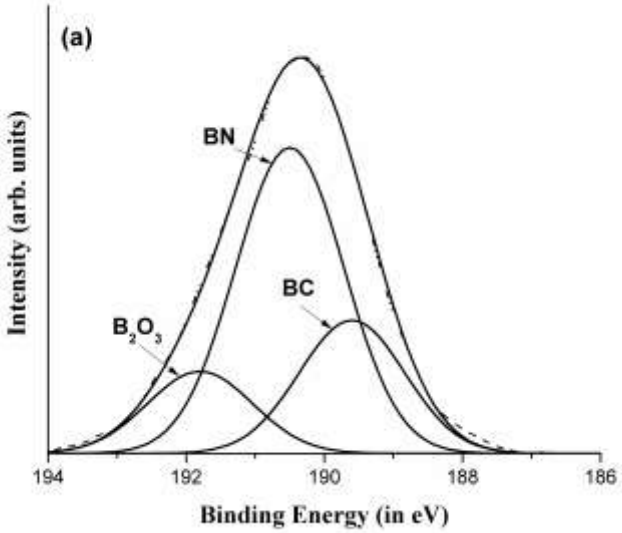
(a)
BN
BC
B_2O_3
Intensity (arb. units)
194
192
190
188
186
Binding Energy (in eV)

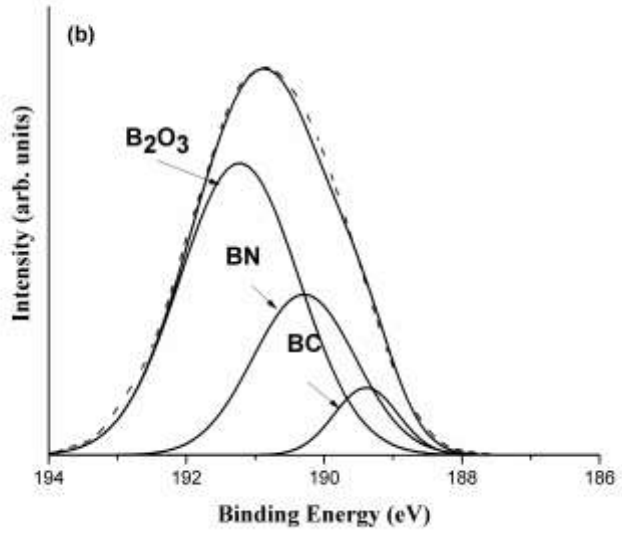
(b)
B_2O_3
BN
BC
Intensity (arb. units)
194
192
190
188
186
Binding Energy (eV)

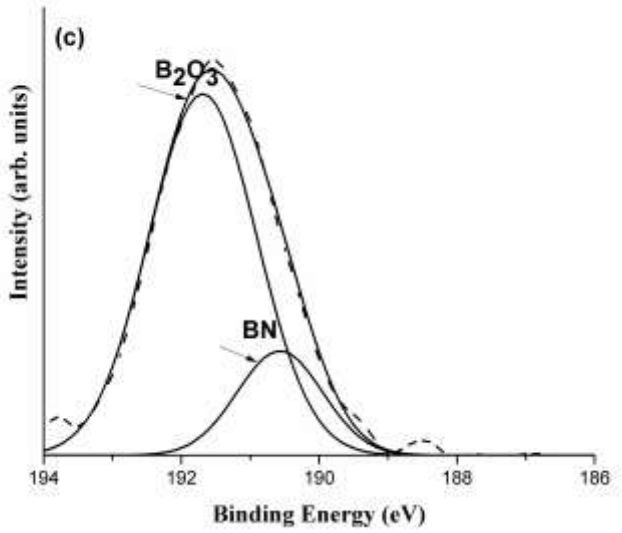

Figure 4.10: XPS B 1s spectra for BCN films deposited at 1 N_2/Ar at different anneal temperatures (a) un-annealed, (b) 500^{o}C and (c) 700^{o}C

4.3 Optical Characterization

In order to investigate the prospects of sputtered BCN thin films as the next generation of optical coatings, it is necessary to understand the optical properties with respect to compositional gas mixtures during film deposition. The effect of annealing on the optical characteristics is also reported in correlation with observed changes in chemical nature of the material.

4.3.1 Band gap studies with different N_2/Ar gas flow ratio at as-deposited temp.

Fig.4.11 shows the optical transmission spectra of the films for various N_2/Ar gas flow ratios. It can be seen that the introduction of N_2 into the sputtering ambient dramatically increases the transmittance of the film. However further increase of the N_2/Ar flow ratio does not produce any significant further change in the transmittance, Thus it appears that the optical transmittance of the BCN films is relatively insensitive to the compositional changes shown in Table 4.1.

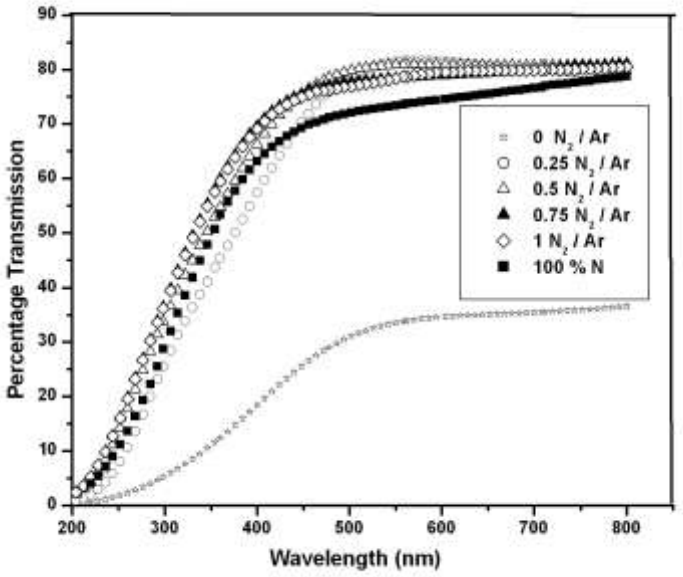

Figure 4. 11: Transmission (%T) curves of as deposited BCN films at various N_2/Ar gas flow ratios.

The transmission (%T) data was used to calculate the optical density (OD) of the films and ultimately used to calculate absorption coefficient as shown in equation 2.

$$\alpha = 2.303 \times \mathrm{OD} = \frac{-2.303}{t} \log_{10}(\%\mathrm{T})$$

Where, α is the absorption coefficient and t is the thickness of the film. Fig. 4.12 shows the calculated absorption coefficient as a function of photon energy for all the gas flow ratios. The absorption coefficient was subsequently used to calculate the optical band gap (E_{opt}) of the amorphous BCN films. This is done using a Tauc plot wherein the data is fitted to the following equation [172].

$$\alpha \cdot h\upsilon^{\frac{1}{2}} = B(h\upsilon - E_{\mathrm{opt}})$$

where, B is a constant factor and hυ is the photon energy.

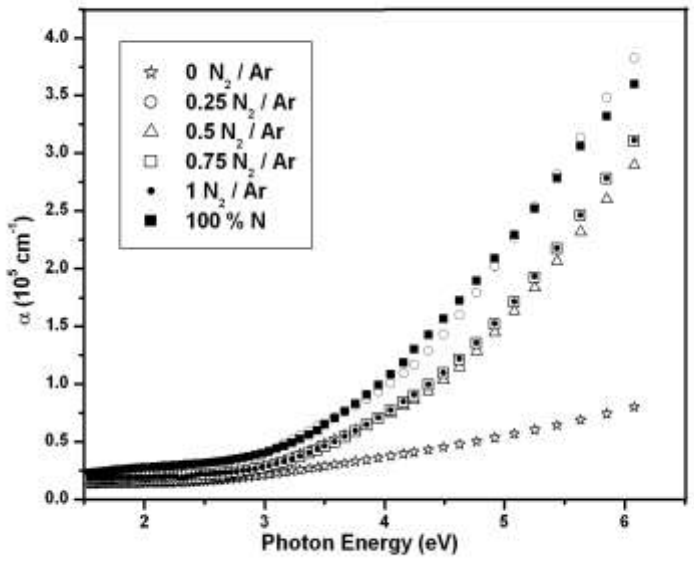

Figure 4. 12: Absorption coefficient (α) with respect to photon energy for various N_2/Ar gas flow ratios.

Fig. 4.13 shows the Tauc plot used to determine E_{opt} for the films. The extrapolation of the linear portion of the Tauc curve to intercept the x-axis provides the E_{opt} values for each material. Fig. 4.14 shows the variation of E_{opt} with respect to the N_2/Ar gas flow ratio. It can be observed that the optical band gap changes significantly when nitrogen is introduced and then increases gradually with N_2/Ar gas flow ratio for the BCN films up to the 0.75 flow ratio, after which a slight decrease is observed. A similar decrease in band gap at a higher N_2/Ar gas ratio has been reported elsewhere. [50]. As expected, the E_{opt} values shown in Fig.10 are intermediate to those of amorphous BC (2.1eV) and that of BN (3.6 eV–6 eV) [173].

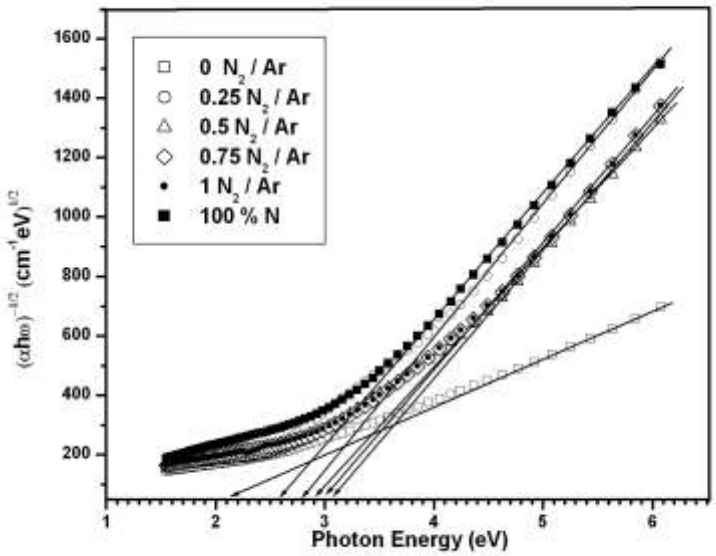

Figure 4. 13: Tauc plot for BCN films. Dotted lines represent extrapolated straight line intercept indicating optical band gap for each curve.

For a well-mixed ternary compounds, one can use the average approximation [174] to calculate the average band gap of the compound. For this calculation the average band gaps assumed were 2.0 eV for BC and 4.2 eV for BN respectively. Assuming a linear increase in band gap from 2 to 4.2 eV for the mixture, the band gaps of different compositions of $BC_{1-x}N_x$ were found based on the value of x obtained for each N_2/Ar ratio. The results are shown in Table 4.3 and the approximation curve with the calculated band gap energies are plotted in Fig. 4.15. These results are in very good agreement with the band gap energies derived from absorption studies.

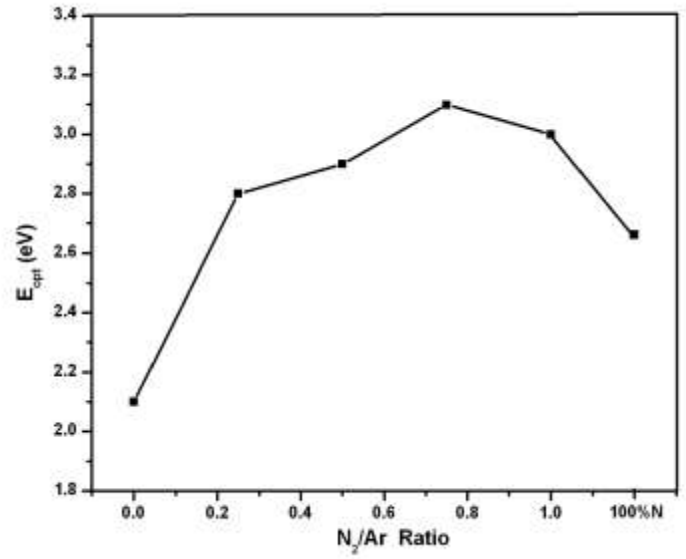

Figure 4. 14: Optical band gap (Eopt) for BCN films with respect to various N_2/Ar gas flow ratios.

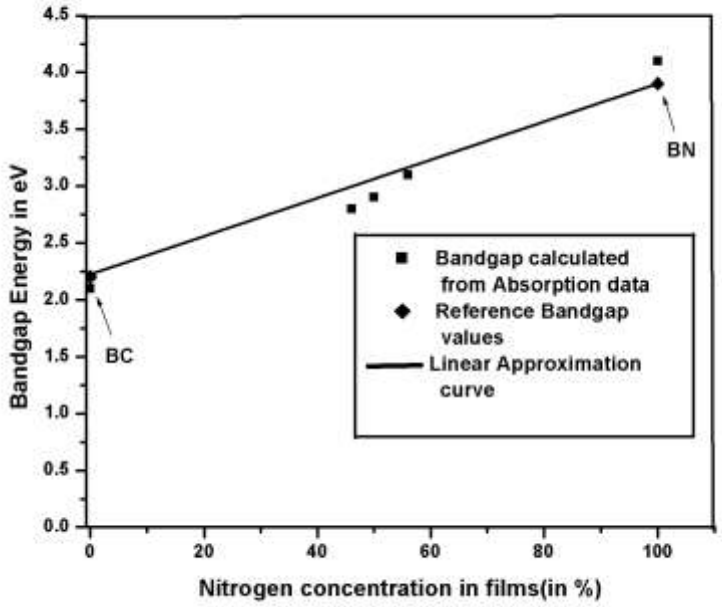

Figure 4. 15: Linear band gap approximation curve between BC and BN to read average band gap values of intermediate ternary alloys.

Table 4. 3: Band gap evaluation.

N_2/Ar Ratio	Nitrogen Concentration (x)	Carbon Concentration (1-x)	E_g (eV) from linear approximation	E_g (eV) from optical absorption
BC	-	-	2.2	2.1
0.25	0.46	0.54	2.9	2.8
0.5	0.51	0.49	3.0	2.9
0.75	0.56	0.44	3.15	3.1
1	0.53	0.47	3.1	3.0
BN	0.7	-	3.8	4.1

4.3.2 Band gap studies with different N_2/Ar gas flow ratio at annealing temp.

Fig. 4.16 shows the transmission data for 1 N_2/Ar gas flow rate for different annealing temperatures. It can be observed that annealing increases transmittance of the films and the film annealed at 700°C is almost completely transparent. The shift in optical transmittance is very gradual initially from as deposited sample up to 300°C annealing. This clearly indicates the temperature stability of the film with respect to optical characteristics. However annealing at temperatures higher than 500°C produces large shift in transmission property. The high transmission properties of the films after 700°C annealing indicate extensive oxide formation. Similar trends were observed in the samples prepared at 0 N_2/Ar and 0.25 N_2/Ar gas flow ratios.

Fig. 4.17 shows the calculated absorption coefficient as a function of photon energy for all the three gas flow ratios under various annealing conditions. It can be seen that there is no distinct absorption edge especially after annealing at higher temperatures. The absorption coefficient was subsequently used to calculate the optical band gap (E_{opt}) of the amorphous BCN films.

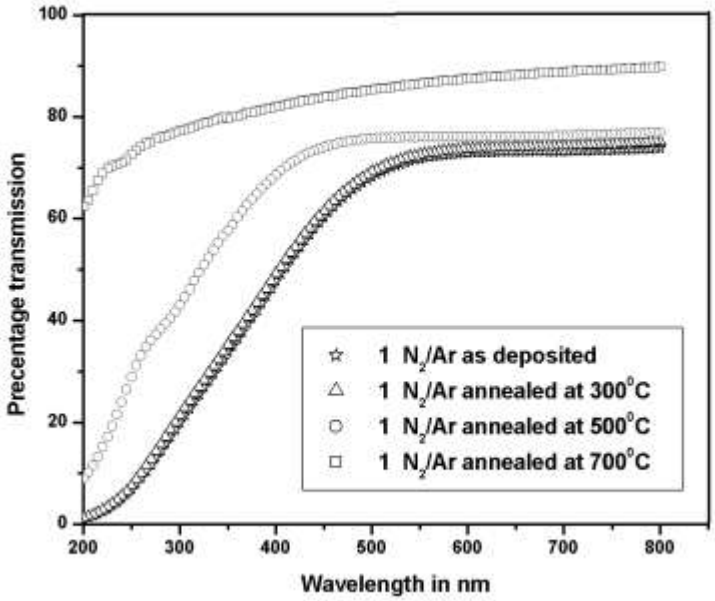

Figure 4. 16: Transmission (%T) curves of 1 N_2/Ar BCN films at different annealing temperatures.

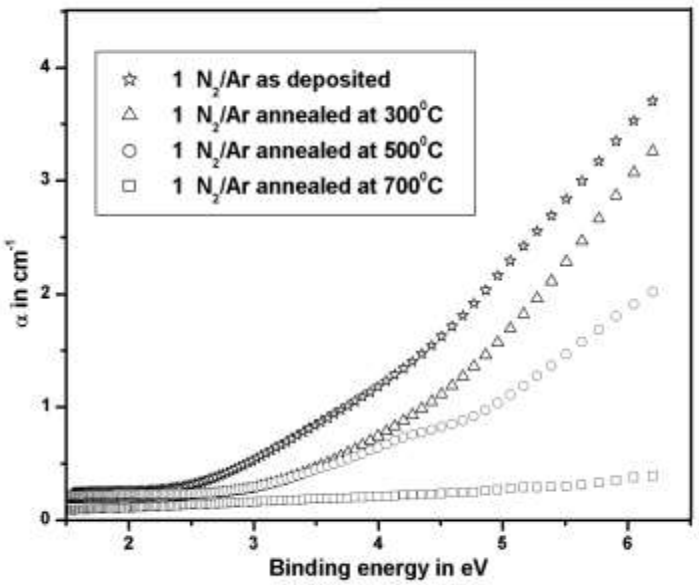

Figure 4. 17: Absorption coefficient with respect to photon energy for 1 N_2/Ar gas flow rtio at different annealing temperatures.

Figure 4.18 shows a Tauc plot for films deposited at $1N_2$/Ar flow rate subject to various annealing conditions. The extrapolation of the linear region of the Tauc curve to intercept the x-axis leads to E_{opt} values for the material and the slope of this line can be used to calculate B. It can be observed that the optical band gap values for the as deposited BCN film is around 2.8eV and increases after annealing. As expected, the E_{opt} values are intermediate to those of amorphous BC (2.1eV) and that of BN (3.6 eV–6 eV).

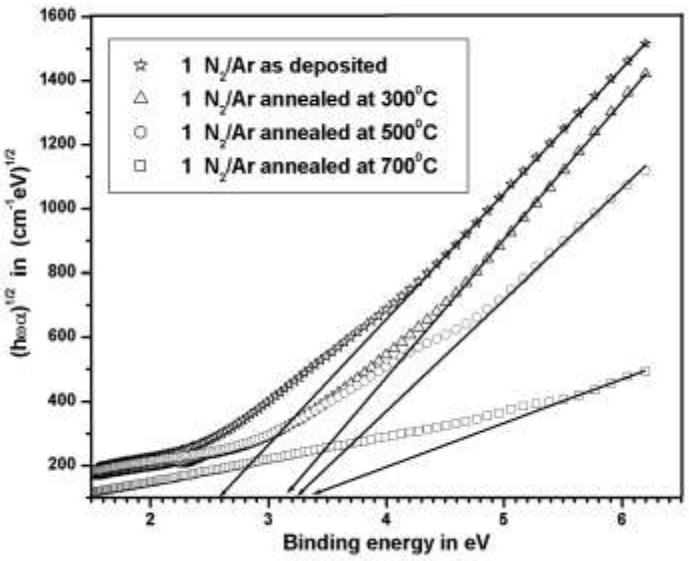

Figure 4. 18: Tauc Plot for 1 N_2/Ar BCN films. Dotted lines represent extrapolated straight line intercept indicating optical band gap for each curve.

Figure 4.19 shows a plot of E_{opt} with respect to annealing conditions for all three deposition gas flow rates. It is evident that the optical band gap increases with annealing in all the three cases. Also, the increase is more prominent at higher temperatures i.e. above 500^{o}C. Furthermore it can be noted that the band gap for 1 N_2/Ar flow ratio is greater than the other two flow ratios and continues the trend after annealing. Compositional changes in the films due to process conditions as well as annealing are believed to cause these variations in optical

properties. In order to investigate this further, we consider the chemical analysis of the films before and after annealing.

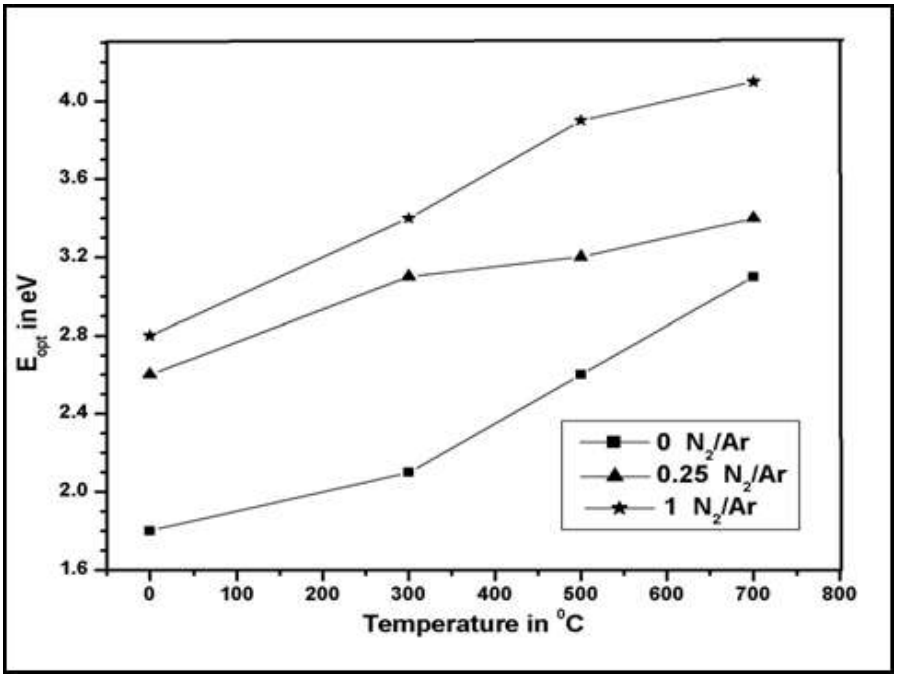

Figure 4. 19: Optical band gap for 0 N_2/Ar, 0.25 N_2/Ar and 1.0 N_2/Ar BCN films with respect to annealing conditions.

4.4 Substrate Heating Studies

Elevated temperatures are employed in thin film deposition processes for three basic reasons:

1) To enhance film adhesion.
2) To control the morphology
3) To activate the reaction between metal and reactive gas in a reactive deposition process.

Hence, elevated temperatures are generally viewed as beneficial in thin film processes. The temperature of the substrate surface is an important and yet difficult parameter to control in the sputtering system. In conventional sputtering systems, the substrate is mounted on a

temperature controlled substrate holder. However the surface of the substrate is heated by the radiant heat of the target. Moreover, the surface of the substrate is heated by the radiant heat of the target. Moreover, bombardment by high energy secondary electrons also heats the substrate. In the rf diode system the temperature of the substrate rises up to 700^{o}C without additional substrate heating, In order to reduce the effect of the radiant heat, the surface of the target must be cooled. Bombardment by the secondary electrons is avoided by negatively biasing the substrate.

Several works have been reported on the BCN films deposited at various temperatures. Ulrich et al. sputtered from the single h-BN target in the atmosphere of argon/acetylene with deposition temperature of 600^{o}C and obtained the B-C-N films with C and BN phase separation. Also, He et al. replaced acetylene with methane as sputtering gas with deposition temperature of 450^{o}C and found that the synthesized films were atomic-level hybrids, which were evidenced by XPS and FTIR data. Liu et al. also obtained the films of atomic-level B-C-N compounds from h-BN and graphite targets under various experimental conditions.

4.4.1 Deposition rate vs substrate heating temperatures

Figure 4.20 shows deposition rate of BN sputtered in pure argon ambient at different deposition temperature. As seen no significant change is seen in the deposition rate of BN even at higher deposition temperatures and the deposition rate is around 7.8 Å/minute.

Fig. 4.21 shows the deposition rate of the BCN films deposited at different deposition temperatures for the N_2/Ar ratios of 0.25 and 1.0. The deposition rate increased with the deposition temperatures for both N_2/Ar gas flow ratios. This increase in the deposition rate is attributed to some kind of a chemical reaction occurring at the surface of the substrate. This is

similar to CVD process in which the growth rate increases at elevated temperatures. The highest deposition rate of 22A^{o}/min was obtained for the samples deposited at 500^{o}C.

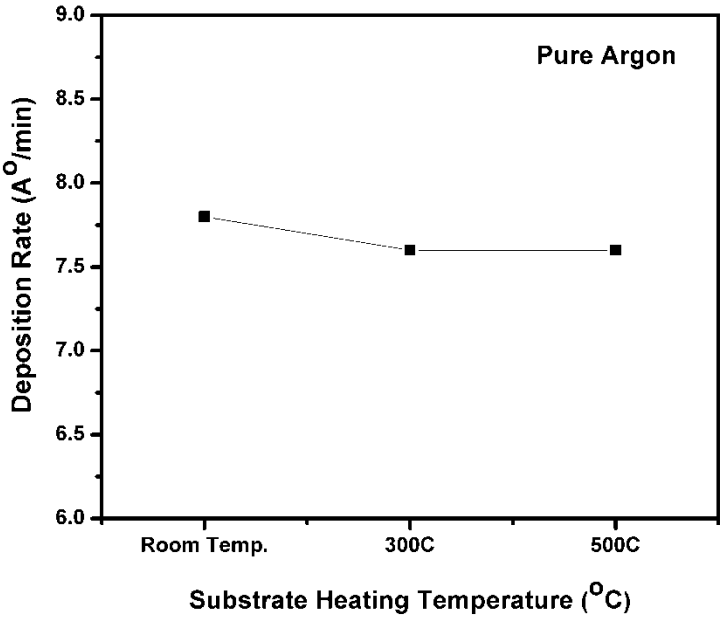

Figure 4. 20: Deposition rate of BN vs deposition temperatures for the samples sputtered in pure argon

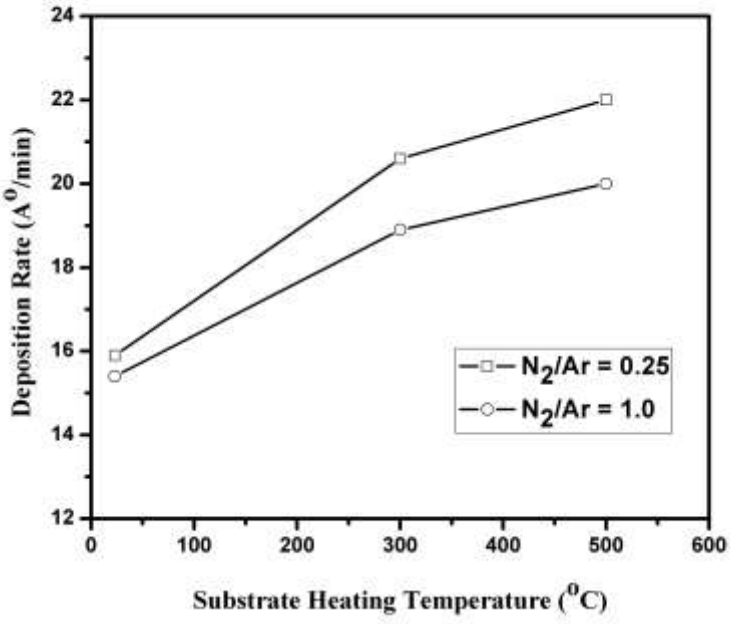

Figure 4. 21: Deposition rate of BCN films vs deposition temperatures.

4.4.2 Chemical Analysis using XPS

The elemental compositions of the films were obtained from XPS surface scans. The relative atomic concentration of boron, carbon and nitrogen are listed in Table 4.4. For all the BCN films obtained, the oxygen concentration was less than 5 at. %. Oxygen results as a contamination because XPS measurements were done ex-situ and thus the atomic concentrations of boron, carbon and nitrogen are normalized with respect to oxygen. As seen in Table 4.4, the boron and nitrogen concentration in the films increased with increasing substrate temperatures. The films deposited at 500^{o}C had the highest amount of boron (40 at. %) and nitrogen (36 at. %) concentration. At the same time the carbon concentration in the films decreased as the substrate temperature was increased. This increase of nitrogen content together with increase in boron and decrease in carbon content could lead to very useful optical properties which are investigated later in this dissertation.

Table 4. 4: Atomic concentrations of B, C and N elements in the B-C-N films deposited at different substrate temperatures from XPS analysis.

Substrate Temp.	Boron (at. %)	Carbon (at. %)	Nitrogen (at. %)
23^{o}C	34	40	26
300^{o}C	36	31	33
500^{o}C	40	24	36

High resolution XPS scans were obtained to analyze the chemical nature of the BCN films. Fig. 4.22 shows the deconvolved high resolution boron (B 1s) spectral data for films deposited at room temperature, 300^{o}C and 500^{o}C respectively. The peak at 190.7eV is a clear indication of a BN peak [167, 168]. The peak at 189.8 eV can be attributed to the BC bonding [169]. Finally, the peak at 192 eV is due to B_2O_3 bonding [170]. It is seen that the intensity of the

BN peaks increases with the deposition temperature and opposite trend is observed for the BC peak. This suggests that boron bonds more with nitrogen then carbon at high deposition temperatures.

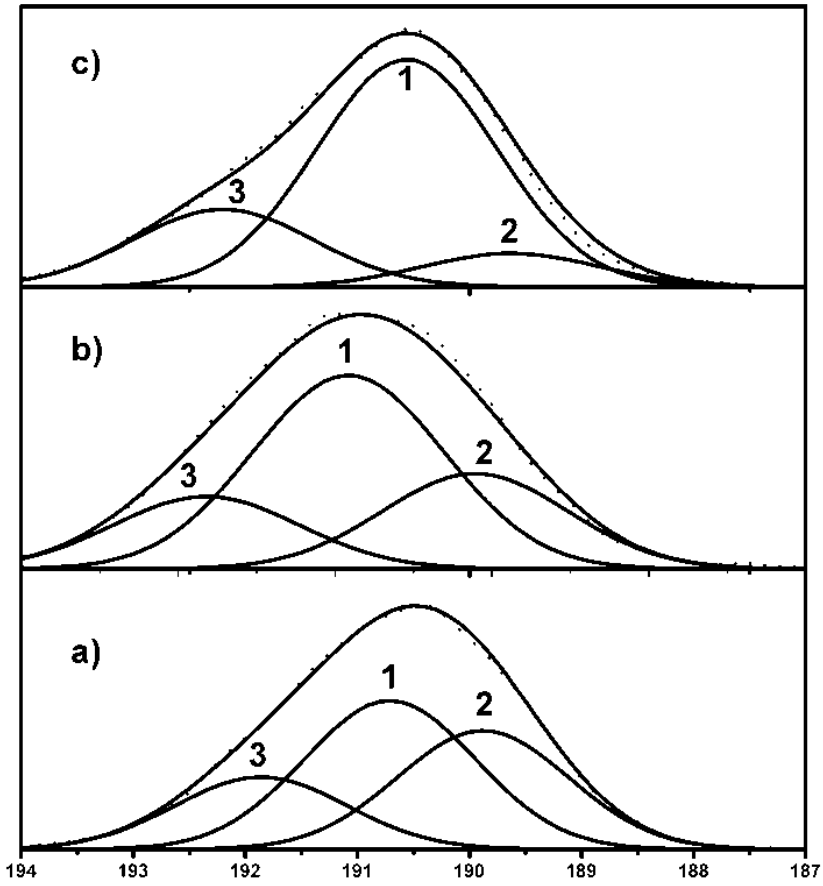

Figure 4. 22: XPS narrow scan spectra of the B1s peak for the BCN films deposited at different deposition temperatures (a) Room Temperature (b) 300^{o}C and (c) 500^{o}C. Peaks identification: 1) BN 2) BC and 3) B_2O_3.

Fig. 4.23 shows the deconvolved high resolution nitrogen (N 1s) spectral data for films deposited at room temperature, 300^{o}C and 500^{o}C respectively. The deconvolved peak found between 397-397.5 eV can be attributed to hexagonal B-N bonding [175], and is evident in all BCN samples, confirming that nitrogen binds well with boron. A second peak between 398-398.5 eV is due to sp^3 N-C bonding (N bonded to sp^3-hybridized C) [163, 164].The peak

between 400-400.5eV can be attributed to the presence of sp^2 C-N bonds (N bonded to sp^2-hybridized C) [176]. It can be seen that the CN peak decreases with increased substrate temperature. At the same time the intensity of sp^3 CN peak increased with increased deposition temperature. The sp^2 CN also shows a decreasing trend but the trend is not that clear. Thus, we can say that the high deposition temperature favors the formation of sp^3 CN bonds in the films.

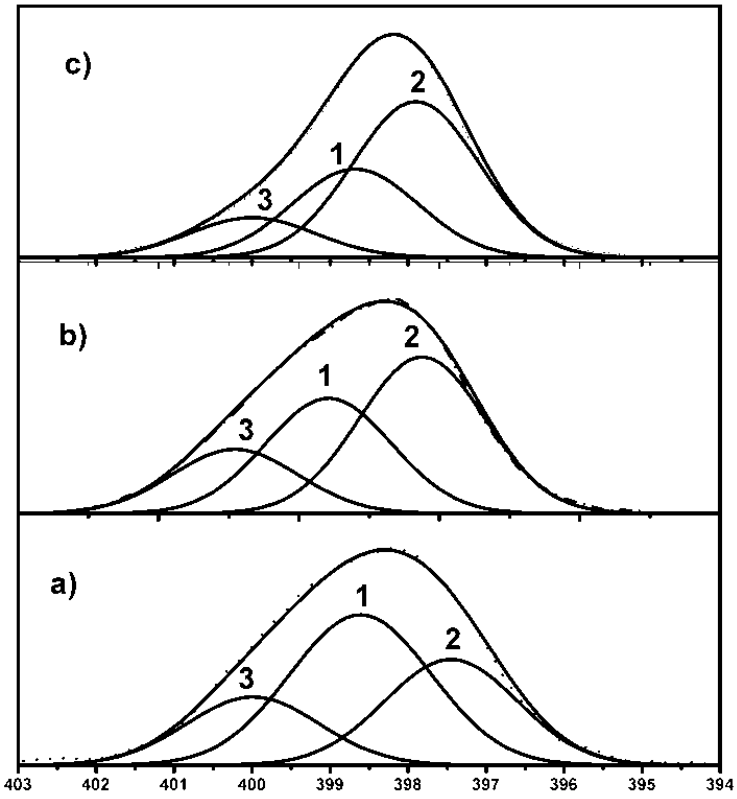

Figure 4. 23: XPS narrow scan spectra of the N1s peak for the BCN films deposited at different deposition temperatures (a) Room Temperature (b) 300^{o}C and (c) 500^{o}C. Peaks identification: 1) NC 2) sp^3 CN and 3) sp^2 CN.

Fig. 4.24 shows the deconvolved high resolution carbon (C 1s) spectral data for films deposited at room temperature, 300^{o}C and 500^{o}C respectively. The peak at 284.6 eV is because of adventitious carbon which is always present in the sample and thus was used as a reference. The deconvolution also leads to two different binding states with peaks centered at 286.5 eV and

288.5 eV. The peak at 286.5 eV corresponds to sp^3 C-N binding. Finally the peak at 288.5 eV results from oxygen contamination and shows the existence of CO bonds.

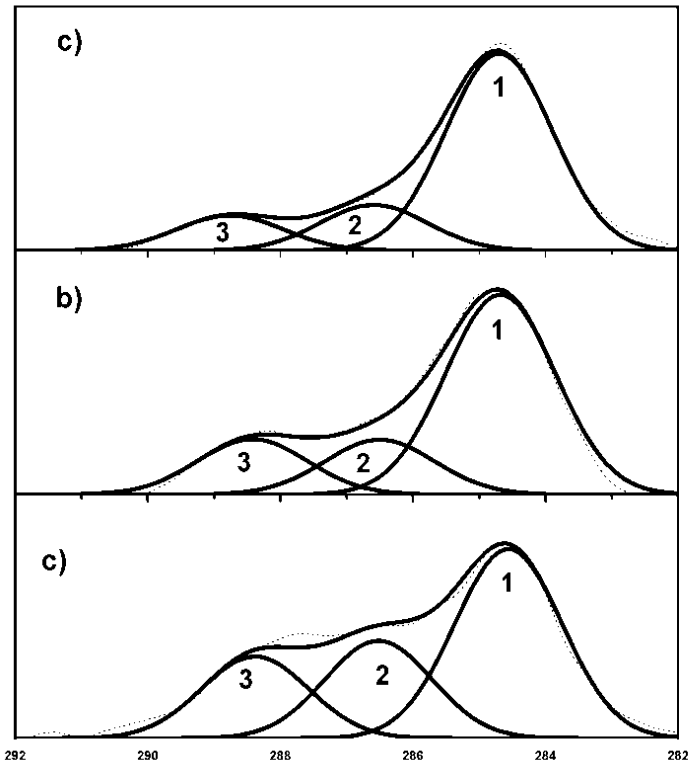

Figure 4. 24: XPS narrow scan spectra of the C1s peak for the BCN films deposited at different deposition temperatures (a) Room Temperature (b) 300^{o}C and (c) 500^{o}C. Peaks identification: 1) C-H 2) sp^3 CN and 3) CO

Thus the deposition temperatures have a significant effect on the composition and structure of the BCN films. The increase in the B/C and B/N ratio of the films was detected as deposition temperature increased. This indicates that higher temperature contributes to the reaction of boron with carbon and nitrogen during deposition. The composition varied in the broad field for the BCN films which eventually led to the complicated structures in the BCN films.

4.4.3 Optical Characterization

Figure 4.25 shows the transmission data for BCN films deposited at different substrate temperatures. It can be observed from the figure that the transmission increases as the deposition temperature was increased from room temperature to 500^{o}C. The films deposited at 500^{o}C have the highest transmission properties. The transmission data is used to calculate the refractive index and the optical band gap of the films. Tauc plot was used to calculate the optical band gap. The refractive indexes were calculated from adjacent maxima from the transmission characteristics.

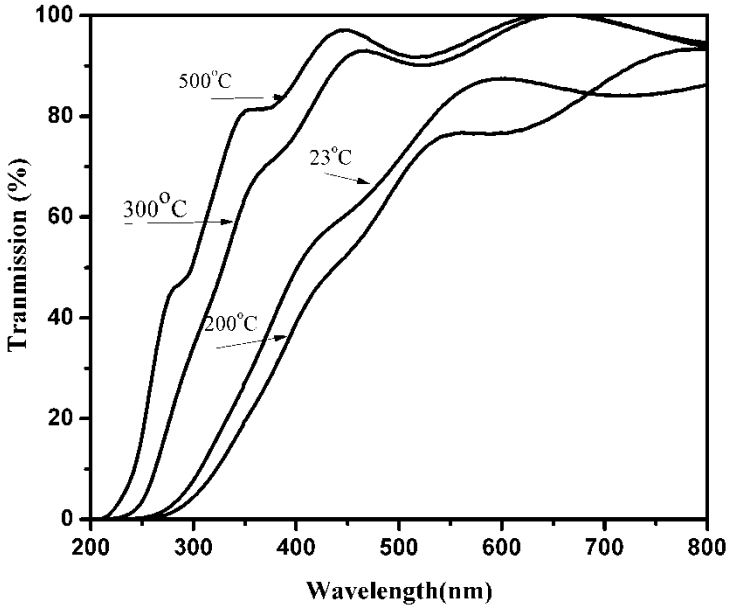

Figure 4. 25: Transmission (%T) curves of BCN films deposited at various deposition temperatures from room temperature to 500^{o}C.

Figure 4.26 shows the refractive index with respect to different substrate heating temperatures. The refractive index decreased from 2.66 to 1.5 as the substrate temperature was increased from room temperature to 500^{o}C. Higher values of refractive index imply poorer optical transparency of the BCN films.

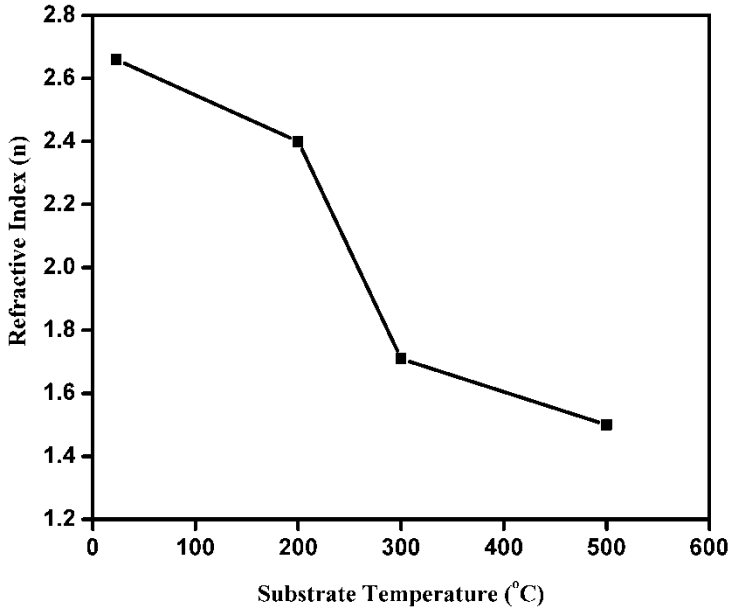

Figure 4. 26: The refractive index of the BCN films deposited at different deposition temperatures.

Figure 4.27 shows the optical band gaps of the BCN films deposited at different deposition temperatures. It is apparent that the optical band gap increased from 3.5eV for samples deposited at room temperature to 4.6eV for the samples deposited at 500^{o}C. The increase in the optical band gap of the films pushes their absorption bands towards the ultraviolet radiation region, which results in higher and flatter optical transparency across the visible wavelength. This increase in band gap can be correlated with the observed increase in boron and nitrogen concentration and decrease in carbon concentration for the BCN films. Park et al. observed decrease in refractive index and increase in optical band gap can result by lowering the fraction of sp^2 binding in the amorphous C:N films. This is consistent with our findings.

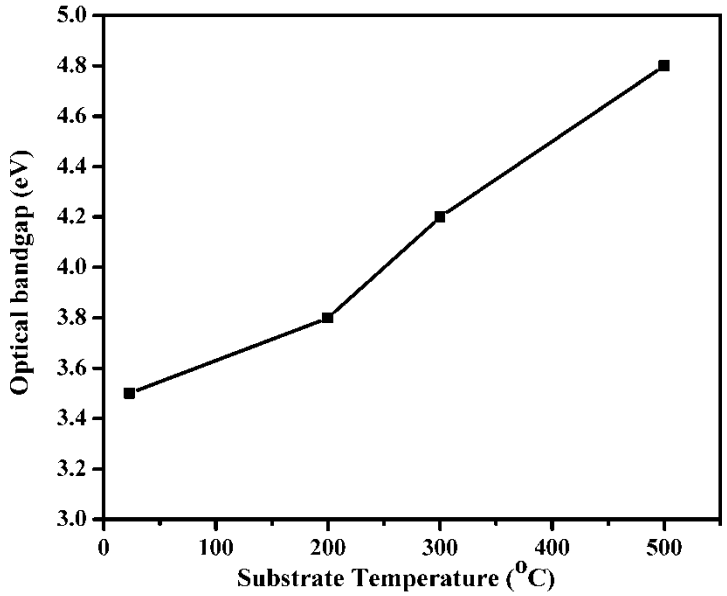

Figure 4. 27: The optical band gap of the BCN films deposited at different deposition temperatures.

There exists a wide range of possible boron, carbon and nitrogen concentration in the BCN films which could result in change of film properties as its composition changes. The microstructure of the BCN films is expected to have a similar effect on their properties. For the amorphous BCN films prepared at the deposition conditions reported here, their optical properties differ from one to another, which is due to the presence of different three-dimensional bonds between boron, carbon and nitrogen. Better optical properties can be achieved with a higher fraction of sp^3 bindings of boron, carbon and nitrogen in the BCN films.

4.4.4 SIMS Depth Profiling

SIMS analysis was performed to verify the distribution of the elemental components of boron, carbon, nitrogen and also oxygen which results due to contamination. Figure 4.28 show the SIMS scans for the BCN thin films deposited at room temperature and 500^{o}C. It can be observed that there exists a very uniform distribution of the three elements B, C and N over the

whole film depth. This suggests that the film is quite homogeneous. The intensities are qualitative and dependant to the analyses conditions, more specifically to the secondary ion yields. For the SIMS data given in the Figure 4.27, the x-axis was converted from time to depth by measuring crater depths obtained during analyses by a profilometer. The thicknesses were in good agreement with the SEM observations with a maximum deviation of 2%. Even for the films deposited at 500^{o}C, the distribution is quite uniform but the films show more of oxygen as compared to the films deposited at room temperature.

Also, the SIMS analysis clearly distinguishes two regions of BCN samples. The first region is the actual BCN films on the surface and the second region is the thermally grown SiO_2 oxide layer.

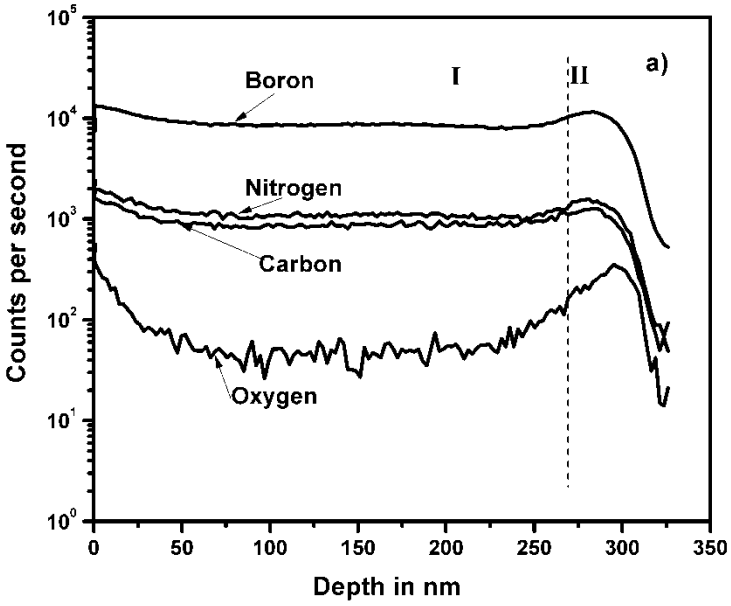

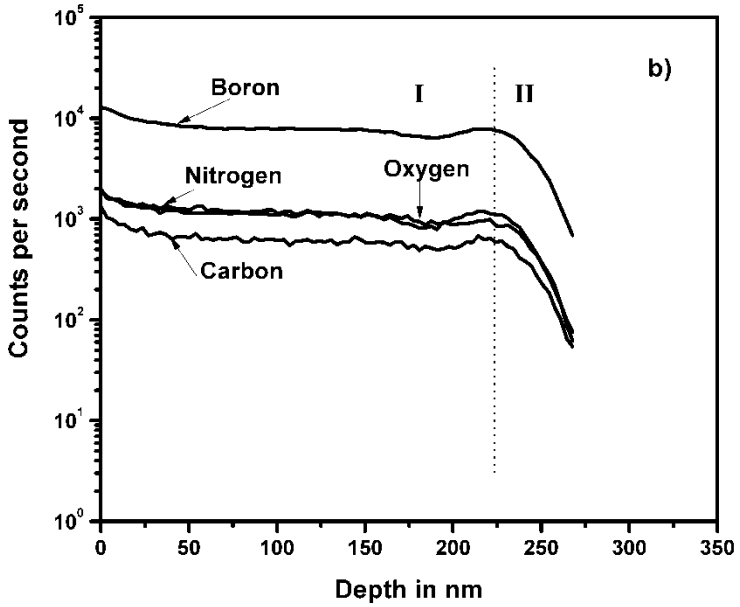

Figure 4. 28: SIMS elemental depth profile of BCN films deposited at a) Room temperature and b) 500°C

4.4.5 AFM Measurements

Surface morphology was characterized by AFM. The roughness data was calculated from AFM measurements for the samples deposited at room temperature and samples deposited at 300°C and 500°C. Figure 4.29 shows a plot of RMS roughness and average roughness for the as deposited samples and samples deposited at different temperatures. As seen from the plot the roughness values are very low which indicates that the films obtained were very smooth. Even for the samples deposited at temperatures of 300°C and 500°C the roughness values increased slightly i.e. from 0.5nm to 0.8nm. This indicated that the deposition temperatures didn't degrade the surface of the films and this is very important for practical purposes.

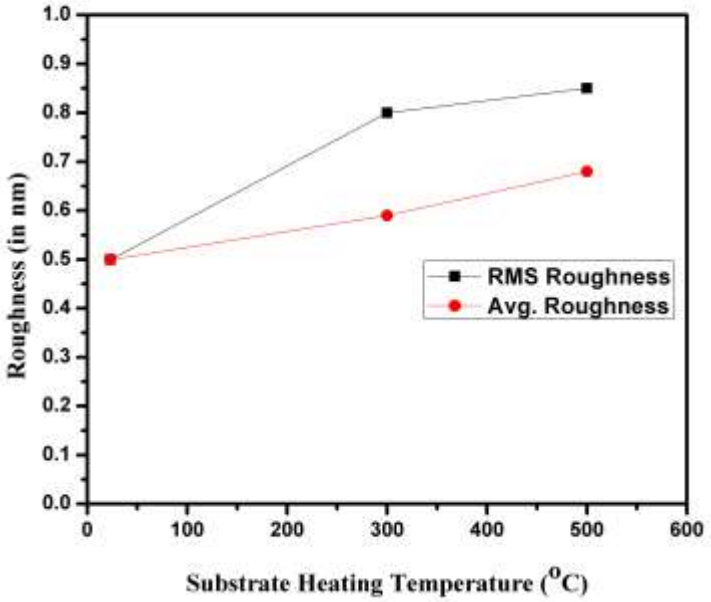

Figure 4. 29: RMS and Average Roughness for as-deposited and samples deposited at different deposition temperatures.

Figure 4.30 shows the AFM images of the samples deposited at room temperature and samples deposited at 300^{o}C and 500^{o}C. As observed from the AFM images not much difference is seen for the surface of the films deposited at room temperature and for the films deposited at higher temperatures. This is in accordance with the roughness values observed and reported in Figure 4.28.

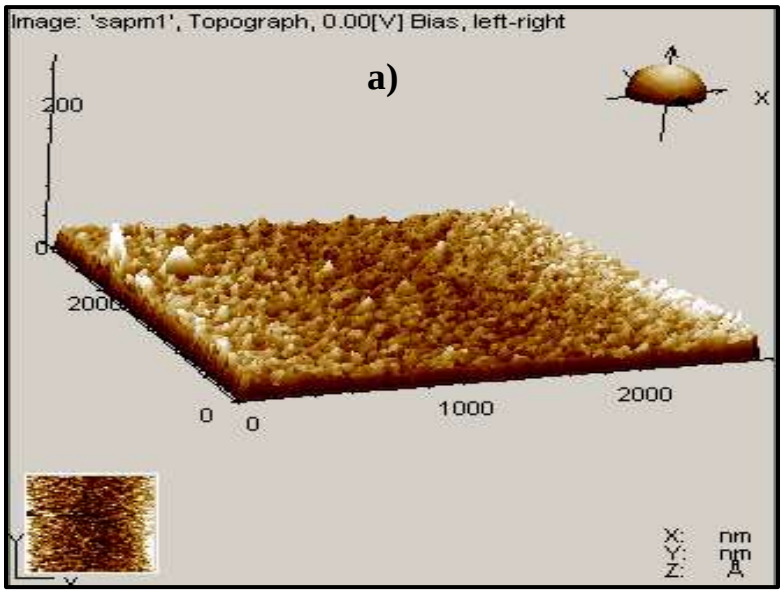

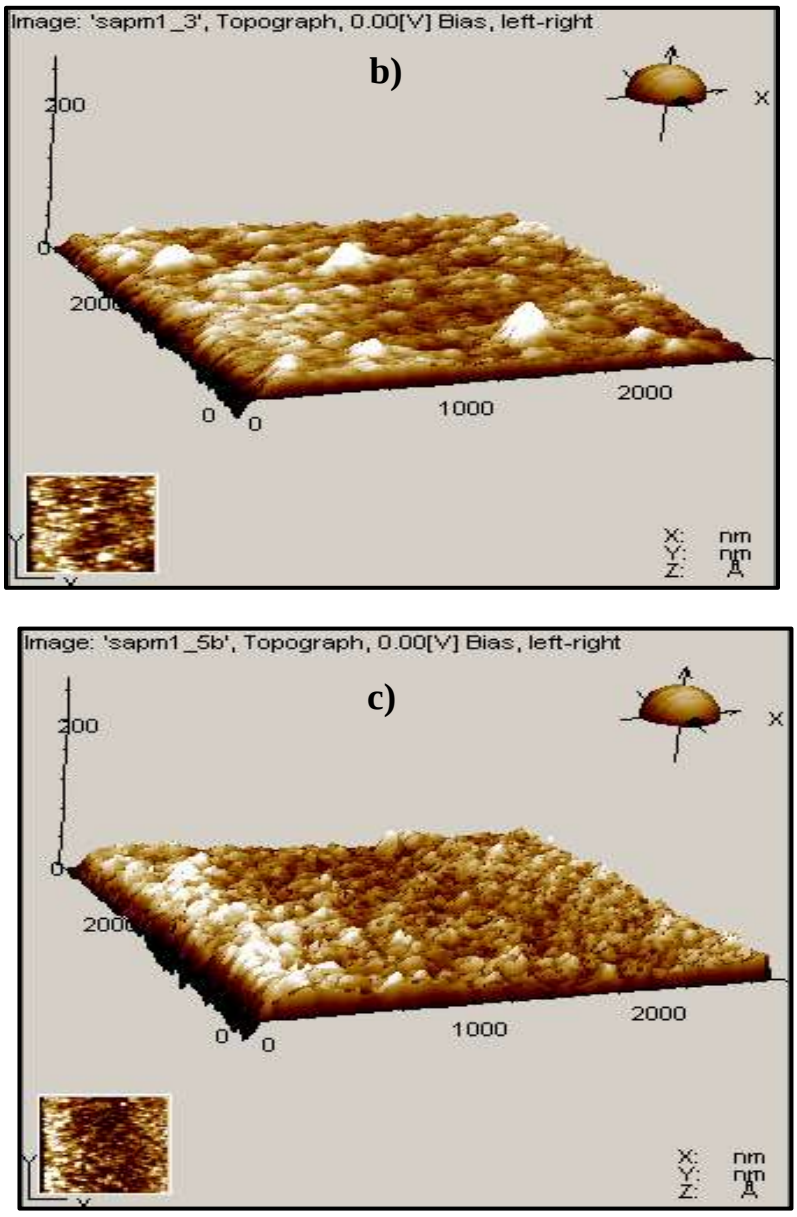

Figure 4. 30: AFM Images for the samples a) as-deposited b) deposited at 300°C c) deposited at 500°C

4.5 Electrical Studies

Electrical properties of the BCN films are evaluated in this section. This mainly includes calculating dielectric constant of the BCN material. For finding the dielectric constant Capacitance-Voltage (C-V) curves across the voltage sweep were plotted for the MOS devices

made with BCN as the dielectric layer. Aluminum was used as the top and bottom electrodes. Dielectric constant was then calculated from the capacitance of the accumulation region.

4.5.1 Dielectric constant v/s deposition temperatures

Figure 4.31 show the C-V plots for the as-deposited samples and the samples deposited at 300^{o}C and 500^{o}C respectively. The N_2/Ar ratio of all the samples was 1 i.e. Ar =10sccm and N_2=10sccm. Voltage was swept from -20 volts to 20 volts for the as-deposited sample, from -30 volts to 30 volts for the sample deposited at 300^{o}C and from -80 volts to 20 volts for the sample deposited at 500^{o}C. The range of voltage sweep had to be varied for different samples to get the good C-V plots covering accumulation and depletion regions. This can be due to the change in process parameters and indicates the device dependability on the fabrication process itself.

The area of the devices was kept the same which eliminates the effect of area on the variation of sweep voltages for samples deposited at different deposition conditions. The different sweep voltages especially -80V for the samples deposited at 500^{o}C may suggest better thermal stability of the devices at that deposition temperature. The y-axis is capacitance represented in nF. As seen from the Figure 4.31, the devices demonstrated good CV curves with capacitance changing from accumulation region for the negative sweep voltages to depletion region for the positive sweep voltages.

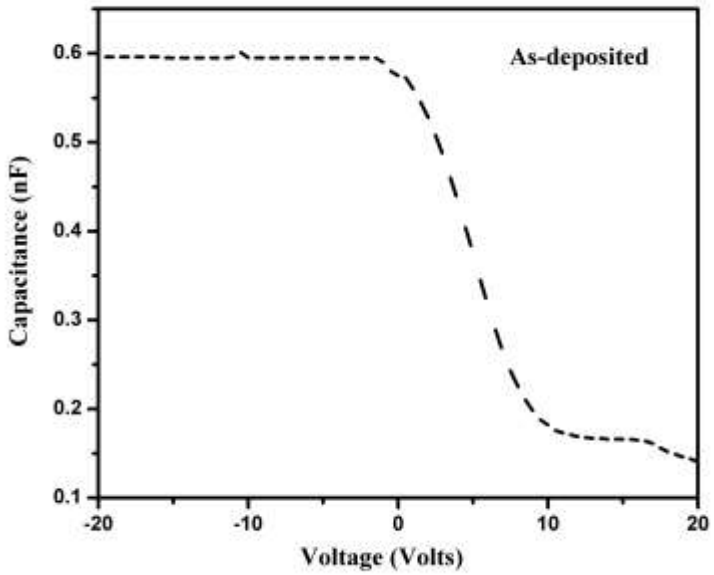
As-deposited
Capacitance (nF)
0.6
0.5
0.4
0.3
0.2
0.1
-20
-10
0
10
20
Voltage (Volts)

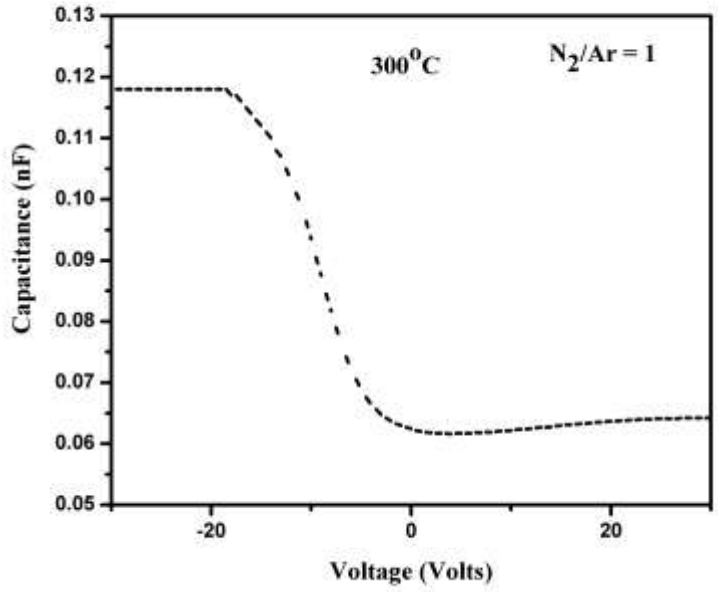
300^{0}C
N_2/Ar = 1
Capacitance (nF)
0.13
0.12
0.11
0.10
0.09
0.08
0.07
0.06
0.05
-20
0
20
Voltage (Volts)

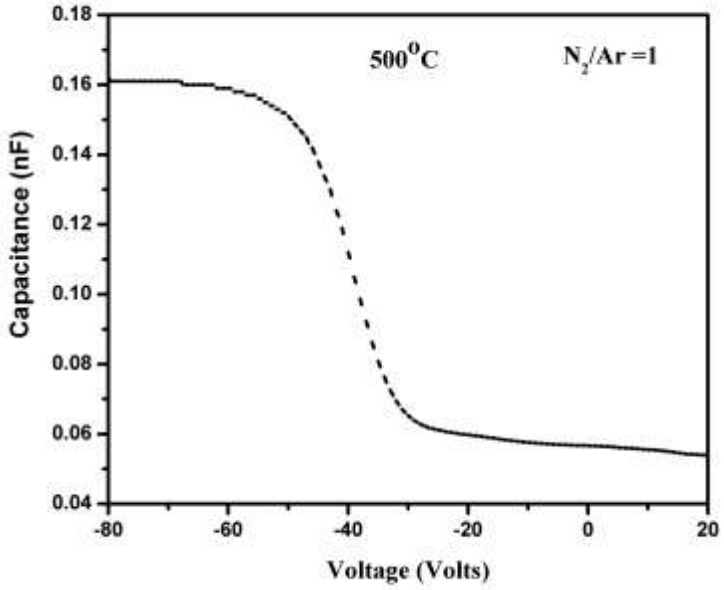

Figure 4. 31: C-V plot of the Al/BCN/p-Si structure for the samples deposited at 1N_2/Ar and a) as-deposited b) deposited at 300°C and c) deposited at 500°C.

The capacitance of the accumulation region was used to calculate the dielectric constant of the BCN films deposited at different deposition conditions. Dielectric constant was calculated by using the following equation;

$$\kappa = C*d / \varepsilon_o*A$$

where, κ = dielectric constant

C = Capacitance (in F)

d = thickness of the material

ε_o = Permittivity of free space

A = Area of the MOS capacitor

Thus we can see from the above equation that the thickness of the material and area of the electrodes needs to be accurately known for finding the values of dielectric constant. The thickness of the material was measured by alpha step profilometer with +/- 0.5nm. The area was accurately known as we used a shadow mask of known area. In order to eliminate the inaccuracy

due to non-uniform thickness over the entire surface of the wafer and also to take into account the tolerance of alpha step profilometer, capacitances on 10 different devices were measured. The dielectric constant values thus have the error bars taking into account the values calculated from ten different devices. Figure 4.32 shows the variation of dielectric constant with respect to various deposition conditions. As seen the dielectric constant calculated were in the range of 4.5-3.5. The samples deposited at 300^{o}C had the least dielectric constant of 3.5 whereby the little difference in dielectric constant was seen for the samples deposited at room temperature and the samples deposited at 500^{o}C. Again the error bars are incorporated in the figure to take into account any non-uniformity and errors due to alpha step profilometer.

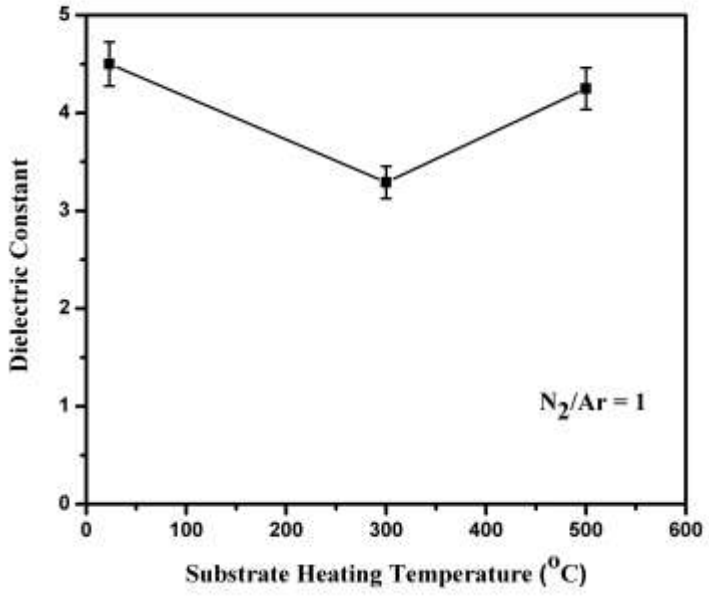

Figure 4. 32: Dielectric constant of BCN films v/s Deposition Temperatures

4.5.2 Dielectric constant vs N_2/Ar gas flow ratios

From the above studies the samples deposited at 300^{o}C yielded the lowest values for dielectric constant. Thus, we studied all the other dielectric constant properties for the samples deposited at 300^{o}C. From our earlier studies, we knew that the nitrogen incorporation into the

sputtering chamber helped in obtaining the films with different composition which showed good optical properties. Hence, we now study the effect of nitrogen incorporation on the dielectric properties of the BCN films. The N_2/Ar gas flow ratio was varied from 0.25, 0.5, 0.75 and 1.0. The total gas in the chamber was kept constant at 20 sccm whereas the individual gas flow of argon and nitrogen was varied to give the desired gas flow ratio.

Figure 4.33 shows the C-V plot for the samples deposited at 300^{o}C for N_2/Ar gas ratios of 0.25, 0.75 and 1.0. Again, the voltage was swept from -30 volts to 20 volts for all the films deposited at different gas flow ratios. As seen we observed good C-V curves for all the films covering capacitance varying from the accumulation region into the depletion region. The C-V plots showed variation with sweep voltages for different ratios. It is seen that the C-V plots does shift for different gas flow ratios suggesting the possibility of variation of dielectric constant with change in nitrogen gas in the sputtering ambient. Dielectric constant was calculated from the accumulation capacitance and by using the equation above.

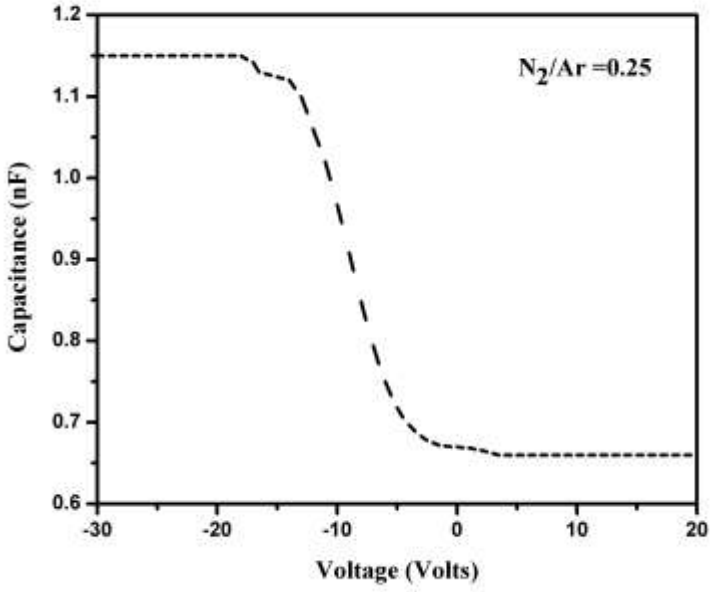

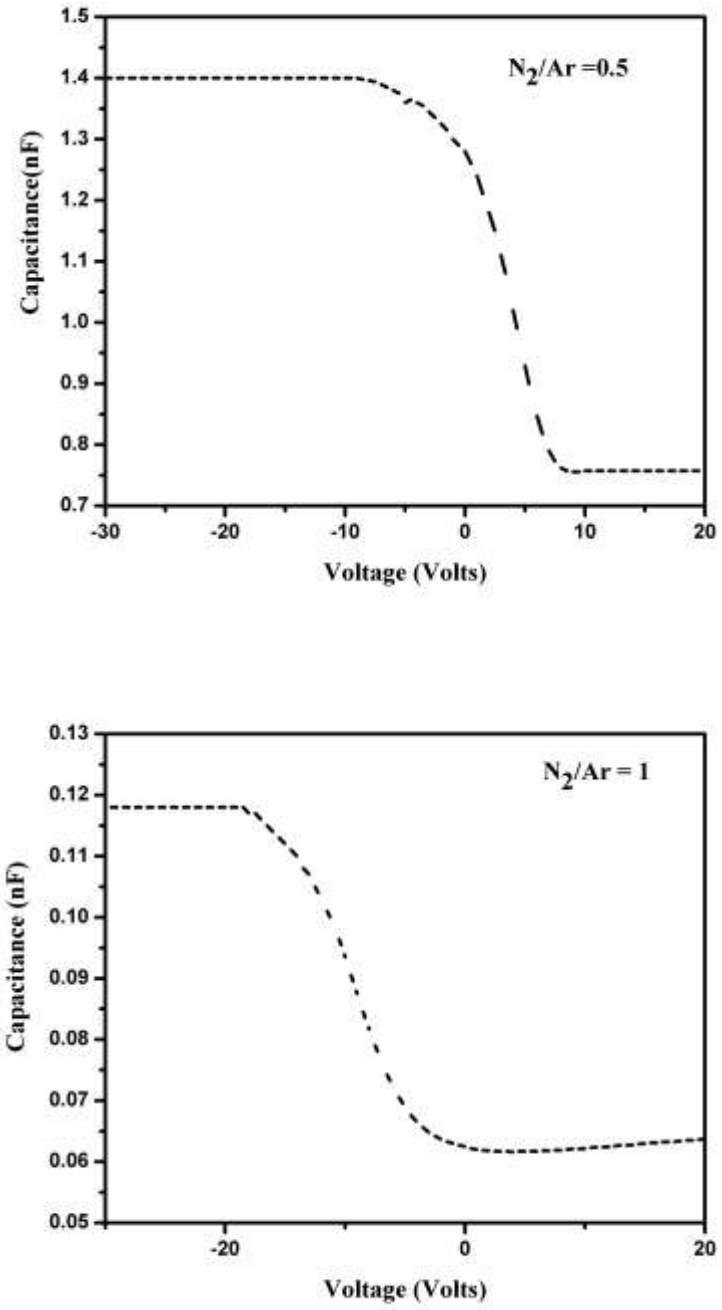

Figure 4. 33: C-V plot of the Al/BCN/p-Si structure for the samples deposited at 300°C and a) 0.25 N_2/Ar b) 0.5 N_2/Ar and c) 1.0 N_2/Ar.

Figure 4.34 shows the values of dielectric constant obtained for different N_2/Ar gas flow ratios. The dielectric constant decreased from 4.91 to 3.49 for the samples deposited at 0.25

N_2/Ar ratio to the samples deposited at 1.0 N_2/Ar gas flow ratio. Thus the films obtained at N2/Ar gas ratio of 1.0 showed the lowest value of dielectric constant.

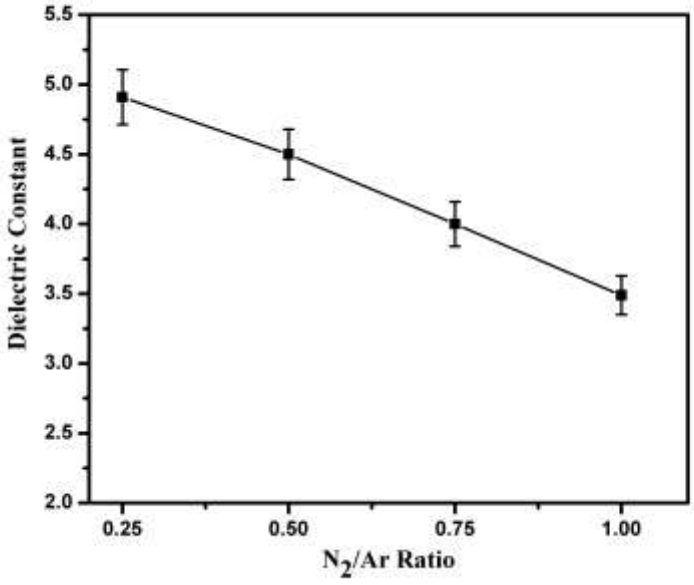

Figure 4. 34: Dielectric constant of BCN films v/s Different N_2/Ar gas flow ratios

The decrease in dielectric constant co-relates very well with the chemical composition obtained by XPS. Figure 4.35 shows the elemental composition of the BCN films obtained by XPS survey scans. It was observed that the carbon concentration in the films decreased at the N_2/Ar ratio was increased and at the same time the nitrogen concentration in the films increased as the N_2/Ar ratio was increased. The boron concentration did show an increasing trend with respect to the increasing N_2/Ar gas ratios but the increase was not that drastic. The boron content increased from 33 at. % to reach a maximum value of 35 at. % at N_2/Ar ratio of 1.0. From the literature it is known that the BN with values of κ reported around 4 has a lower dielectric constant as compared to BC with values of κ reported around 8. Thus decreasing carbon content together with increasing nitrogen content is considered to be a reason for lower values of κ.

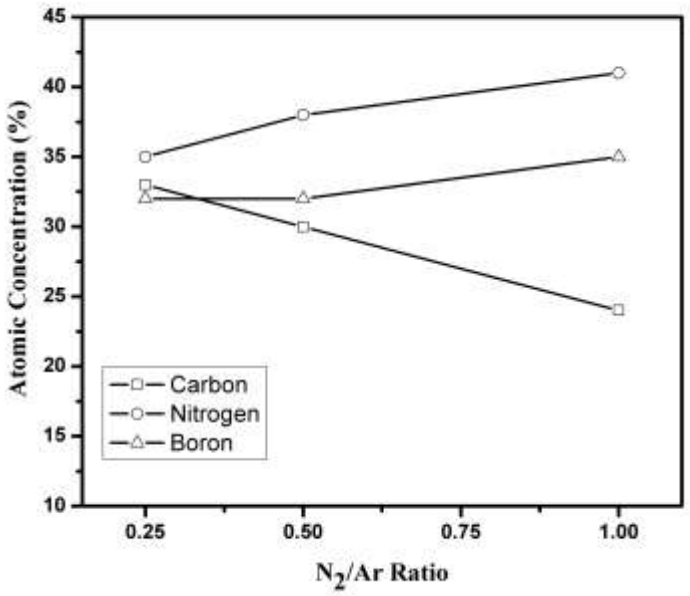

Figure 4.35: Atomic concentration of the elementals C, B and N obtained from XPS survey scans for the samples deposited at different N_2/Ar gas flow ratios.

4.5.3 Effect of annealing on dielectric constant

It is important to study the degradation of the insulating property of the BCN thin film after annealing if the material is considered as an interlayer dielectric layer. Annealing was performed in programmable box furnace at 400^{o}C. The annealing was performed in argon gas ambient and the sample was annealed at 400^{o}C for 20 minutes. The sample was loaded in the box furnace and the furnace was flushed with argon gas for about two hours. This was done to eliminate the effect of any reaction of atmospheric oxygen with the BCN MOS structures. The furnace was then programmed to ramp up to 400^{o}C at the rate of 10^{o}C and the soak time was set for 20 minutes. The sample was allowed to cool down to the room temperature with the argon still flowing in the furnace. C-V measurements were then performed on the MOS structures and dielectric constant was calculated from the accumulation region capacitance.

Figure 4.36 a) and b) shows the C-V plots for the as-deposited and samples deposited at 300^{o}C after annealing at 400^{o}C in argon gas ambient for 20 minutes. It is important to note that even after annealing we were able to get the good C-V plots which indicated that the aluminum did not diffuse into the BCN layer after annealing at 400^{o}C. We see a shift in the C-V plot after annealing and we see a variation from as deposited samples to the samples deposited at 300^{o}C. This suggests change in the values of dielectric constant which is represented in the next figure.

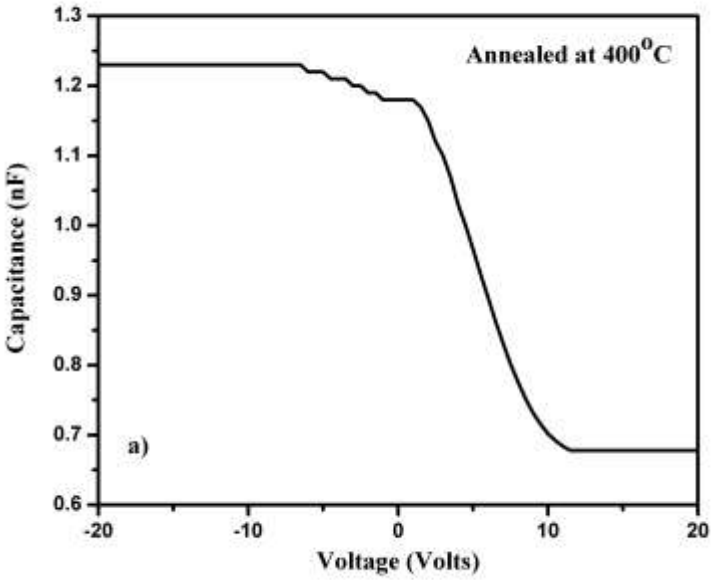

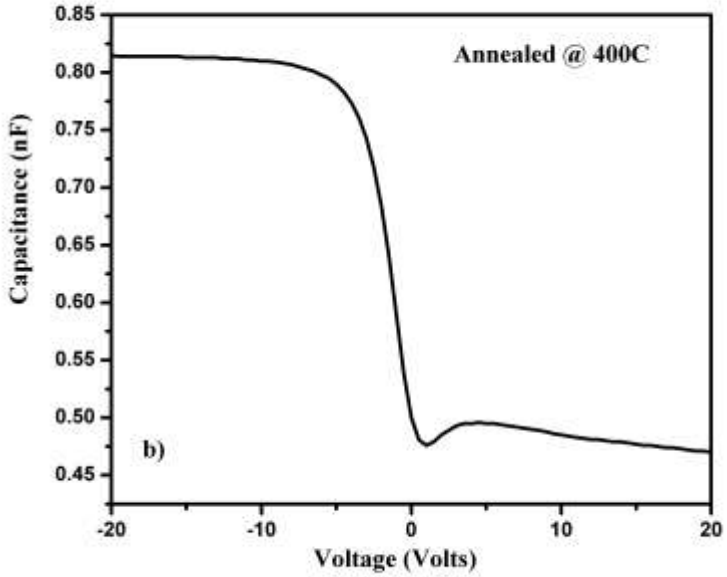

Figure 4. 36: C-V plot of the Al/BCN/p-Si structure for the samples annealed at 400^{o}C and a) as-deposited and b) annealed at 400^{o}C

Fig 4.37 shows the values of dielectric constant before and after annealing for the samples deposited at room temperature and the samples deposited at 300^{o}C. It can be seen that the dielectric constant decreases after annealing for both the as-deposited and the films deposited at 300^{o}C. A dielectric constant as low as 2.52 is achieved for the BCN films studied . The error bars are incorporated to take into account the errors caused due to non-uniformities of the sample. The value of 2.52 is the lowest value reported for the insualting film deposited by sputtering. Sugiyama et al. have reported the effect of annealing on dielectric constant of BCN films deposited by plasma assisted chemical vapor deposition [].

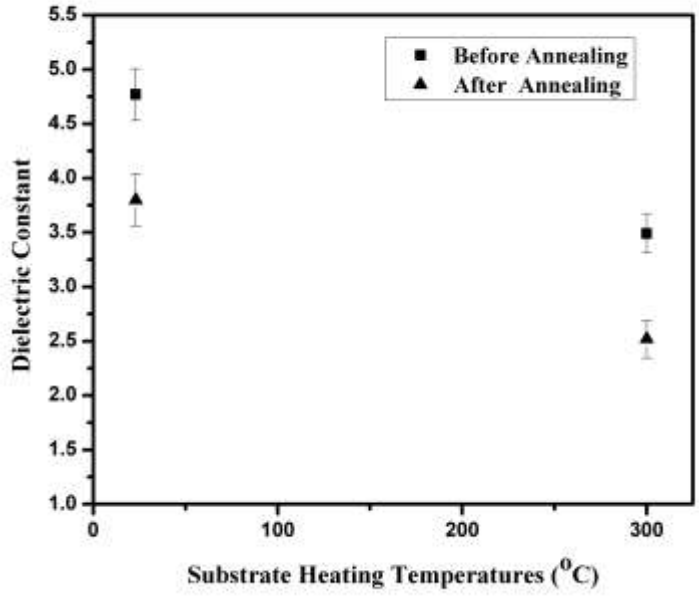

Figure 4.37: Relationship between dielectric constant before and after annealing for as-deposited samples and the samples deposited at 300°C.

4.5.4 Resistivity vs deposition temperatures

The electrical resistivity of the BCN films was examined from Metal-Insulator-Metal (MIM) structures with BCN film used a the insulator. I-V characteristics of the junction were then measured under forward and reverse bias conditions. The resistance value extracted from the I-V curves was used to calculate the resistivity of the BCN films and is plotted in the figure. As seen from the Figure 4.38, the resistivity of the BCN films increased with increase in the deposition temperatures. At room temperature the resistivity was very low in the range of 10^3 Ω and increased significantly when the films were deposited at 100°C. The resistivity increased from 10^3 Ω for as-deposited sample to 2.5 x10^9 Ω for samples deposited at 100°C. For temperatures higher than 100°C, the resistivity showed an increasing trend but the increase in resistivity was not that drastic and the films deposited at 400°C had the resistivity values of 3 x10^{10} Ω. The deposition temperature of around 400°C is ideal for the films used in the ULSI

integration schemes thereby making BCN a very promising candidate for applications in CMOS back-end technology.

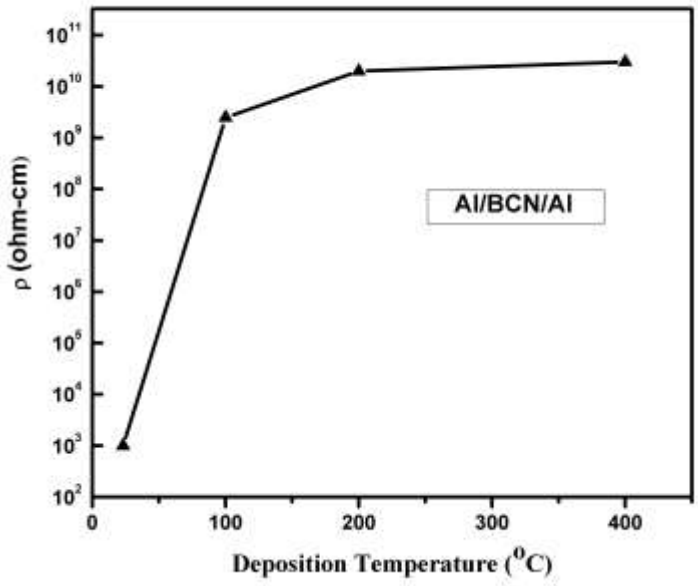

Figure 4. 38: Resistivity vs Deposition Temperatures.

CHAPTER 5: CONCLUSION

5.1: Concluding Remarks

Thin BCN films were successfully deposited by reactive sputtering from B_4C target in argon and nitrogen gas ambient. The formation of BCN is evident from XPS analysis. Film stoichiometry is strongly dependent on the N_2 flow ratio during deposition. Boron content in the film is observed to remain fairly constant even at higher N_2 flow ratios. Carbon content decreased as the ratio of N_2/Ar was increased and the nitrogen content in the films showed an increasing trend at higher N_2/Ar gas flow ratios. Higher nitrogen concentrations during deposition also show increased probability of formation of BN bonds in the deposited films. The deposition rate was found to be dependent on the N_2/Ar gas flow ratio and increased as the ration was increased from zero to 0.5. Further increase in the N_2/Ar ratio causes the deposition rate to reduce. Nitrogen flow rate change in the sputtering chamber also affects the film surface characteristics. Roughness of the films increases with higher N_2 flow rates and could be due to increased ion activity in the chamber at these flow rates. The optical studies revealed that the transmittance of the films improved with the initial nitrogen incorporation but did not significantly change with further increase of the N_2/Ar gas flow ratio. The optical band gap of the films increased with increasing N_2/Ar flow ratio up to 0.75. The band gap values in the range of 2.2-3.0 eV reveal a possible linear trend between that of BC (2.0 eV) to BN (4.0 eV) for potential band gap engineering applications.

Oxidation studies on thin BCN films obtained by reactive sputtering were carried out. Surface chemical composition and state of the annealed films were studied using XPS. Carbon and Nitrogen content in the film decreased significantly at higher temperatures. No nitrogen can

be seen in the films after 700°C anneal. The effect is primarly due to the breaking of C-N bonding in the film and the loss of N_2 and CO/CO_2 as gases during anneal. Oxygen interaction with boron in the film seems to increase with annealing temperatures. Optical properties of amorphous BCN thin films were studied at annealing temperatures up to 700^{o}C. High temperature annealing also leads to considerable increase in transmission. Optical energy gap is significantly influenced by annealing temperatures. Annealing at higher temperatures leads to broken C-N bonds and formation of B_2O_3 phases in the films. This is believed to be the primary cause for variations in optical properties of the films.

The properties of the BCN films were studied at deposition temperatures ranging from room temperature to 500^{o}C. The deposition temperature had a significant effect on the composition and the optical properties of the BCN films. The refractive index of the BCN films was observed to be in the range of 2.66-1.5. The optical band gap was in the range of 3.5-4.6 eV and increased with increasing deposition temperatures. The films were observed to have more BN bonds than BC bonds at higher deposition temperatures. The increase in optical band gap can be correlated to the loss of carbon and increase of boron content in the films.

The electrical properties of the reactively sputtered BCN films have been studied to see its feasibility as a material having a low dielectric constant to be used as a interlayer dielectric in the ultra large scale integration (ULSI). The Capacitance-Voltage (C-V) plots were obtained for the Al-BCN-p-Si (MOS) structures. Dielectric constant of the BCN films was calculated from capacitance of the accumulation region. The samples deposited at 300^{o}C showed the lowest value of dielectric constant. The dielectric constant was observed to decrease as the ratio of N_2/Ar was increased. This was attributed to the decreasing carbon content and increasing nitrogen content in the films at higher N_2/Ar gas flow ratio. Lastly, the dielectric constant

decreased after annealing at 400^{o}C in the argon gas ambient for 20 minutes. The lowest value of dielectric constant of 2.5 was obtained for the samples deposited at 300^{o}C and annealed at 400^{o}C in argon gas ambient. This by far is the lowest value obtained for the BCN films prepared by sputtering.

5.2: Future Work

Several avenues for exploring the potential applications for such materials are still open for investigation. Some are listed below;

5.2.1: Diffusion Barrier Studies

The microelectronics industry continues to scale down feature sizes and develop new materials for applications where performance is limited by material properties. The insulating copper diffusion barrier used in the interconnect integration represents one current materials opportunity. This barrier, critical for device reliability, prevents copper from diffusing into the underlying transistors by surrounding the copper wire in combination with the conductive diffusion barrier [177]. Silicon nitride deposited by plasma-enhanced chemical vapor deposition PECVD has been the insulating barrier since the implementation of Cu. However, SiN_x has a relatively high dielectric constant, k~7, compared to interlayer dielectric materials with k~2.7 now being developed (e.g., porous dielectrics). The higher k of SiN_x contributes to a higher overall effective k (k_{eff}) of the insulating materials in the interconnect; developing barriers with lower k would reduce the k_{eff}. Indeed, Martin *et al.* lowered k_{eff} 9% by replacing a 50 nm barrier with k of ~7 (silicon nitride) with a barrier having k of ~5 (silicon carbo-nitride) [178].

Studies of films with k~7 to replace silicon nitride have focused on PECVD-grown Si-based insulating barriers that incorporate carbon with or without nitrogen, e.g., SiC_xN_y and SiC_x [179-180]. These films have k *as* low as 5 for SiC_xN_y and 4 for SiC_x. However, as k drops in these Si-

based films, their barrier and electrical properties can degrade. B-based films are a potential alternative to current barrier materials. Numerous studies of boron nitride and boron carbo-nitride films using PECVD and thermal CVD deposition processes have reported *k* less than 5. Recent work by the authors on CVD boron carbo-nitride films deposited at 360^{o}C using dimethylamine borane with ammonia and/or ethylene demonstrated deposition of films with *k* less than 4.

The feasibility of BCN films as a diffusion barrier can be studied through SIMS. One way could be to make a sandwich structure with Cu/BCN/SiO_2/Si and then anneal these films at various temperatures in the ambient of inert gas such as argon or nitrogen. These films can then be characterized by SIMS depth profiling. The barrier studies can be analyzed by studying the Cu diffusion into the BCN layer at high temperatures.

5.2.2: Optical and surface characterization using reactive co-sputtering from B_4C and BN targets

Another way to prepare BCN films is by reactive co-sputtering from two targets namely B_4C and BN. In this case, there are two sources of boron as compared to only one in B_4C case and thus more boron content can be expected in the deposited films. The film elemental composition can be analyzed using XPS and SIMS depth profile techniques. Optical properties can be studied by UV-Visible Spectrophotometer. The substrate heating effect can be studied on the films deposited by co-sputtering from B_4C and BN targets. The optical properties at various deposition temperatures can be studied to see the possibility of tuning the band gap.

LIST OF REFERENCES

[1] A. Vijayakumar, R.M. Todi, K.B. Sundaram, "Amorphous-SiCBN-Based Metal–Semiconductor–Metal Photodetector for High-Temperature Applications", IEEE Electron Devices Letters, vol.28, no.8, (2007) pp. 713-715.

[2] A. Vijayakumar, R.M. Todi, V.O. Todi, K.B. Sundaram, "In-situ high temperature electrical characterization of RF sputtered SiCBN thin films", Journal of The Electrochemical Society, 154(10), (2007) pp. H875-H878.

[3] M.K. Lei, Q.Li, Z.F.Zhou, I.Bello, C.S.Lee and S.T.Lee, "Characterization and optical investigation of BCN film deposited by RF magnetron sputtering", Thin Solid Films, vol. 389, no.1/2. (2001), pp. 194-199,

[4] M.O.Watanabe, S.Itoh, K.Mizushima, T.Sasaki, Applied Physics Letters, 68 (21), (1996), pp. 2962.

[5] A.Y. Liu, M.L. Cohen, "Carbon nitride and other speculative super hard materials", Science, 245, (1989), pp. 841-842.

[6] W.D.Sproul, Surface coatings technology 81 (1996)

[7] D.C. Reigada, F.L. Freire, Diamond and related materials 16 (2007) 1441.

[8] D.C. Reigada, F.L. Freire Jr., "Nitrogen incorporation into boron carbide films deposited by dc-magnetron sputtering: Film microstructure and tribological properties," Surface and Coatings Technology, vol. 142-144, (2001), pp. 889-893.

[9] M.P.Johansson, N.Hellgren, T.Berlind, E.Broitman, L.Hultman and J.E.Sundgren. "Growth of CN_x/BN:C multilayer films by magnetron sputtering", Thin Solid Films, vol. 360, no.1/2, (2000), pp. 17-23.

[10] C. Morant, D. Caceres, J.M.Sanz and E. Elizalde, “Nano-mechanical properties of BCN/CN/BN multilayer films”, Diamond and related materials, 16 (2007), pp.1441-1444.

[11] M, Kawaguchi, Advanced Materials, vol. 9, 1997, pp. 615.

[12] S.Umeda, T.Yuki, T. Sugiyama and T. Sugino, “ Boron carbon nitride film with low dielectric constant as passivation film for high speed electronic devices”, Diamond and related materials, 13 (4-8), (2004) 1135.

[13] T Sugiyama, T. Tai and T. Sugino, “Effect of annealing on dielectric constant of boron carbon nitride films synthesized by plasma-assisted chemical vapor deposition”, Applied Physics Letters, vol. 80, no. 22, June 2002, pp. 4214-4216.

[14] T Yuki, S Umeda, T Sugino, “Electrical and optical characteristics of boron carbon nitride films synthesized by plasma-assisted chemical vapor deposition”, Diamond and related materials, vol. 13, (2004) pp. 1130-1134.

[15] Montasser, S. Hattori, S. Morita, Thin Solid Films, vol. 117, 1984, pp. 71

[16] A Weber, U. Bringmann, R. Nikulski, C.P. Klages, Diamond and Related Materials, vol. 2, 1993, pp. 201

[17] M.N.Oliveira, A.M. Botelho do Rego, O. Conde, “XPS investigation of $B_xN_yC_x$ coatings deposited by laser assisted chemical vapour deposition”, Surface Coatings and technology, 100-101, (1998), pp. 398-403.

[18] E.H.A Dekempeneer, J. Meneve, S. Kuypers, J. Smeets, Thin Solid Films, 281-282, (1996), pp.331.

[19] A. Mannan, M. Nagano, T. Kida, N. Hirao and Y. Baba, “ Characterization of BCN films synthesized by radio frequency plasma enhanced chemical vapor deposition”, 70, (2009), pp. 20-25.

[20] D. Watanabe, H. Aoki, R. Moriyama, M.K. Mazumder, C. Kimura and T.Sugino, "Characterization of BCN film after wet process for interconnection integration", 17, (2008), pp. 669-672.

[21] A. Perrone, A.P.Caricato, A.Luches, M. Dinescu, C.Ghica, V. Sandu and A. Andrei, "Boron carbonitride films deposited by pulsed laser ablation", *Applied Surface Science*, 133 (1998), pp. 239-242.

[22] C.Y. Zhang, X.L.Zhong, J.B. Wang and G.W. Yang, "Room temperature growth of cubic nitride boron film by RF plasma enhanced pulsed laser deposition", Chem. Physics Letters, 370, (2003), pp. 522-527.

[23] W.J. Pan, J. Sun, H.Ling, N.Xu, Z.F.Ying and J.D.Wu, "Preparation of thin films of carbon based compounds", Applied Surface Science, 218, (2003), pp. 297-304.

[24] S. Kouptsidis, H. Luthje, K. Bewilogua, A. Schutze, P. Zhang, "Deposition of c-BN films by DC magnetron sputtering", Diamond and related materials, vol. 7, (1998), pp. 26-31.

[25] J.Yue, W.Chang, X. Zhng, D.He nd G.Chen, "Ternary BCN thin films deposited by reactive sputtering", Thin Solid Films, 375 (2000), pp. 247-250.

[26] G.Bejarano, J.M.Caicedo, E.Baca, P.Prieto, A.G.Balogh and S.Enders, "Deposition of B_4C/BCN/c-BN multilayered thin films by r.f. magnetron sputtering", Thin Solid Films, 494 (2006), pp. 53-57.

[27] T. Komatsu, M. Samedima, T. Awano, Y. Kahadate, S. Fujiwara, Journal of Material Process Technology, vol. 85, 1999, pp. 69.

[28] S. Nakano, M. Akaishi, R. Sasaki, S. Yamaoka, Chemical Materials, vol. 6, 1994, pp. 2246.

[29] S. Itoh, Diamond Films Technology, vol. 7, 1997, pp. 195

[30] V.S. Teodorescu, A. Luches, R. Dinu, A. Zocco, M.E. Cioabanu, M. Martino, V. Sandu, M. Dinesu, Applied Physics A vol. 69, 1999, pp. 667.

[31] Z.F.Zhou, I.Bello, M.K.Lei, K.Y.Li, C.S.Lee, S.T.Lee, "Synthesis and characterization of boron carbon nitride films by radio frequency magnetron sputtering", Surface Coatings Technology, 128 (2000), pp. 334-340.

[32] J. Loeffler, E. Steinbach, J. Bill, J. Mayer, E. Aldinger, Z. Metallkd, vol. 87, 1996, pp. 170

[33] A. Lousa, J. Esteve, S.Muhl and E. Martinez. " BCN thin films near the B_4C composition deposited by radio frequency magnetron sputtering", Diamond and related materials, 9 (2000), pp. 502-505.

[34] E. Martinez, A. Lousa and J. Esteve "Micromechanical and microtribological properties of B4C thin films near the B_4C composition deposited by r.f magnetron sputtering", Diamond and related materials, 10 (2001), pp. 1892-1896.

[35] Thévenot, F., "Boron carbide–A comprehensive review", *Journal of the European Ceramic Society*, 6, (1990), pp. 205.

[36] Lattemann, M., Ulrich, S., "Investigation of structure and mechanical properties of magnetron sputtered monolayer and multilayer coatings in the ternary system Si-B-C", *Surf. Coat. Tech.*, 201, (2007), pp. 5564.

[37] Lee, K.E., Lee, J.Y., Park, M.J., Kim, J.H., Lee, C.B., Kim, C.O., " Preparation of boron carbide thin films for HDD protecting layer", *Journal of Magnetism and Magnetic Materials*, 272–276, (2004), pp. 2197.

[38] Lousa, A., Martinez, E., Esteve, J., Pascual, E., "Effect of ion bombardment on the properties of B4C thin films deposited by RF sputtering", *Thin Solid Films*, 355-356, (1999), pp. 210.

[39] Chen, Y., Chung, Y.W., Li, S.Y., "Boron carbide and boron carbonitride thin films as protective coatings in ultra-high density hard disk drives", *Surface Coatings Technology*, 200, (2006), pp. 4072.

[40] Sezer, A.O., Brand, J.I., "Chemical vapor deposition of boron carbide", *Materials Science and Engineering B*, 79, (2001), pp. 191.

[41] Erdemir, A., Bindal, C., Zuiker, C., Savrun, E., "Tribology of naturally occurring boric acid films on boron carbide", *Surface Coatings Technology*, 86-87, (1996), pp. 507.

[42] Conde, O., Silvestre, A.J., Oliveira, J.C., "Influence of carbon content on the crystallographic structure of boron carbide films", *Surface Coatings Tech*nology, 125, (2000), pp. 141.

[43] Harris, S.J., Krauss, G.G., Simko, S.J., Baird, R.J., Gebremariam, S.A., Doll, G., "Abrasion and chemical-mechanical polishing between steel and a sputtered boron carbide coating", *Wear*, 252, (2002), pp. 161.

[44] Eckardt, T., Bewilogua, K., Van der Kolk, G., Hurkmans, T., Trinh, T., Fleischer, W., "Improving tribological properties of sputtered boron carbide coatings by process modifications", *Surface Coatings Tech*nology, 126, (2000), pp. 69.

[45] Suematsu, H., Kitajima, K., Ruiz, I., Kobayashi, K., Takeda, M., Shimbo D., Suzuki, T., Jiang, W., Yatsui, K., "Thermoelectric properties of crystallized boron carbide thin films prepared by ion beam evaporation", *Thin Solid Films*, 407, (2002), pp. 132.

[46] Ahmad, A.A., Ianno, N.J., Hwang, S.D., Dowben, P.A., "Sputter deposition of high resistivity boron carbide", *Thin Solid Films*, 335, (1998), pp. 174.

[47] Aoqui, S., Miyata, H., Ohshima, T., Ikegami, T., Ebihara, K., "Preparation of boron carbide thin film by KrF excimer laser depositon process", *Thin Solid Films*, 407, (2002), pp. 126.

[48] Lin, S.H., Feldman, B.J., Li, D., "Microhardness study of amorphous hydrogenated boron carbide deposited on a cathode substrate by plasma deposition", *Applied Physics Letters*, 69, (1996), pp. 2373.

[49] Annen, A., Sab, M., Beckmann, R., Von Keudell, A., Jacob, W., "Structure of plasma-deposited amorphous hydrogenated boron-carbon thin films", *Thin Solid Films*, 312, (1998), pp. 147.

[50] Kosinova, M.L., Rumyantsev, Y.M., Golubenko, A.N., Fainer, N.I., Ayupov, B.M., Dolgovesova, I.P., Kolesov, B.A., Kaichev, V.V., Kuznetsov, F.A., "Chemical composition of boron carbonitride films grown by plasma-enhanced chemical vapor deposition from trimethylamineborane", *Inorganic Materials*, vol. 39, no. 4, (2003), pp. 366.

[51] Lee, S., Mazurowski, J., Ramseyer, G., Dowben, P.A., "Characterization of boron carbide thin films fabricated by plasma enhanced chemical vapor deposition from boranes", *Journal of Applied Phys*ics, vol. 72, no. 10, (1992), pp. 4925.

[52] Oliveira, J.C., Conde, O., "Deposition of boron carbide by laser CVD: A comparison with thermodynamic predicitions", *Thin Solid Films*, 307, (1997), pp. 29.

[53] Suematsu, H., Kitajima, K., Suzuki, T., Jiang, W., Yatsui, K., Kurashima, K., Bando, Y., "Preparation of polycrystalline boron carbide thin films at room temperature by pulsed ion-beam evaporation", *Applied Physics Letters*, vol. 80, no. 7, (2002), pp. 1153.

[54] Kokai, F., Taniwaski, M., Ishihara, M., Koga, Y., "Effect of laser fluence on the deposition and hardness of boron carbide thin films", *Applied Physics A,* 74, (2002), pp. 533.

[55] Sun, J., Ling, H., Pan, W.J., Xu, N., Ying, Z.F., Shen, W.D., Wu, J.D., "Chemical structure and micro-mechanical properties of ultra-thin films of boron carbide prepared by pulsed-laser deposition", *Tribology Letters*, vol. 17, no. 1, (2002), pp. 99.

[56] Greuner, H., Balden, M., Boeswirth, B., Bolt, H., Gadow, R., Grigull, P., Hofmann, G., Huber, T., Kasparek, W., Kumric, H., Lindig, S., Matern, G., Mayer, M., Neu, R., Renner, H., Roth, J., Riegert- Escribano, M., Simon-Weidner, J., Wacker, R., "Evaluation of vacuum plasma-sprayed boron carbide protection for the stainless steel first wall of WENDELSTEIN 7-X, *Journal of Nuclear Materials*, 329–333, (2002), pp. 849.

[57] Zhou, M.J., Wong, S.F., Ong, C.W., Quan, L., "Microstructure and mechanical properties of B_4C films deposited by ion beam sputtering", *Thin Solid Films*, 516, (2007), pp. 336.

[58] Hu, T., Steihl, L., Rafaniello, W., Fawcett, T., Hawn, D.D., Mashall, J.G., Rozeveld, S.J., Putzig, C.L., Blackson, J.H., Cermiagnani, W., Robinson, M.G., "Structures and properties of disordered boron carbide coatings generated by magnetron sputtering", *Thin Solid Films*, 332, (1998), pp. 80.

[59] Jacobsohn, L.G., Nastasi, M., "Sputter-deposited boron carbide films: Structural and mechanical characterization", *Surface Coatings Technology*, vol. 200, no. 5-6, (2005), pp. 1472.

[60] Wu, M.L., Kiely, J.D., Klemmer, T., Hsia, Y.T., Howard, K., "Process property relationship of boron carbide thin films by magnetron sputtering", *Thin Solid Films*, 449, (2003), pp. 120.

[61] Ahn, H.S., Cuong, P.D., Shin, K.H., Lee, K.S., "Tribological behavior of sputtered boron carbide coatings and the influence of processing gas", *Wear*, 259, (2005), pp. 807.

[62] Pierson, H.O. 1996: *Handbook of Refractory Carbides and Nitrides*, pp. 118- 154, Noyes Publications, New Jersey, USA.

[63] Chiang, C.L., Holleck, H., Meyer, O., "Properties of RF sputtered B_4C thin films", *Nucl. Instrum. Meth. Phys. Res. B*, vol. 91, no. 1-4, (1994), pp. 692.

[64] Han, Z., Li, G., Tian, J., Gu, M., "Microstructure and mechanical properties of boron carbide thin films", *Materials Letters*, 57, (2002), pp. 899.

[65] Chen, H.Y., Wang, J., Yang, H., Li, W.Z., Li, H.D., "Synthesis of boron carbide films by ion beam sputtering", *Surface Coatings Technology*, 128-129, (2002), pp. 329.

[66] Kulikovsky, V., Vorlicek, V., Bohac, P., Ctvrtlik, R., Strayanek, M., Dejneka, A., Jastrabik, L., "Mechanical properties and structure of amorphous and crystalline B_4C films", *Diamond and Related Materials*, 18, (2009), pp. 27.

[67] Monteiro, O.R., Delplancke-Ogletree, M.P., Klepper, C.C., "Boron carbide coatings prepared by cathodic arc deposition", *Journal of Material Science*, 38, (2003), pp. 3117.

[68] Ulrich, S., Ehrhardt, H., Schwan, J., Samlenski, R., Bren, R., "Subplantation effect in magnetron sputtered super hard boron carbide thin films", *Diamond and Related Materials*, 7, (1998), pp. 835.

[69] Cuong, P.D., Ahn, H.S., Yoon, E.S., Shin, K.H., "Effects of relative humidity on tribological properties of boron carbide coating against steel", *Surface Coatings Technology* 201, (2006), pp. 4230.

[70] Hu, T., Steihl, L., Rafaniello, W., Fawcett, T., Hawn, D.D., Mashall, J.G., Rozeveld, S.J., Putzig, C.L., Blackson, J.H., Cermiagnani, W., Robinson, M.G., "Structures and properties of disordered boron carbide coatings generated by magnetron sputtering", *Thin Solid Films*, 332, (1998), pp. 80.

[71] Pascual, E., Martinez, E., Esteve, J., Lousa, A., "Boron carbide thin films deposited by tuned-substrate RF magnetron sputtering", *Diamond and Related Materials*, 8, (1999), pp. 402.

[72] Lee, K.E., Kim, C.O., Park, M.J., Kim, J.H., "Preparation of boron carbide thin films from reactive sputtering of boron", *Phys. Stat. Sol. (b)*, vol. 241, no. 7, (2004), pp. 1637.

[73] Knotek, O., Lugscheider, E., Siry, C.W., "Tribological properties of BC thin films deposited by magnetron-sputter ion plating method," *Surface Coatings Technology*, 91, (1997), pp. 167.

[74] Erdemir, A., Eryilmaz, O.L., Fenske, G.R., "Self-replenishing solid lubricant films on boron carbide", *Surface Engineering*, 15, (1999), pp. 291.

[75] Larsson, P., Axén, N., Hogmark, S., "Tribofilm formation on boron carbide in sliding wear", *Wear*, 236, (1999), pp. 73.

[76] Guruz, M.U., Dravid, V.P., Chung, Y.W., "Synthesis and characterization of single and multilayer boron nitride and boron carbide thin films grown by magnetron sputtering of boron carbide", *Thin Solid Films*, 414, (2002), pp. 129.

[77] Reigada, D.C., Prioli, R., Jacobsohn, L.G., Freire Jr. F.L., "Boron carbide films deposited by a magnetron sputter-ion plating process: Film composition and tribological properties", *Diamond and Related Materials*, 9, (2000), pp. 489.

[78] Kustas, F., Mishra, B., Zhou, J., "Wear behavior of B_4C-Mo co-sputtered wear coatings", *Surface Coatings Technology*, 141, (2000), pp. 48.

[79] Lee, S., Mazurowski, J., Ramseyer, G., Dowben, P.A., 1992: Characterization of boron carbide thin films fabricated by plasma enhanced chemical vapor deposition from boranes, *Journal of Applied Phys*ics, Vol. 72, no. 10, (1992), pp. 4925.

[80] Sylyester B., Lin S.H., Feldman B.J., "Doping v/s alloying in amorphous hydrogenated boron carbide", *Solid State Communications*, vol. 93, no. 12, (1995), pp. 969-971.

[81] Jones J.D., Stewart A.D., *Phil. Mag.*, 46, (1982), pp. 423.

[82] Ahmad, A.A., Ianno, N.J., Hwang, S.D., Dowben, P.A., "Sputter deposition of high resistivity boron carbide", *Thin Solid Films*, vol. 335, no. 1-2, (1998), pp. 174.

[83]

[84] L. Vel, G. Demazeau and J. Etourneau, "Cubic Boron Nitride: Synthesis, Physiochemical Properties and Applications", *Materials Science and Engineering B*, (1991), pp. 149-164.

[85] C. Ronning, H. Feldermann and H. Hofsass, "Growth, doping and applications of cubic boron nitride thin films", *Diamond and Related Materials*, vol. 9, (2000), pp. 1767-1773.

[86] Wentorf Jr. RH., *J. Chem Phys*. 26, (1957), pp. 956.

[87] V. L. Solozhenko, S. N. Dub and N. V. Novikov, "Mechanical properties of cubic BC_2N new super hard phase", *Diamond and Related Materials*, vol. 10, (2001), pp. 2228-2231.

[88] N. V. Novikov. "New trends in high pressure synthesis of diamond", *Diamond and Related Materials*, vol. 8, (1999), pp. 1427-1432.

[89] R. Ganzetti and W. Gissler, "The Deposition of Cubic Boron Nitride Films by Ion Beam Assisted Sputter Deposition", *Materials and Manufacturing Processes*, vol. 9, (1994), pp. 507-517

[90] J. Hahn, M. Friedrich, R. Pintaske, M. Schaller, N. Kahl, F. Richter and D. R. T. Zahn, "Cubic boron nitride films by dc and r.f magnetron sputtering: Layer characterization and process diagnostics", *Diamond and Related Materials*, vol. 5, (1996), pp. 1103-1112.

[91] S. Matsumoto and W. Zhang, "Synthesis of Boron Nitride Films by Microwave Plasma Chemical Vapor Deposition in Flourine containing gases", *Japanese Journal of Applied Physics*, vol. 40, (2001), pp. 570.

[92] Riedel R., *Advanced Materials*, 4, (1992), pp. 759.

[93] Mishima O, Era K, Tanaka J, Yamaoka S., *Applied Physics Letters*, 53, (1988), pp. 962.

[94] Mishima M, Tanaka J, Yamaoka S, Furunaga O., *Science*, 238, (1987), pp. 181.

[95] Taniguchi T, Tanaka J, Mishima O, Osawa T, Yamaoka S., *Applied Physics Letters*, 62, (1993), pp. 576.

[96] A. Lipp, K. A. Schwetz, and K. Hunold, "HEXAGONAL BORON NITRIDE: FABRICATION, PROPERTIES AND APPLICATIONS", Journal of the European Ceramics Society, vol. 5, (1989), pp. 3-9.

[97] S. Watanabe, S. Miyake, and M. Murakawa, "Tribological properties of cubic, amorphous and hexagonal boron nitride films," *Surface & coatings technology*, vol. 49, (1991), pp. 406-410.

[98] M. Neuberger, *Handbook of Electronic Materials* 2, IFI/Plenum, New York (1971).

[99] Sugino T., Tai T, Etou Y., "Synthesis of boron nitride films with low dielectric constant for in application to silicon ultra large scale integrated semiconductors", *Diamond and Related Materials*, 10, (2001), pp. 1375-1379.

[100] Karim M.Z., Cameron D.C., Hashmi M.SJ. Surface and Coatings Technology, 60, (1993), pp. 502.

[101] Pauling L, The Nature of Chemical Bond, (1967), New York: Cornell University Press.

[102] Tong C.J., Silversten J.M., Judy J.H. and Chang C., *Journal of Material Research*, 5, (1990), pp. 2490.

[103] Yu K.M., Cohen M.L., Haller E., Hansen W.L., Liu A.Y. and Wu I., *Physics Review B*, 49, (1994), pp. 5034.

[104] Kumar S and Tansley T., *Solid State Communications*, 88, (1993), pp. 803.

[105] Kumar S and Tansley T., *Journal of Applied Physics*, 76, (1994), pp. 4390.

[106] Han H and Feldman B., *Solid State Communication*, 65, (1988), pp. 921

[107] Diani M, Mansour A, Kubler L, Bischoff J and Bolmont D, *Diamond and Related Materials*, 3, (1994), pp. 264

[108] Niu C, Lu Y. and Lieber M., *Science*, 261, (1993), pp. 334.

[109] Lieber C.M. and Zhang Z., *Advanced Materials*, 6, (1994), pp. 497.

[110] Fujimoto F and Ogata K, *Japanese Journal of Applied Physics*, 32, (1993), pp. L420.

[111] Chubaci J, Sakai T, Yamamoto T, Ogata K, Ebe A and Fujimoto F, *Nucl. Instrum. Methods B*, 80/81, (1993), pp. 463.

[112] Riviere J, Texier D, Delafond J, Jaouen M, Mathe E and Chaumont J, *Materials Letters*, 22, (1995), pp. 115.

[113] Kouvetakis J, Bhandari A, Todd M, Wilkens B and Cave N, *Chem. Mater.*, 6, (1994), pp. 811.

[114] Nakayama N, Tsuchiya Y, Tamada S, Kosuge K, Nagata S, Takahiro K and Yamaguchi S, *Japanese Journal of Applied Physics*, 32, (1993), pp. L1465.

[115] Mubumbila N., Tessier P., Angleraud B., Turban G., "Effect of nitrogen incorporation in CN_x thin films deposited by RF magnetron sputtering", *Surface and Coatings Technology*, 151-152, (2002), pp. 175-179.

[116] Kumar S., Tansley T and Wielunski L.S., "Structural characterization of reactively sputtered carbon nitride thin films with high nitrogen content", *Journal of Physics D: Applied Physics*, 28, (1995), pp. 2335-2339.

[117] Ulrich, S., Theel, T., Schwan, J., Ehrhardt, H., "Magnetron-sputtered super hard materials", *Surface and Coatings Technology*, 97, (1997), pp. 45.

[118] Freire, F.L., Reigada, D.C., Prioli, R., "Boron carbide and boron-carbon nitride films deposited by DC-magnetron sputtering: Structural characterization and nanotribological properties", Phys. Stat. Sol. (a), vol. 187, no. 1, (2001), pp. 1.

[119] Tsai, T.H., Yang, T.S., Cheng, C.L., Wong, M.S., "Synthesis and properties of boron carbon nitride (BN: C) films by pulsed-DC magnetron sputtering", *Materials Chemistry and Physics*, 72, (2001), pp. 264

[120] Linss, V., Hermann, I., Scwarzer, N., Kreissig, U., Richter, F., "Mechanical properties of thin films in the ternary triangle B-C-N", *Surface and Coatings Technology*, 163-164, (2003), pp. 220-226.

[121] M.O. Watanabe, S. Itoh, K. Mizushima, "Electrical properties of BC_2N thin films prepared by chemical vapor deposition," *Journal of Applied Physics*, 78, (1995), pp. 2880.

[122] P.R. Fitzpatrick, J.G. Ekerdt, *Journal of Vacuum Science and Technology A*, 26, (2008), pp. 1397.

[123] H. Aoki, D.Watanabe, R.Moriyama,M.K.Mazumder, N. Komatsu, C. Kimura, T. Sugino, *Diamond and Related Materials* 17, (2008), pp. 628.

[124] O. Baake, P.S.Hoffmann,A. Klein, B.Pollakowski, B.Beckhoff,W. Ensinger,M. Kosinova, N. Fainer, V.S. Sulyaeva, V. Trunova, X-Ray Spectrom. 38, (2009), pp. 68.

[125] I. Caretti, J.M. Albella, I. Jiménez, *Diamond and Related Materials*, 16, (2007), pp. 1445.

[126] F. Zhou, K. Adachi, K. Kato, *Thin Solid Films*, 497, (2006), pp. 210.

[127] P.-C. Tsai, "The deposition and characterization of BCN films by cathode arc plasma evaporation", *Surface and Coatings Technology*, 201, (2007), pp.5108-5113.

[128] A. Perrone, A.P. Caricato, A. Luches, M. Dinescu, C. Ghica, V. Sandu, A. Andrei, *Applied Surface Sciences*, 133, (1998), pp. 239.

[129] V. Linss, S.E. Rodil, P. Reinke, M.G. Garnier, P. Oelhafen, U. Kreissig, F. Richter, *Thin Solid Films*, 467, (2004), pp. 76.

[130] S. Ulrich, A. Kratzsch, H. Leiste, M. Stüber, P. Schloßmacher, H. Holleck, J. Binder,

D. Schild, S.Westermeyer, P. Becker,H.Oechsner, Surface and Coatings Technology, 116–119 (1999), pp. 742.

[131] Yang Q., Wang C.B., Zhang S., Zhang D.M., Shen Q., Zhang L.M., "Effect of nitrogen on structure and optical properties of pulsed laser deposited BCN thin films", *Surface and Coatings Technology*, 204, (2010, pp. 1863-1867.

[132] Yap Y.K., Wada Y., Yamaoka M., Yoshimura M., Mori Y., Sasaki T., "Bond modification of BCN films on Ni substrate", *Diamond and Related Materials,* 10, (2001), pp. 1137-1141.

[133] Dinescu M., Perrone A., Caricato A.P., Mirenghi L., Gerardi C., Ghica C., Frunza L., "Boron carbon nitride films deposited by sequential pulses laser deposition", *Applied Surface Science*, 127-129, (1998), pp. 692-696.

[134] Mannan M.A., Nagano M., Shigezumi K., Kida T., Hirao N. and Baba Y., Characterization of Boron Carbonitride (BCN) thin films deposited by radio frequency and microwave plasma enhanced chemical vapor deposition", *American Journal of Applied Sciences*, 5 (6), (2007), pp. 736-741.

[135] Pan W.J., Sun J., Ling H., Xu N., Ying Z.F., Wu J.D., "Preparation of thin films of carbon –based compounds", *Applied Surface Science,* 218, (2003), pp. 297-304.

[136] Kimura C., Okada K., Funakawa S., Sakata S., Sugino T., "Electron affinity and field emission characteristics of boron carbon nitride film", *Diamond and Related Materials,* 14, (2005), pp. 719-723.

[137] Liu L., Wang Y., Feng K., Li Y, Li W, Zhao C., Zhao Y., "Preparation of boron carbon nitride thin films by radio frequency magnetron sputtering", *Applied Surface Science,* 252, (2006), pp. 4185-4189.

[138] Yokomichi H., Funakawa T., Masuda A., "Preparation of boron-carbon-nitrogen thin films by magnetron sputtering", *Vacuum*, 66, (2002), pp. 245-249.

[139] Martinez C., Krysta S., Cremer R., Neuschutz, "Influence of the composition of BCN films deposited by reactive magnetron sputtering on their properties", Anal. Bioanal Chem., 374, (2002), pp. 709-711.

[140] Kusano Y., Evetts J.E., Hutchings I.M., "Deposition of boron carbon nitride films by dual cathode magnetron sputtering", *Thin Solid Films*, 343-344, (1999), pp. 250-253.

[141] Xu S., Ma X., Su M., "Investigation of BCN films deposited at various N_2/Ar flow ratios by DC reactive magnetron sputtering", IEEE Transactions of Plasma Science, vol. 34, no.4, (2006), pp. 1199-1203.

[142] Johansson M.P., Hellgren N., Berlind T., Broitman E., Hultman L., Sundgren J.E., "Growth of CN_x/BN:C multilayer films by magnetron sputtering", *Thin Solid Films*, 360, (2000), pp. 17-23.

[143] S. P. Jeng, R. H. Havemann and M. C. Chang, "Process integration and manufacturability issues for high performance multilevel interconnect," *Proc. Advanced Metallization for Devices and Circuits-Science, Technology and Manufacturability Symp.* Pittsburgh, PA, (1994), pp. 25-31.

[144] T. Licata, E. G. Colgan, J. M. Harper and S. E. Luce, "Interconnect fabrication processes and the development of low-cost wiring for MOS products," *IBM J. Res. Develop.*, vol. 39, no. 4, pp. 419-435, July 1995.

[145] The International Technology Roadmap for Semiconductors (ITRS) (2000). [Online]. Available at www.sematech.org

[146] A. Ishii, S. Amadatsu, S. Minomo, M. Taniguchi, M. Sugiyo, and T. Kobayashi, *Journal of Vacuum Science and Technology*, A 12, (1994), pp. 1068.

[147] T. Mandel, M. Frischholz,'R. gelbig and A. Hammerschmidt, *Applied Physics Lett*ers, 64, (1994), pp. 3637.

[148] T. Mandel, M. Frischholz, R. Helbig, *S* . Birkle, and A. Hammerschmidt, *Applied Surface Science*, 65/66, (1993), pp. 795.

[149] K. K. Chan, S. R. P. Silva, and G. A. J. Amaratunga, *Thin Solid Films*, 212, (1992), pp. 232.

[150] S.V. Nguyen, T. Nguyen, H. Treichel and 0. Spindler, *Journal of Electrochemical Society*, 141, (1994), pp. 1633.

[151] D. C. Cameron, M. Z. Karim and M. S. J. Hashmi, *Thin Solid Films*, 236, (1993), pp. 96

[152] M. Maeda, T. Makino, E. Yamamoto, and *S* . Konaka, *IEEE Trans. Electron Devices*, 36, (1989), pp. 1610.

[153] W. Schmolla and H. L. Hartnagel, *Solid State Electronics*, 26, (1983), pp. 931.

[154] M. Hirayama and K. Shohno, *Journal of Electrochemical Society*, 122, (1975), pp. 1671.

[155] M. J. Rand and J. F. Roberts, *Journal of Electrochemical Society*, 115, (1968), pp. 423.

[156] J. E. Parmeter, D. R. Tallant, and M. P. Siegal, *Materials Research Society*, 349, 513 (1994); D. R. Tallant, J. E. Parmeter, M. P. Siegal, and R. L. Simpson, *Diamond Relat. Mater*. 4, (1995), pp. 191.

[157] M. P. Siegal, T. A. Friedmann, S. R. Kurtz, D. R. Tallant, R. L. Simpson, F. Dominguez, and K. F. McCarty, *Material Research Society. Proc*. 349, (1994), pp. 507

[158] J. P. Sullivan “Novel Low-Permittivity Dielectrics for Si-Based Microelectronics”, Sandia Report SAND97-2092.

[159] T. L. Barr and S. Seal, "Nature of the use of adventitious carbon as a binding energy standard," *Journal of Vacuum Science & Technology A: Vacuum, Surfaces, and Films*, vol. 13, pp. 1239, 1995.

[160] J. F. Husein, Y. Zhou, F. Li, R. C. Allen, C. Chan, J. J. Kleiman, Y. Gudimenko, C. V. Cooper, “Synthesis of carbon nitride thin films by vacuum arcs”, Material Science Engineering, 1996, vol. 209, pp.10-15.

[161] C. D. Wagner, W. M. Riegs, L. E. Davis, J. F. Moulder, In:G.E. Mulienberg (Ed.), Handbook of X-ray Photoelectron spectroscopy, Perkin-Elmer, 1979.

[162] F. Fujimoto, K. Ogata, “Formation of carbon nitride films by means of ion assisted dynamic mixing (IVD) method”, Japanese Journal of Applied Physics, vol. 32, (1993) L420-L423.

[163] T. Ichiki, T. Momose, T. Yoshida, “Effects of the substrate bias on the formation of cubic boron nitride by inductively coupled plasma enhanced chemical, vapor deposition”, Journal of Applied Physics, vol. 75, (1994), pp.1330-1334.

[164] H. Sjostrom, W. Lanford, B. Hjorvarson, K. Xing, J.E. Sundgren, “Growth of CNx:Hy films by reactive magnetron sputtering of carbon in Ar/NH_3 discharges, Journal of Materials Research, vol. 11, (1996), pp. 981-988.

[165] M.Tabbal, P.Merel, S.Moisa, M.Chaker, A.Ricard, M.Moisan, “X-ray photoelectron spectroscopy of carbon nitride films deposited by graphite laser ablation in a nitrogen postdischarge”, Applied Physics Letters, vol. 69, (1996) pp. 1698-1700.

[166] Y.K.Yap, Y.Mori, S.Kida, T.Aoyama, J.Sasaki, "Carbon nitride thin films synthesized at high temperature by using RF-plasma PLD", Journal of crystal growth, vol. 199, (1999), pp. 1028-1031.

[167] M.N.Uddin, I.Shimoyama, Y.Baba, T. Sekiguchi, M. Nagano, "X-ray photoelectron spectroscopic observation on B-C-N hybrids synthesized by ion beam deposition of borazine", Journal of Vacuum Science and Technology, A23 (3), (2005), pp. 497-502.

[168] M.O.Watanabe, T.Sasaki, S.Itoh, K. Mizushima, "Structural and electrical characterization of BC_2N thin films", Thin Solid Films, 281-282, (1996), pp. 334-336.

[169] H. Kunzli, P. Gantenbein, R. Steiner, P. Oelhafen, "Deposition and characterization of thin boron-carbide coatings", Journal of Analytical Chemistry, vol. 346, no. 1-3, (1993), pp. 41-44.

[170] C.Morant, P. Prieto, J.Bareno, J.M.Sanz, E.Elizalde, "Hard BC_xN_y thin films grown by dual ion beam sputtering", Thin Solid Films 515, (2006), pp. 207-211.

[171] D. Li and W. Y. Ching, "Electronic structures and optical properties of low and high pressure phases of crystalline B_2O_3", Physics Review B54, (1996), pp. 13616-13622.

[172] J. Tauc, R. Grigorovici, A. Vancu, Phys. Status Solidi B, 15 (1966) 627-637.

[173] A. Vijayakumar, R. M. Todi, A. Warren, K. B. Sundaram, " Influence of N_2/Ar gas mixture ratio and annealing on optical properties of SiCBN thin films prepared by rf Sputtering", Diamond and Related Materials, 17, (2008), pp. 944-948.

[174] B. G. Streetman, S. Banerjee, Solid State Electronic Devices, 5^{th} edition, Prentice Hall, New Jersey, 2000

[175] R. Trehan, Y. Lifshitz and J. W. Rabalais, "Auger and x-ray electron spectroscopy studies of *h*-BN, *c*-BN, and N^+_2 ion irradiation of boron and boron nitride", Journal of Vacuum Science and Technology A8, (1990), pp. 4026-4032.

[176] K. J. Boyd, D. Marton, S. S. Todorav, A. H. Al-Bayati, J. Kulik, R. A. Zuhr and J. W. Rabalis, " Formation of C-N thin films by ion bean deposition", Journal of Vacuum Science and Technology A13, (1995), pp. 2110-2122.

[177] A. A. Istratov, C. Flink and E. R. Weber, "Impact of the unique physical properties of copper in silicon on characterization of copper diffusion barriers", Physics Status Solidi B 222, (2000), pp.261-277.

[178] J. Martin, S. Filipiak, T. Stephens, F. Huang, M. Aminpur, J. Mueller, E. Demircan, L. Zhao, J. Werking, C. Goldberg, S. Park, T. Sparks and C. Esber, 2002 IEEE International Interconnect Technology Conference (2002), pp. 42.

[179] S. G. Lee, Y. J. Kim, S. P. Lee, H. S. Oh, S. J. Lee, M. Kim, I.-G, Kim, J.-H. Kim, H.-J Shin, J.-G. Hong, Japanese Journal of Applied Physics, Part 1 40, (2001), pp. 2663.

[180] K. Goto, H. Yuasa, A. Andatsu and M. Matsura, 2003 IEEE International Interconnect Technology Conference (2003), pp. 6.